UV LASER PROTEIN-PROTEIN CROSS-LINKING IN LIVING CELLS: A NOVEL APPROACH TO IDENTIFY PROTEIN TARGETS

Francesco Itri

Dottorato in Scienze Biotecnologiche – XXVIII ciclo
Indirizzo Biotecnologie Industriali e Molecolari
Università di Napoli Federico II

Dottorato in Scienze Biotecnologiche – XXVIII ciclo
Indirizzo Biotecnologie Industriali e Molecolari
Università di Napoli Federico II

UV LASER PROTEIN-PROTEIN CROSS-LINKING IN LIVING CELLS: A NOVEL APPROACH TO IDENTIFY PROTEIN TARGETS

Francesco Itri

Dottorando:	Francesco Itri
Relatore:	Prof. Renata Piccoli
Coordinatore:	Prof. Giovanni Sannia

Alla mia famiglia e a tutti coloro che in questi anni mi hanno supportato ma soprattutto…sopportato

"Progress is impossible without change and those who cannot change their minds cannot change anything"

George Bernard Shaw

INDEX

RIASSUNTO

BASE SCIENTIFICA DEL PROGETTO DI RICERCA

Lo studio delle interazioni proteina-proteina (PPIs) è di fondamentale importanza per la comprensione dei processi biologici a livello cellulare. Infatti, basti pensare che mentre il genoma umano consiste di circa 20,000 geni codificanti proteine, è stato stimato che queste ultime sono coinvolte in centinaia di migliaia di interazioni. Per tale motivo, lo studio delle interazioni proteiche all'interno del proteoma cellulare (il cosiddetto "interattoma") risulta essere uno dei principali obiettivi della ricerca scientifica.

Numerose sono le tecniche sviluppate per studiare e caratterizzare tali interazioni. Tra di esse ricordiamo il sistema del doppio ibrido, saggi di co-immunoprecipitazione e co-localizzazione e il trasferimento di energia per risonanza (FRET). Tuttavia tali metodiche presentano numerose limitazioni, quali ad esempio l'impossibilità di identificare le interazioni transienti e l'elevata incidenza di falsi postivi e/o falsi negativi.

Per tale motivo, l'attenzione del mondo scientifico si è rivolta verso lo sviluppo di nuove strategie basate sull'utilizzo combinato del *cross-linking* e della spettrometria di massa per stabilizzare ed identificare le interazioni proteina-proteina.

Il *cross-linking* è una tecnica basata sulla capacità di indurre la formazione di legami covalenti tra due proteine, che sono fisicamente in contatto tra di loro, attraverso l'utilizzo di reagenti chimici o di una sorgente di luce UV.

Nel primo caso si fa riferimento al *cross-linking* di tipo chimico dove vengono utilizzati reagenti chimici bi-funzionali, come l'NHS, capaci di instaurare legami covalenti con i diversi gruppi reattivi delle proteine, tra i quali ricordiamo i gruppi amminici e sulfidrilici. Tuttavia, la resa di *cross-linking* è molto bassa e i prodotti ottenuti sono spesso eterogenei, perciò difficili da analizzare. A tal scopo, sono stati introdotti nuovi reagenti che semplificano le successive analisi di identificazione, ma che spesso richiedono una ingegnerizzazione delle cellule, alterando così il normale contesto cellulare.

Nel secondo caso, la reazione di *cross-linking* è basata sull'utilizzo della luce UV che è considerata capace di indurre la formazione dei cosiddetti legami a "lunghezza zero". In questo caso, infatti, non c'è necessità di utilizzare reattivi per ottenere il *cross-linking*. Tale sistema è stato ampiamente utilizzato per lo studio delle interazioni DNA-proteina; infatti, l'esposizione delle cellule alla luce UV ad una lunghezza d'onda di 260 nm induce la formazione di legami covalenti tra il DNA e le proteine che vi interagiscono. Anche questo sistema presenta, però, diversi svantaggi, quali i lunghi tempi di esposizione a cui sono soggetti i campioni, che possono causare danni cellulari e rendere tale metodica inadeguata per lo studio di interazioni transienti.

Per superare tali limiti, nel corso degli ultimi anni, la luce UV è stata sostituita dall'uso della luce laser UV. Infatti è stato dimostrato che l'uso del fascio laser UV come agente di *cross-linking* ha gli stessi vantaggi della luce UV, tra i quali la possibilità di formare i legami a lunghezza zero, e l'incremento delle rese del processo, ciò consente di ridurre notevolmente i tempi di reazione, rendendo quindi possibile lo studio delle interazioni transienti.

IL PROGETTO DI RICERCA

Il mio progetto di ricerca si propone come obiettivo lo sviluppo di una nuova strategia di *cross-linking* proteina-proteina in cellule vitali, basata sull'utilizzo di luce laser UV nella scala dei femtosecondi, capace di stabilizzare le interazioni senza alterare il contesto biologico in cui esse avvengono.

Inizialmente ho valutato l'uso del fascio laser per indurre la formazione di *cross-linking* proteina-proteina irraggiando cellule vitali in sospensione. Successivamente, ho analizzato come la resa del processo di *cross-linking* è influenzata dalla variazione dei parametri che caratterizzano il fascio laser, in modo da massimizzare la resa del processo e consentire l'isolamento e l'identificazione dei prodotti ottenuti.

Infine, durante il periodo di lavoro svolto presso i Laboratori della Prof.ssa Zurzolo a Parigi e del Prof. Tramier a Rennes, ho acquisito una metodologia indipendente che sarà utilizzata per validare e caratterizzare, le dinamiche spazio-temporali delle interazioni stabilizzate attraverso l'uso del fascio laser. Tale sistema è basato sulla metodica FRET combinata con l'analisi e la misura dell'emivita di fluorescenza attraverso la tecnologia FLIM ("Fluorescence Lifetime Imaging Microscopy").

IRRAGGIAMENTO MEDIANTE UV LASER

Partendo dalla recente dimostrazione che è possibile indurre la formazione di *cross-linking* mediante l'esposizione di peptidi in soluzione ad un fascio laser, e che tale fenomeno coinvolge principalmente gli amminoacidi aromatici, ho applicato, durante il mio progetto di Dottorato, tale tecnologia ad un sistema più complesso, ovvero cellule in coltura. A tal scopo, sono state utilizzate come sistema modello cellule tumorali della cervice uterina (HeLa) e come proteina oggetto di studio la gliceraldeide 3-fostato deidrogenasi (GAPDH), un enzima tetramerico costituito da 4 subunità identiche del peso di 37 kDa ciascuna. Si tratta di una proteina costitutiva molto abbondante nella cellula, in quanto rappresenta tra il 10-20% del totale delle proteine cellulari. Oltre al suo ben noto ruolo nella via glicolitica, in cui catalizza la conversione della gliceraldeide-3-fosfato in 1,3-bisfosfoglicerato, l'enzima GAPDH è coinvolto in numerosi processi cellulari.

Il primo passo è stato, quindi, irraggiare le cellule HeLa in sospensione in cuvetta ($4x10^5$ cellule/mL) con un fascio laser UV (260 nm) usando diverse combinazioni dei parametri fisici interessati, ovvero la frequenza di ripetizione degli impulsi (f_{rate}), l'energia del singolo impulso (E_{pulse}) ed il tempo di irraggiamento (T_{irr}). In particolare, tenendo conto che la dose totale di irraggiamento (D) è calcolata come $D = E_{pulse} \times T_{irr} \times f_{rate}$, sono stati utilizzati valori di energia variabili da 1.2 J fino a 13 J. Dopo lisi delle cellule, le analisi sono state condotte mediante Western blotting usando un anticorpo specifico per la GAPDH. I risultati hanno rivelato che nei campioni sottoposti ad irraggiamento, oltre alla presenza della specie monomerica della GAPDH del peso molecolare di 37 kDa, sono presenti anche altre specie proteiche a più alto peso molecolare, di cui la prioritaria corrisponde al peso di circa 90 kDa.

Queste analisi rappresentano una chiara evidenza che il fascio laser è in grado di stabilizzare complessi molecolari, che potrebbero derivare da una reazione

di *cross-linking* tra le subunità della GAPDH, o anche da interazioni della GAPDH con altre proteine. In ogni caso, tali risultati sono un incoraggiante punto di partenza per valutare la potenzialità di questa nuova metodologia.

OTTIMIZZAZIONE DELLE CONDIZIONI DI IRRAGGIAMENTO

Allo scopo di ottimizzare le rese del processo di *cross-linking*, ho analizzato come i parametri che caratterizzano il fascio laser influenzino la reazione di *cross-linking*.

Per tale motivo sono stati effettuati tre diversi set di irraggiamento, in cui abbiamo mantenuto costante uno dei tre parametri del fascio laser e variato gli altri due, in modo tale da mantenere costante la dose totale di irraggiamento al valore di 4.0 J. Le analisi sono state condotte determinando, sulla base dell'intensità delle bande proteiche riconosciute tramite Western blotting, la percentuale della specie monomerica e del prodotto di *cross-linking* di 90 kDa nelle varie condizioni di irraggiamento saggiate. Tali analisi hanno evidenziato che la resa del processo di *cross-linking* rimane costante intorno al valore del 10%. Ciò ci permette di assumere che la resa di *cross-linking* nell'intervallo di energia saggiata ($4x10^8$ - $10x10^8$ W/cm^2) può essere facilmente modulata, in quanto funzione della sola dose totale di irraggiamento.

Successivamente, per massimizzare l'efficienza del processo, ho effettuato una nuova serie di esperimenti mantenendo costante la frequenza di ripetizione e l'energia del singolo impulso, mentre il tempo di irraggiamento è stato variato da 24 a 44 secondi così da modulare la dose totale da 2.4 J a 4.4 J. Tali esperimenti hanno mostrato l'esistenza di una doppia correlazione lineare tra l'aumento della dose totale di irraggiamento e la diminuzione della specie monomerica con il concomitante aumento nella percentuale della specie ad alto peso molecolare. Inoltre, è stato osservato che alte dosi di energia causano un'apparente drastica diminuzione del totale delle proteine cellulari, dovuto probabilmente ad un eccessivo ed incontrollato processo di *cross-linking*. Tali analisi ci hanno permesso anche di definire i parametri della condizione ottimale di irraggiamento, che sono risultati essere: 2 kHz di frequenza di ripetizione, 50 µJ di energia del singolo impulso e 42 secondi di tempo di irraggiamento, per una dose totale di energia pari a 4.2 J.

In conclusione, queste osservazioni indicano che il processo di *cross-linking* proteina-proteina è altamente riproducibile. Esse suggeriscono anche che il processo è determinato dall'assorbimento di un singolo fotone da parte delle catene laterali degli amminoacidi aromatici, rendendolo così differente dal *cross-linking* DNA-proteina, che invece è un fenomeno di assorbimento bi-fotonico.

ISOLAMENTO E IDENTIFICAZIONE DI UN PRODOTTO DI *CROSS-LINKING*

Allo scopo di identificare i complessi ad alto peso molecolare ottenuti tramite irraggiamento, sono state effettuate analisi di spettrometria di massa in collaborazione con la Prof.ssa Leila Birolo del Dip. di Scienze Chimiche (Università di Napoli Federico II).

I lisati cellulari del campione irraggiato e non irraggiato sono stati prima frazionati tramite elettroforesi bidimensionale e poi colorati con blu di Coomassie

colloidale o analizzati tramite Western blotting con un anticorpo specifico per l'enzima GAPDH. Quest'ultima analisi ha rivelato la presenza nel solo campione irraggiato di un segnale (spot) ad alto peso molecolare e corrispondente allo stesso pI della GAPDH monomerica. L'area del gel corrispondente a tale spot, così come la corrispondente area del campione di controllo, è stata escissa dal gel e sottoposta ad analisi di spettrometria di massa, le quali hanno rivelato la presenza della sola GAPDH, suggerendo che il prodotto di *cross-linking* è un oligomero della GAPDH stessa.

Per convalidare tale dato, sono state effettuate ulteriori analisi attraverso esperimenti di immunoprecipitazione sul campione irraggiato e, come controllo, sul campione non irraggiato utilizzando un anticorpo specifico per la GAPDH. Le proteine immuno-selezionate sono state poi sottoposte ad analisi mediante SDS-PAGE, seguita da colorazione con blu di Coomassie colloidale. Tale analisi ha rivelato la presenza della specie monomerica della GAPDH in entrambi i campioni immuno-selezionati, mentre solo nel campione irraggiato è stata identificata la specie proteica dal peso apparente di 90 kDa. Su quest'ultima è stata effettuata un'analisi mediante spettrometria di massa, che ha rivelato ancora una volta la presenza della sola GAPDH, confermando quindi che essa rappresenta un oligomero della GAPDH.

ANALISI *IN VITRO* ED *IN SILICO*

Ho quindi effettuato un'analisi comparativa dei prodotti di *cross-linking* generati *in vivo* con quelli generati *in vitro* irraggiando l'enzima GAPDH disponibile in commercio. Le analisi effettuate mediante SDS-PAGE seguita da Western blotting hanno permesso di paragonare la mobilità elettroforetica dei due campioni; ciò ha evidenziato che il prodotto di *cross-linking* ottenuto dall'irraggiamento *in vitro* corrisponde anch'esso al peso molecolare di 90 kDa come riscontrato per le cellule vitali, supportando così le evidenze sperimentali finora ottenute.

Allo scopo poi di fornire una base strutturale per i nostri risultati, in collaborazione con il gruppo della Prof.ssa Angelina Lombardi del Dip. di Scienze Chimiche (Università di Napoli Federico II), ho analizzato la struttura cristallografica della GAPDH, recentemente risolta da Jenkins & Tanner, che nella sua forma funzionale si presenta come un omo-tetramero con simmetria D_2 e tre interfacce indipendenti. Tale analisi ha evidenziato la presenza di alcuni possibili siti di *cross-linking* in una sola delle tre interfacce della proteina. In particolare, il triptofano in posizione 196 di una delle quattro subunità è in prossimità di tre tirosine (Y42, Y45, Y49) della subunità adiacente. Inoltre, poiché il meccanismo di eccitazione di questa tecnica è basato sull'assorbimento di un singolo fotone, possiamo affermare che la formazione di un omo-dimero della GAPDH, che coinvolge il triptofano 196 ed una sola della tre tirosine sopra menzionate, è l'unico prodotto atteso, in quanto è il solo che può essere generato a seguito di cross-linking mediante UV laser.

ANALISI SPETTROSCOPICHE

Per analizzare l'effettivo coinvolgimento dei residui aromatici nel fenomeno di *cross-linking*, abbiamo effettuato una caratterizzazione spettroscopica della GAPDH irraggiata *in vitro*. In particolare, è stato effettuato uno spettro UV-Vis, nel range 200-800 nm, che ha mostrato la chiara presenza di una nuova banda centrata alla

lunghezza d'onda di 330 nm, che può essere interpretata come la formazione di un cromoforo aromatico, mentre l'assorbimento a 280 nm è rimasto pressoché invariato. Analisi di fluorescenza intrinseca hanno poi mostrato solo una piccola variazione nell'intensità di fluorescenza rispetto alla proteina non irraggiata, suggerendo una diminuzione nel numero di fluorofori eccitati a 280 nm. Quest'ultima ipotesi è stata supportata da un concomitante aumento dell'intensità dell'emissione a 420 nm della proteina a seguito di eccitazione a 340 nm. Ciò indica che una frazione dei residui aromatici è coinvolta in uno spostamento della fluorescenza verso lunghezze d'onda più alte. Infine, sono state effettuate analisi di dicroismo circolare (CD) dalle quali è emerso che la struttura secondaria della proteina rimane pressoché inalterata dopo irraggiamento. Le uniche differenze spettrali riscontrate, in quest'ultima analisi, sono presenti nella regione di lunghezza d'onda nel campo UV, in accordo con i dati precedenti.

In conclusione, possiamo affermare che la formazione di prodotti di *cross-liknking* indotta dall'esposizione alla luce laser UV è principalmente basata sul coinvolgimento dei residui aromatici.

MARCATURA DELLA MEMBRANA CITOPLASMATICA ED ESPERIMENTI DI FLIM-FRET

Ultimo obiettivo del progetto è la messa a punto di un sistema independente per l'analisi delle interazioni proteina-proteina, allo scopo di validare i risultati ottenuti con la nuova metodologia laser UV e di analizzare le dinamiche spazio-temporali delle interazioni proteina-proteina che il nostro sistema è in grado di stabilizzare. A tal scopo, ho effettuato esperimenti volti a combinare le tecnologie FRET (*Fluorescence Resonance Energy Transfer*) e FLIM (*Fluorescence Lifetime Imaging Microscopy*). Infatti, le analisi mediante FRET permettono di determinare le interazioni attraverso il trasferimento di energia per risonanza da un fluoroforo donatore ad uno accettore. Applicando la tecnica FLIM è possibile analizzare queste interazioni monitorando l'emivita del fluoroforo donatore in presenza o in assenza dell'accettore, ricavando perciò informazioni spazio-temporali sull'interazione oggetto di studio.

Tali esperimenti sono stati effettuati durante la mia esperienza di ricerca nei laboratori di "Unitè de Trafic Membranaire et Pathogenèse" all'Istituto Pasteur (Parigi, Francia) e nel "Département de Biologie Cellulaire et Developpement" all'Università di Rennes 1 (Rennes, Francia). In particolare, è stata utilizzata una sonda fluorescente del colesterolo, di cui è stata monitorata l'emivita, al fine di analizzare l'ambiente chimico della membrana citoplasmatica in diverse linee cellulari epiteliali. Una volta acquisite tali informazioni, la stessa sonda è stata utilizzata come donatore per effettuare esperimenti di FLIM-FRET usando come accettore proteine di membrana con ancora di glicosil fosfatidil inositolo (GPI-APs).

Diversi studi hanno evidenziato che l'organizzazione della proteine con ancora GPI nelle cellule epiteliali è differente rispetto a quella dei fibroblasti. Infatti, le GPI-APs presenti sulla membrana apicale delle cellule epiteliali sono organizzate in *cluster* della stesse specie, denominati *omo-cluster*, indipendenti dalla presenza di colesterolo. Tali raggruppamenti si possono poi fondere in *cluster* più grandi, composti da specie diverse di GPI-APs, denominati *etero-cluster*, la cui formazione è invece dipendente dal colesterolo di membrana. Nei fibroblasti, invece, le GPI-APs sono presenti sulla membrana citoplasmatica come monomeri e non come omo-

cluster e possono formare direttamente etero-cluster, a seconda della quantità del colesterolo di membrana.

Inoltre, recentemente è stato dimostrato che nei fibroblasti l'organizzazione in cluster è influenzata anche dall'actina, la cui strutturazione è a sua volta influenzata dalla quantità di colesterolo presente nella cellula. Quindi, anche se ancora non sono ben chiari i meccanismi di azione, risulta evidente che actina e colesterolo hanno un ruolo ben diverso nell'organizzazione delle GPI-APs nei fibroblasti e nelle cellule epiteliali.

Perciò, allo scopo di acquisire e mettere a punto un'efficace metodologia per analizzare l'influenza che actina e colesterolo esercitano sull'organizzazione delle GPI-APs sulla membrana citoplasmatica nelle diverse linee cellulari, abbiamo utilizzato una sonda fluorescente per il colesterolo, denominata TopFluorcholesterol, per misurare l'emivita del colesterolo di membrana nelle cellule epiteliali renali di cane (MDCK) e nelle cellule di ovario di criceto (CHO) in presenza o in assenza del trattamento con la latrunculina A che, prevenendo la polimerizzazione dell'actina, destabilizza l'integrità del citoscheletro.

Tali esperimenti hanno rivelato che effettivamente l'intorno chimico della membrana cellulare delle cellule epiteliali e dei fibroblasti è differente. Inoltre, mentre nei fibroblasti sottoposti a stress con la latrunculina A, l'emivita del colesterolo scende drasticamente, nelle cellule epiteliali rimane costante, sottolineando che nelle due diverse linee cellulari esiste una differente relazione tra colesterolo e actina.

Infine, abbiamo messo a punto un esperimento di FLIM-FRET, nella linea cellulare CHO, con lo scopo di misurare l'emivita del TopFluorcholesterol in presenza o in assenza di un putativo accettore, quale la fosfatasi alcalina placentare (PLAP), che rappresenta un esempio di GPI-AP. A tale scopo, abbiamo trasfettato in modalità transiente cellule CHO con un plasmide codificante la proteina PLAP fusa alla proteina fluorescente mCherry. Le cellule sono state quindi trattate con la latrunculina A, o direttamente marcate con il TopFluorcholesterol, e analizzate mediante FLIM.

Tali analisi hanno rivelato che, in tale linea cellulare, vi è un forte segnale FRET tra il Topfluorcholesterol e la GPI-AP, in quanto l'emivita del colesterolo scende da 4.08 ns ± 0.23 a 3.8 ns ± 0.03. Inoltre, abbiamo osservato che il segnale FRET diminuisce drasticamente quando le cellule sono sottoposte a trattamento con la latrunculina A, dal momento che l'emivita del colesterolo passa da 3.87 ns ± 0.17 a 3.75 ns ± 0.05. Tali risultati confermano quindi che l'organizzazione delle GPI-APs nei fibroblasti è influenzata dall'actina del citoscheletro.

L'acquisizione dei principi di base di questa metodologia sarà di grande utilità per validare la metodologia innovativa messa a punto nel corso del presente progetto di Dottorato e sarà, in particolare, utilizzata per delucidare le dinamiche spazio-temporali delle interazioni identificate in seguito ad irraggiamento delle cellule vitali con luce laser UV.

SUMMARY

The study and the characterization of protein-protein interactions (PPIs) are essential to define the molecular networks that contribute to cellular physiological processes or to the development of a disease.

To this purpose, my research project was focused on the development of an innovative methodology aimed at identifying protein-protein interaction networks in living cells by inducing UV laser cross-linking between two interacting bio-partners in close molecular contact without altering proteins and their natural environment.

In particular, we used a femtosecond UV laser to irradiate human living cells, i.e. HeLa cells, in order to cross-link proteins *in vivo*. We focused our attention on glyceraldehyde-3-phosphate dehydrogenase (GAPDH), a protein implicated in many cellular activities, which is a homo-tetrameric enzyme, structurally and functionally well characterized.

Our experiments allowed us to demonstrate that the exposure of HeLa cells to UV laser induces the formation of covalent adducts of GAPDH inside the cells and that the phenomenon can be modulated, since the amount of cross-linked products was found to be a linear function of the total irradiation energy. By this way, we were able to setting up the optimal parameters to maximize UV laser protein-protein cross-linking yield without damaging cells.

Immunoprecipitation experiments and mass spectrometry analyses allowed us to isolate and identify, among the cross-linked products, stable dimers of GAPDH, as also observed upon *in vitro* UV laser irradiation of the pure protein.

Since aromatic residues are supposed to be involved in the cross-linking reaction, we performed GAPDH structural and spectroscopic analyses to add knowledge to the molecular bases of UV laser cross-linking. Interestingly, a detailed structure analysis of the distances between aromatic residues showed the presence of a defined aromatic patch at the C2 symmetric R-interface of GAPDH natural tetramer, so that a dimer is the sole product expected to be generated by light excitation. Furthermore, spectroscopic analyses, performed on rabbit muscle GAPDH irradiated *in vitro*, suggested that a cross-coupled aromatic moiety is produced upon laser irradiation.

Taken together, collected data confirmed that UV laser acts as an agent able to photo-fix protein surfaces that are in direct contact. Due to the ultra-short time scale of UV laser induced cross-linking, this technique may represent a powerful tool to weld transient protein interactions (at zero length) in their native context.

Since this novel methodology needs to be validated and deeply characterized, in the period I spent in the laboratories of Professor C. Zurzolo in Paris and Professor M. Tramier in Rennes, I set up a suitable system based on FLIM-FRET microscopy, which will be helpful to validate by an independent approach data obtained by UV laser cross-linking in living cells and which will allow the spatio-temporal characterization of the dynamics of interactions “photo-fixed” by UV laser irradiation.

The impact of the UV laser technique will be relevant both in the generation of scientific knowledge and insight, as well as in practical applications. Our results pave the way to understand the basic mechanisms of interaction between biomolecules in a native context at a molecular level, what represents a consistent boost in physics, chemistry, and so-called "omics" sciences, such as genomics, epigenomics and proteomics.

CHAPTER 1

BACKGROUND

1.1 Protein-protein interactions

The study of protein-protein interactions (PPIs) is the key to understand all biological processes at the molecular level. While the human genome consists of only approximately 20,000 protein-encoding genes, their products are estimated to engage in hundreds of thousands of PPIs [Stumpf MP et al, 2008]. Thus, characterization of protein interactions in the cellular proteome (interactome) will be the next milestone along the road to understand cell biochemistry. The interactome is dynamic: every significant cellular event – growth, motility, division – is accompanied by changes in PPIs networks. Moreover, at the organism level, alterations in the protein interactome are clearly fundamental to physiological processes and to pathological events. Therefore, mapping PPIs and their interaction interfaces in living cells is critical for a comprehensive understanding of protein function and regulation, as well as for identifying protein partners and key targets.

Interactions among proteins can be classified as stable or transient and be either strong or weak [Nooren IM & Thorton JM, 2003; Jones S & Thorton JM, 1996]. Stable interactions are those associated with proteins that are purified as multi-subunit complexes, where subunits of the complex are made of identical or different polypeptide chains. For example, hemoglobin and core RNA polymerase are considered as stable multi-subunit complexes where protein chains are stably bound. By contrast, a transient interaction associates and dissociates *in vivo*. It is possible to distinguish weak transient interactions, characterized by a dynamic oligomeric equilibrium in solution, since the interaction is broken and formed continuously, and strong transient associations that require a molecular trigger to shift the oligomeric equilibrium [Lander ES et al, 2001]. While in contact with their binding partners, transiently interacting proteins are expected to be involved in numerous cellular processes including protein modification, transport, folding, signaling or cell cycling.

To date, the interactome map remains incomplete and functional and structural insights are often lacking, even for known interactions.

Primary challenges associated with the study of biological systems, hence, include identification of protein interactions and measurement of topological/structural features of protein interactions *in vivo*. Several strategies have been developed to identify and map protein interactions in complex biological samples, such as the Yeast Two-Hybrid (Y2H) [Vidal M & Fields S, 2014], co-immuno-precipitation [Elion EA, 2006], protein microarray [Liu BA et al, 2012], co-localization microscopy [Buser & McDonald K, 2010], affinity purification mass spectrometry (AP-MS) [Kocher T & Superti-Furga G, 2007], fluorescence protein Förster resonance energy transfer (FRET) [Piston DW & Kremers G, 2007] and microscopic imaging strategies based on FRET, such as acceptor bleaching, sensitized emission, polarization anisotropy and fluorescence lifetime imaging microscopy (FLIM) [Ishikawa-Ankerhold HC et al, 2012]. Even though these approaches have provided a wealth of information on protein complexes, none of these methods is fully comprehensive, and the obtained large data sets often suffer from high rates of false negative and false positive

results. Furthermore, in most of the cases low-affinity interactions are dismissed as non-specific, although these transient interactions play a key role in critical cellular processes.

It appears clearly evident that a significant improvement in the field of PPIs analyses would be the development of methodologies aimed at identifying relevant and/or transient PPIs directly in living cells, thus minimizing artefacts.

This is the driving force to develop and optimize MS-compatible protein chemistry-based strategies that rely on chemical or UV light cross-linking to stabilize, isolate, and finally identify individual protein components of functional complexes [Sinz A, 2006].

1.2 Cross-linking

In the cell, a single protein may often engage in transient interactions with a variety of partners in a specific pathway. If two proteins physically interact with each other, they can be covalently cross-linked. The formation of cross-links between two distinct proteins is a direct and convincing evidence of their close proximity. In addition to information on the identity of the interacting proteins, cross-linking experiments can reveal interaction sites.

1.3 Chemical cross-linking

Chemical cross-linking represents a direct method to identify both transient and stable interactions. This methodology takes advantage of the enormous diversity of available cross-linking reagents that differ in chemical functionality, reactivity, and size [Wong SS & Jameson DM, 2012]. Homo-bifunctional and hetero-bifunctional chemical cross-linkers carry two reactive groups able to form bonds with the same or different functional groups of proteins, respectively. These reactive groups can react with amine-, sulfhydryl- or photo-reactive ends of biomolecules. The most commonly used cross-linking reagent is N-hydroxysuccinimide ester (NHS) [Boeri Erba E et al, 2015], which forms stable amide bonds with primary amines at physiological pH and it may be used for *in vivo* labeling.

Upon the formation of covalent bonds between interacting partners, affinity purification of covalent complexes may be performed under stringent and fully denaturing conditions, thus reducing non-specific background and preserving stable and weak/transient interactions [Guerrero C et al, 2006; Guerrero C et al, 2008; Kaake RM et al, 2010]. Subsequent mass spectrometric analyses can reveal not only the identity of interacting proteins, but also that of the cross-linked amino acid residues. This provides a direct molecular evidence of the physical contacts occurring between and within proteins [Leitner A et al, 2010]. Thus, cross-linking mass spectrometry (XL-MS) strategies represent a powerful and emergent technology that possesses unparalleled capabilities to study PPIs.

In general, cross-linked products are heterogeneous and low in abundance with respect to non-cross-linked products. In addition, their MS fragmentation is too complex to be interpreted using conventional database searching tools [Sinz A, 2006]. It has to be noticed that in most of the current *in vivo* PPIs studies, formaldehyde is used as cross-linking reagent, since it is able to permeate cell membranes and enter the cells. However, in comparison to the most commonly used

amine reactive NHS ester cross-linkers, identification of formaldehyde cross-linked peptides is even more challenging because of its non-specific reactivity and extremely short spacer length [Sutherland BW et al, 2008]. Therefore, further developments in reagents and methods are urgently needed to enable simpler MS detection and effective identification of *in vivo* cross-linked products. This would allow mapping of authentic interaction sites in protein complexes.

Various efforts have been performed to overcome the limitations of XL-MS studies, such as development of bioinformatics tools for improved data interpretation [Rinner O et al, 2008; Panchaud A et al, 2010; Walzthoeni T et al, 2012; Yang B et al, 2012] and design of novel cross-linking reagents for enhanced MS analysis of cross-linked peptides [Weisbrod CR et al, 2013; Chu F et al, 2006; Chowdhury SM et al, 2009].

These novel approaches include Stabilized Affinity-Capture Mass Spectrometry (SAC-MS) [Subbotin RI & Chiat BT, 2014], protein interaction reporter (PIR) technology [Zhang H et al, 2009], or methods based on novel membrane permeable and MS-cleavable cross-linking reagents [Kaake RM et al, 2014].

However, all the available techniques are based on the use of chemical reagents, chemical treatments or engineering of living cells, which may alter the proteins under test and their physiological context.

1.4 UV light cross-linking

In the early 1960s [Alexander P & Moroson H, 1962], ultraviolet (UV) light irradiation was found to induce stable cross-linking between protein and DNA. Later this technique was used to cross-link a specific protein to DNA. Nowadays, UV cross-linking combined with immunoprecipitation (UV-X-ChIP) represents an effective tool to detect DNA-protein or protein-protein interactions [Carr A & Biggin MD, 1999; Dimitrov SI & Moss T, 2001].

UV light is a zero length cross-linker, whose main advantage with respect to a chemical cross-linker is that of determining a significantly less pronounced perturbation of protein complexes. In particular, irradiation of living cells with UV light at wavelength near 260 nm produces covalent bonds between interacting nucleic acids and proteins [Dimitrov SI & Moss T, 2001]. In fact, following irradiation, the electronic state of proteins and DNA is excited and relaxes by means of the formation of a covalent bond in a bi-photonic reaction [Meisenheimer KM & Koch TH, 1997].

In particular, the excitation mechanism involves the adsorption of two photons and results in the production of reactive cation radicals (Figure 1). The first photon excites the S_0–S_1 transition. From the excited S_1 state the molecule can absorb a second photon, which promotes the molecule to high singlet level S_N allowing the cross-linking reaction. Since there is a certain probability for intersystem crossing (typical intersystem crossing rate is $k = 10^9\ s^{-1}$), a fraction of the excited molecules will relax from the S_1 to the first excited triplet state T_1, which has a longer lifetime compared to the S_1 state. From T_1 a second photon can lead to excitation of high triplet states T_N, which can also cause cross-linking. The ratio between excitation *via* the singlet or triplet path depends on the pulse length of the exciting laser, the effective lifetime of the excited singlet state S_1 and the intersystem crossing rate [Russmann C et al, 1997; Russmann C et al, 1998].

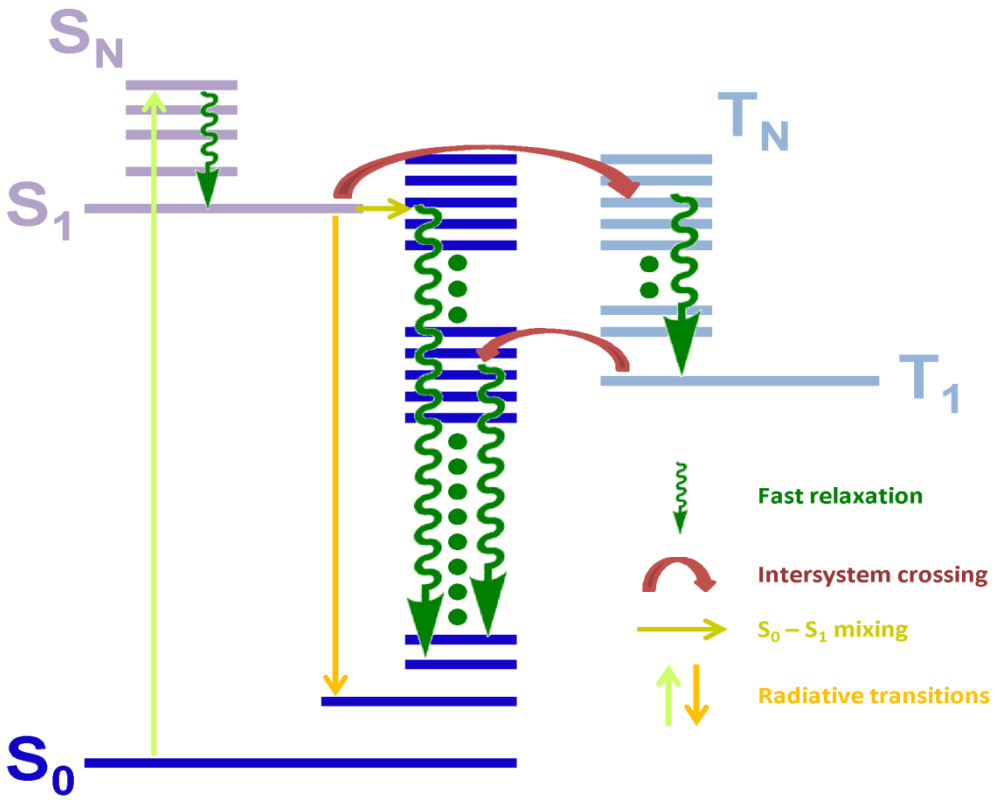

Figure 1. Simplified energy level diagram. The pathways leading to cross-linking *via* the singlet S_1 and the triplet T_1 states are indicated. Following excitation of the singlet S_1 state, the bases are promoted either directly with a second photon to high lying S_N states above the ionization threshold, or after intersystem crossing to the T_1 level, to states T_N.

However, this reaction is relatively inefficient and the formation of photo-induced products strongly depends on structural parameters, such as distance between reactive amino acids and/or bases. Moreover, not all amino acids and bases are equally reactive. The amino acids more responsive to UV cross-linking are those containing an aromatic ring, since they possess free electrons [Greenberg JR, 1979].

To overcome this problem, protein photo-cross-linking is often obtained by replacing amino acids (e.g. leucine and methionine) with their photo-sensitive analogs containing diazirine rings activated by UV light [Rotili D et al, 2011; Mizdrak J et al, 2008; Suchanek M et al, 2005]. Upon irradiation, highly reactive intermediates are generated and react with neighboring functional groups, with the consequent formation of covalent bonds. However, this method still suffers from high false positive and negative rates, with the main limit that non-native photo-cross-linking groups are introduced into biomolecules of interest *via* the metabolic labelling and the genetic code expansion strategies [Suchanek M et al, 2005].

Another photo-cross-linking limit is linked to the long exposure times required, ranging from minutes to several hours, thus determining protein redistribution and cross-linking of photo-damaged molecules [Moss T et al, 1997]. This makes UV light cross-linking not suitable to study rapid binding kinetics. As a consequence, research activities were aimed to develop a novel tool able to induce UV cross-linking by using an UV laser pulsed system [Russmann C et al, 1997].

1.5 The laser theory

The term "laser" was used for the first time in the late 1950s by Gordon Gould. It represents an acronym for *Light Amplification by Stimulated Emission of Radiation.*

A laser is an electronic-optical device that emits temporally and spatially coherent, monochromatic, bright and unidirectional light radiation. Laser theory is based on the central concept of quantum mechanics: atomic energies are confined to certain allowed, discrete values. The atomic population of any system at equilibrium in nature, without an external source of energy, is stabilized at values predicted by the Boltzmann's distribution. If the temperature of the entire system is raised, the atomic distribution shifts towards higher energy values. Hence, the population of a lower energy level will always exceed that of a higher level.

The energy variation between the upper and lower energy states of any radiative transition is the photon energy, i.e. the wavelength of the emitted (decay to the lower level) or the absorbed (jump to the higher level) light. Normally, light emission is the result of a spontaneous decay from excited to low-lying energy states, and it ends when system ground state is reached. During decay process, the system exceeding energy is emitted as light in the so-called "spontaneous emission" (Figure 2) [Paschotta R, 2008].

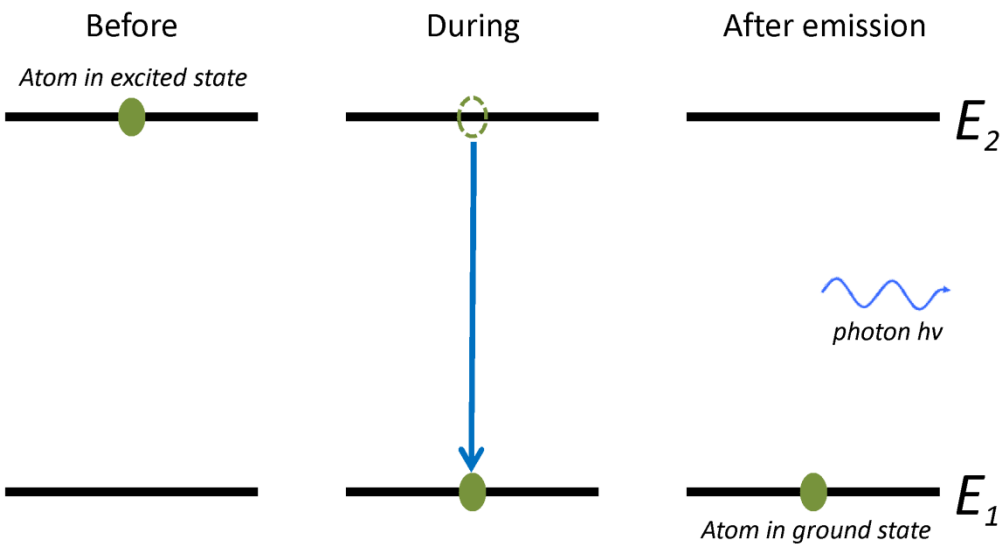

Figure 2. Spontaneous emission. An atom in the excited state E_2 can decay in the ground sate E_1 by spontaneous emission of a photon of energy $hv=E_2-E_1$.

Another mechanism, known as “stimulated emission”, can take place, even if this is not dominant over the spontaneous emission until ground state atomic population excides the excited state population. Stimulated emission occurs when an atom in the excited state is subjected to an external radiation source, having a wavelength resonating with that of the photon associated to an atomic transition. Hence, there is a finite probability for the external radiation field to induce a transition to the atomic ground state determining emission of a photon with an energy and a direction identical to that of the incident radiation photons, for energy and momentum conservation. This makes the radiation emitted by stimulated emission coherent and monochromatic, two key properties of laser light. The laser beam is also collimated, since the two emitted photons have the same direction. In essence, the original photon is amplified by this process; this is the reason why it is called stimulated emission (Figure 3) [Paschotta R, 2008].

Generally, a non-equilibrium condition is required for lasing action. By this way, energy may be selectively injected to pump an upper energy level from which transitions occur to a lower level. This phenomenon is known as pumping. Pumping may be realized in several ways, including electrical, thermal, optical, chemical, or nuclear. Lasers often utilize electrical or optical pumping. In the latter case, when the target medium (active medium) is a solid material, light from a flash-lamp or an arc-lamp is focused onto a rod containing the lasing atoms. Commonly used solid state laser active media include ruby (chromium ions in an aluminium oxide host glass) and YAG (neodymium ions in an yttrium–aluminium–garnet host glass) [Huber G et al, 2010]. The lasing atoms absorb photons of incident pump light and become excited to upper energy levels.

Regardless of the method, the ultimate goal of pumping is to excite high-energy states within the lasing medium so that the population of atoms at a high-energy state is greater than the population of atoms at a low-energy state for the lasing transition. This population inversion is a pre-requisite to ensure laser action: if it is not maintained, atoms will absorb rather than emit photons and the light intensity will decrease rather than being amplified while crossing a medium.

A laser source is an optical cavity, constituted by an active medium between two mirrors, pumped by an external energy source. When energy is pumped into the gain medium it causes population inversion and the release of a great number of photons via stimulated emission.

This population inversion can be achieved in the three- or four-level systems (Figures 4 A and B). In a three-level system (Figure 4 A), energy injected into the gain medium excites atoms to a pump level above the upper lasing level. From there atoms very quickly decay to the upper lasing level, with no radiation emission (non-radiative transition). The lifetime in this upper level is long enough to ensure the population inversion. By this way, the lasing transition can occur between the upper level and the ground state, which plays the role of lower level in the lasing transition, with consequent laser light emission in the process.

An improvement of this scheme is obtained with a four-level structure, where the laser transition takes place between the third and second excited states on the energy axes (Figure 4 B).

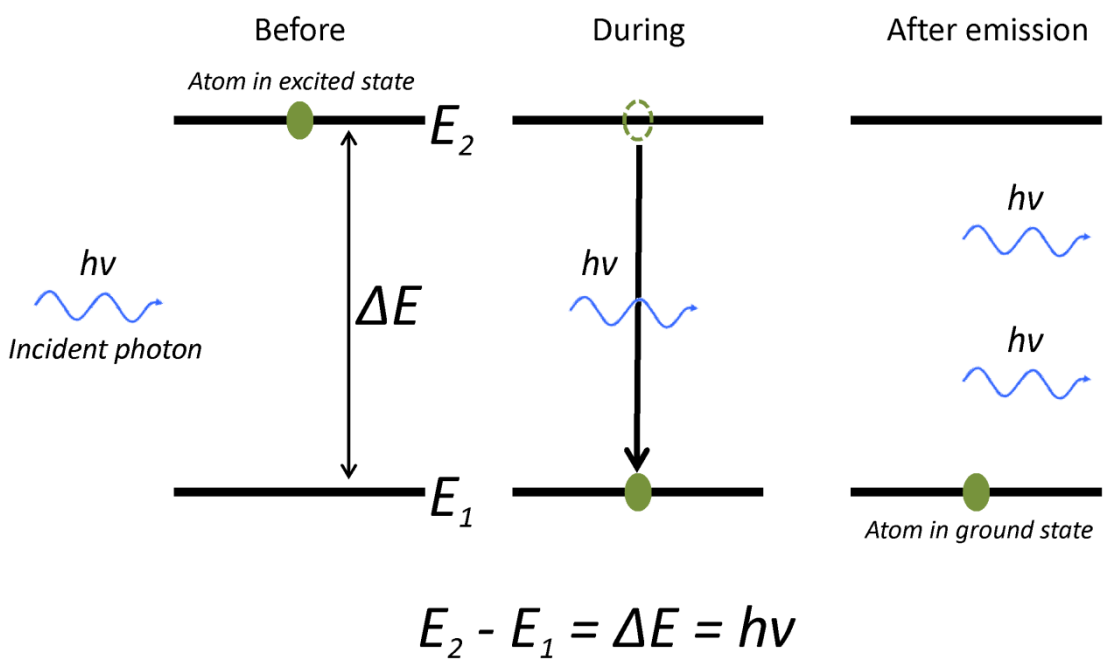

Figure 3. Stimulated emission. A photon of energy hv=E_2-E_1 finds an atom in the excited state E_2; the atom can decay to the ground state E_1 releasing a photon with an energy and a direction identical to that of the incident photon in, for energy and momentum conservation.

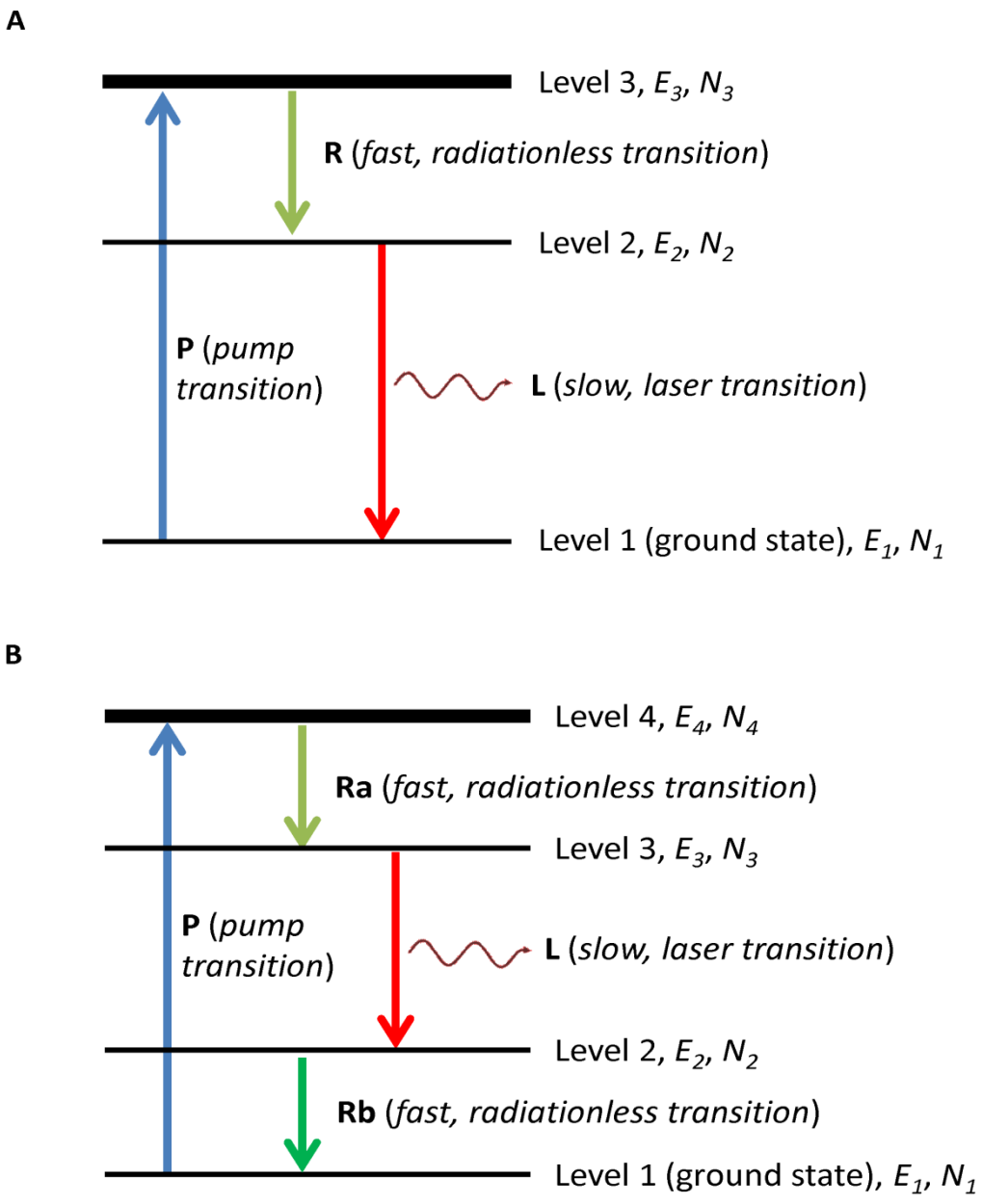

Figure 4. Three-level laser energy diagram (A) and four-level laser energy diagram (B). Atoms can be excited to a level above the upper lasing level (blue arrows). From there atoms quickly decay to the upper lasing level, with no radiation emission (pale green arrows). The lasing transition can occur between the second and first levels of Figure A and between the third and second levels of Figure B (red arrows).

1.6 UV laser cross-linking

Cross-linking by UV laser has been presented in the literature as a revolutionary technique to increase the otherwise low process yield of conventional methods based on chemical catalysts [Solomon MJ et al, 1988], conventional UV sources [Zhang L et al, 2004], or longer UV pulses [Russmann C et al, 1997; Russmann C et al, 1998].

In fact, it has been demonstrated that this technique reaches cross-linking yields twice (or even more) those obtained with ordinary alternative methods. [Angelov D et al, 2003; Moss T et al, 1997].

UV laser cross-linking is a potentially powerful tool to investigate DNA-protein and protein-protein interactions, especially transient interactions and binding kinetics, since the number of photons required for covalent complex formation can be delivered very rapidly, in nano-, pico- or even femtosecond intervals.

Moreover, UV laser technology offers the possibility to study molecular interactions *in vivo* and to take “snapshots” at various steps during the assembly of a protein complexes. It is known that cross-linking induced in cells by ultrashort laser pulses can occur only between species that are in close proximity of the absorbed photons (“zero length” covalent bonds), what unfavours unspecific bonds. Furthermore, it can only occur until the radiation is incident on the sample, thus allowing time-resolved studies of transient interactions [Altucci C et al, 2012]. Moreover, when combined with biochemical techniques, such as immunoprecipitation (IP), the UV laser method will make feasible the characterization and the identification of protein interactions occurring in a natural context, i.e. *in vivo*.

Actually, the critical parameter in UV laser cross-linking is not the total amount of energy but a combination of intensity and pulse length.

In 1998, a combination of two wavelengths, UV and blue, and the use of specific time intervals between pulses allowed to greatly increase the cross-linking yield and concomitantly to reduce the molecular damaging [Russmann C et al, 1997].

Moreover, Christoph Russmann and co-workers demonstrated that, using a femtosecond UV laser source, cross-linking efficiency is increased by more than a factor of six compared with cross-linking efficiency obtained with picosecond and nanosecond pulses, reaching a cross-linking yield of about 30%.

In conclusion, unlike conventional light sources, lasers represent stable, high-energy sources of UV radiation. Their use ensure high reproducibility of cross-linking yield. Furthermore, lasers use allows very short irradiation times of biological samples. The rapidity by which UV laser-induced cross-linking occurs should also significantly reduce artefacts and allow kinetic studies in intact cells.

AIMS OF THE THESIS

Laser UV-induced cross-linking might in principle be applied to any system in which the understanding of protein-protein interactions represents the molecular basis to learn about physiological or pathological processes. This method could strongly impact the general understanding of protein complexes in living cells and could provide new avenues for therapeutic intervention.

The overall aim of this research project is the development of an innovative UV laser induced protein-protein cross-linking strategy able to reveal protein-protein interactions (PPIs) without perturbing their physiological environment, where native interactions occur with intended partners inside the cells.

The objectives of the project are:

1. Development of the UV laser cross-linking procedure;
2. Setting up of FLIM-FRET system as a suitable independent method to validate this innovative methodology.

The main goals concerning the 1st objective are the following:

a) Inspection on the potentiality of femtosecond UV laser pulses as inductor of protein-protein cross-linking in living cells;
b) Study on the correlation between irradiation parameters and cross-linking efficiency, in order to maximize the cross-linking yield;
c) Isolation and identification of cross-linking products.

Since a novel method need to be validated, the 2nd objective is aimed at setting up a FLIM-FRET methodology to independently assess the PPIs detected in living cells by the UV laser approach. The prefixed aims concerning this objective are:

a) Setting up of experimental protocols to measure fluorescence lifetime in living cells by fluorescence lifetime imaging microscopy (FLIM);
b) Evaluation of fluorescence protein Förster resonance energy transfer (FRET) occurrence as a measure of protein-protein interactions.

CHAPTER 2

SETTING UP OF A NOVEL PROCEDURE FOR PROTEIN-PROTEIN IN VIVO CROSS-LINKING BY UV LASER IRRADIATION

2.1 UV laser irradiation: state of art

This PhD project is aimed at providing a novel strategy based on the use of a femtosecond-UV laser to cross-link interacting proteins in a physiologic environment.

Cross-linking with pulsed UV lasers has been heralded as a revolutionary technique to increase the photochemical yield of protein-nucleic acid cross-linking by one to two orders of magnitude and to significantly reduce the timescale of the reaction [Lejnine S et al, 1999; Angelov D et al, 2003; Altucci C et al, 2012].

Based on previous knowledge on DNA-protein cross-linking, the first assumption for a potential UV laser directed protein-protein cross-linking was that proteins absorb UV radiations producing reactive radicals that are able to react and eventually introduce covalent bonds between peptides [Sun G et al, 2006].

As a first approach, in order to demonstrate the radical nature of the reaction mechanism, a pulsed UV laser irradiation was performed in the presence of spin trap molecules [Nakagawa K, 1992; Nakagawa K, 1993]. These molecules can react with radical sites in proteins, both *in situ* and in real time. During this reaction, a spin trap molecule forms a covalent bond at the radical site, with the consequent formation of a protein-spin trap radical adduct. The protein radical adduct is more stable than a protein radical and, consequently, his lifetime is higher (i.e. seconds to minutes) and can be detected by electron spin resonance (ESR) spectroscopy [Leinisch F et al, 2011].

Though spin trapping was initially developed to examine reactive radicals formed from low molecular mass compounds [Davies MJ et al, 1987], developments over the last three decades have shown that this methodology can also be used to study radical formation on proteins and other macromolecules, in both isolated and complex biological systems. The spin trap molecules form a covalent bond with the protein resulting in a new nitroxide radical, which may be stable under electrospray ionization mass spectrometry conditions. By using this procedure in combination with peptide mapping by mass spectrometry, it is possible to investigate the formation and structure of radical adducts generated on proteins. To identify the precise amino acid residues (i.e. radical site) trapped by the spin trap, mass spectrometry-based sequencing can be used.

Recently, Leo and co-workers demonstrated that cross-links can be induced by exposure of peptides in solution to UV laser [Leo G et al, 2013]. The Authors observed that, once irradiated, peptides, such as angiotensin, interleukin 1-β and xenopsin, are able to form covalent adducts with spin trap molecules, demonstrating the radical nature of the reaction mechanism. Interestingly, mass spectrometric analyses demonstrated that “zero-length” covalent bonds were formed with good

efficiency, and on an extremely rapid time scale only if aromatic amino acids are present in the peptide sequence. Among these, tryptophan was found to be the most reactive site [Leo G et al, 2013].

Based on these results, this PhD project is aimed at transferring this basic know how to a complex system, such as living cells, to cross-link interacting proteins within their physiologic environment. Cells from human epithelial adenocarcinoma (HeLa cell line) were selected as the cell system for our experiments and the enzyme glyceraldehyde-3-phosphate dehydrogenase (GAPDH) as the model protein.

2.2 The laser station

The experiments were carried out taking advantage of a femtosecond pulsed laser source (PHAROS source, Light Conversion Ltd) available at the Dept. of Physics of University of Naples. This ultrashort laser source, based on a single-unit integrated system, has unique characteristics in terms of tuneability of the output radiation wavelength and pulse repetition rate, which makes this source ideal to freeze transient, but relevant, interactions between biomolecules while occurring.

The system is equipped with a sophisticated pulse picker which allows to separately select any possible repetition rate within single-shot to 200 kHz together with any possible total amount of pulses for irradiation. This unique feature is very useful when studying laser pulses-biomolecules interactions, since the role of the overall radiation dose and of the single pulse peak intensity can be separately studied and enlightened. This, for example, allows to understand whether the response of the sample to the irradiation is linear or nonlinear to some extent.

The fourth harmonic of the fundamental pulse (257 nm), having a pulse energy up to 170 μJ, is sent to the liquid sample, which is contained in a cuvette. A magnetic stirrer ensures for homogeneity of the irradiation conditions. The fourth harmonic pulse has been chosen so far, as it is a suitable radiation to excite the aromatic amino acids, which exhibit strong absorption bands around 250-300 nm. Thus, this radiation is very appropriate to trigger transient interactions between biomolecules. The interaction geometry can be also easily modified by either the insertion of a focusing lens mounted on a flipping stage or the insertion of a telescope, which can make the collimated beam larger or tighter, depending on the specific need of the experiment.

A schematic diagram of the apparatus used for irradiations is shown in Figure 5.

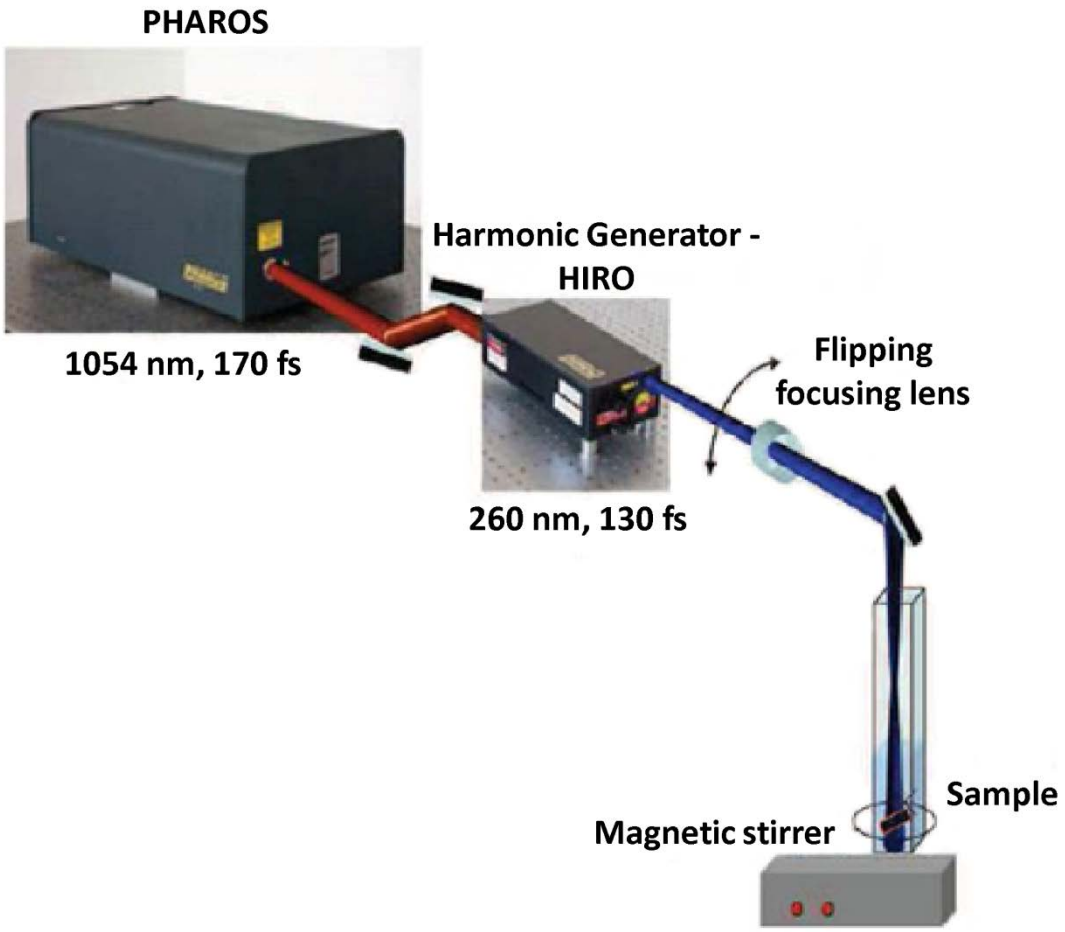

Figure 5. Geometry of the Laser apparatus device, coupled with a focusing lens, mounted on a flipping mount, that can be replaced by a telescope to modify the beam size, and with a cell irradiating support.

2.3 The model protein: human GAPDH

Glyceraldehyde-3-phosphate dehydrogenase (GAPDH) is considered a housekeeping protein involved in basic cell catabolic processes. It constitutes between 10-20% of total cellular proteins and plays an important role in glycolysis and gluconeogenesis by reversibly catalyzing the oxidation and phosphorylation of D-glyceraldehyde-3-phosphate to 1,3-bisphospho-glycerate with concomitant reduction of NAD^+ to NADH. The enzyme exists as a homo-tetramer made up of four identical 37 kDa subunits. The three-dimensional structure of human GAPDH has been solved at high resolution (Figure 6) [Jenkins JL &Tanner JJ, 2006]. Each subunit contains two major domains, the NAD^+ binding domain (residues 1→150) and the catalytic or glyceraldehyde-3-phosphate domain (residues 151→335) which includes the active site cysteine [Sirover MA, 2014].

Recent experimental evidences suggest that beyond its glycolytic functions, GAPDH is in reality a multifunctional protein and is now considered to be a classic example of a moonlighting protein. GAPDH seems to be involved in membrane, cytoplasmic and nuclear functions in endocytosis, mRNA regulation, tRNA export, DNA replication, and DNA repair. GAPDH has been reported to bind to DNA and RNA [Sirover MA, 1999; Baxi MD & Vishwanatha JK, 1995], regulate transcription [Zheng L et al, 2003], possess kinase/phosphotransferase activity [Engel M et al, 1998; Ashmarina LI et al, 1988], catalyze microtubule formation and polymerization [Volker KW & Knull H, 1997], facilitate vesicular transport [Bryksin AV & Laktionov PP, 2008], and to bind to integral membrane ion pumps associated with Ca^{2+} release [Patterson RL et al, 2005], as well as to interact with a number of small molecules, including tumor necrosis factor (TNF)-α ribozymes [Sioud M & Jespersen L, 1996], glutathione (GSH) [Lind C et al, 1998], p53 [Chuang DM et al, 2005], and nitric oxide (NO) [Hara MR et al, 2006].

These functions, summarized in Figure 7, have been linked to different intracellular localizations of the enzyme, which has been found in the cytosol, the nucleus, ER-Golgi-vesiculae, mitochondria, as well as associated to the plasma membrane.

Recent studies also indicate GAPDH as an essential part of the program of gene expression observed in apoptosis and as part of the cellular phenotype of age-related neuronal disorders. In the former, GAPDH might be translocated into the nucleus without the induction of nuclear GAPDH glycolytic activity. Moreover, in stress conditions, such as serum starvation and exposure to DNA-damaging agents, a pool of GAPDH molecules is translocated to the mitochondria and induces pro-apoptotic mitochondrial membrane permeabilization *via* association with voltage-dependent anion channel 1 [Tarze A et al, 2007]. In the latter, GAPDH might physically associate to the L-amyloid precursor protein in Alzheimer's disease [Berry MD, 2004].

Moreover, GAPDH is subjected to numerous post-translational modifications - acetylation, phosphorylation and nitrosylation - that, as indicated in Table I, provide the basis for GAPDH diverse functional activities [Sirover MA, 2014].

These features make GAPDH an ideal candidate to be used as a model protein for a study aimed at setting up, learning about and optimizing the *in vivo* laser-induced protein-protein cross-linking.

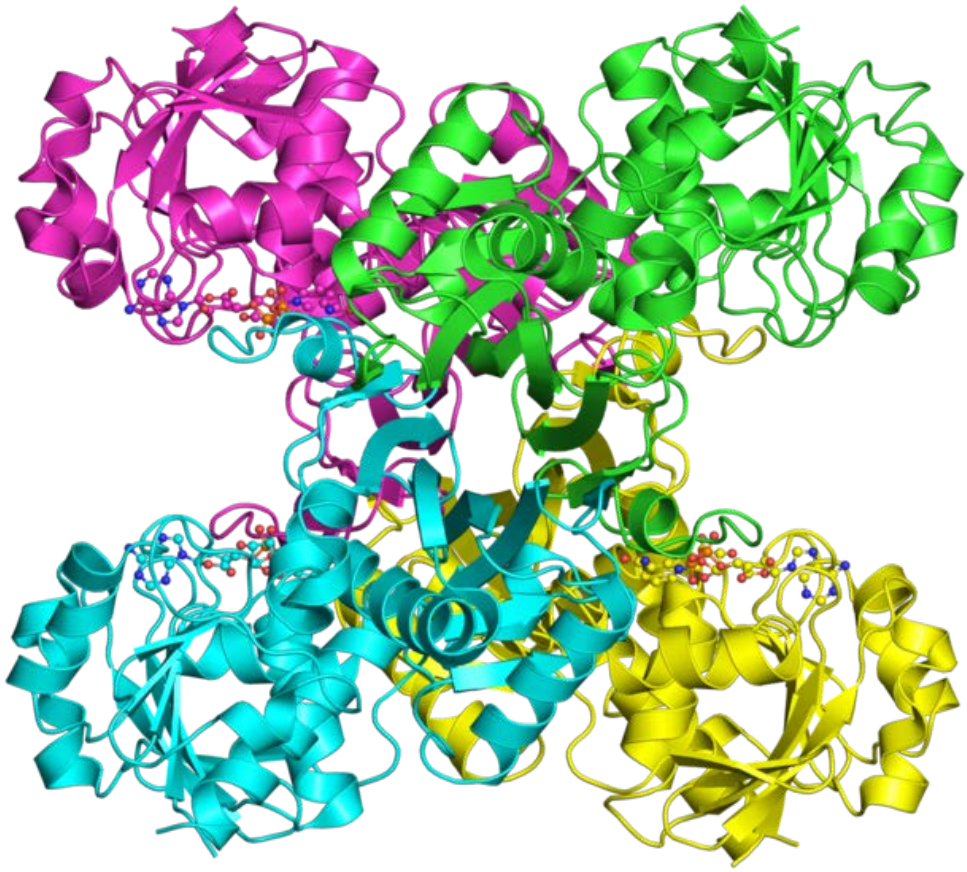

Figure 6. 3D structure of tetrameric GAPDH. The four identical subunits are reported with different colours. In each active site is shown the cofactor NAD^+.

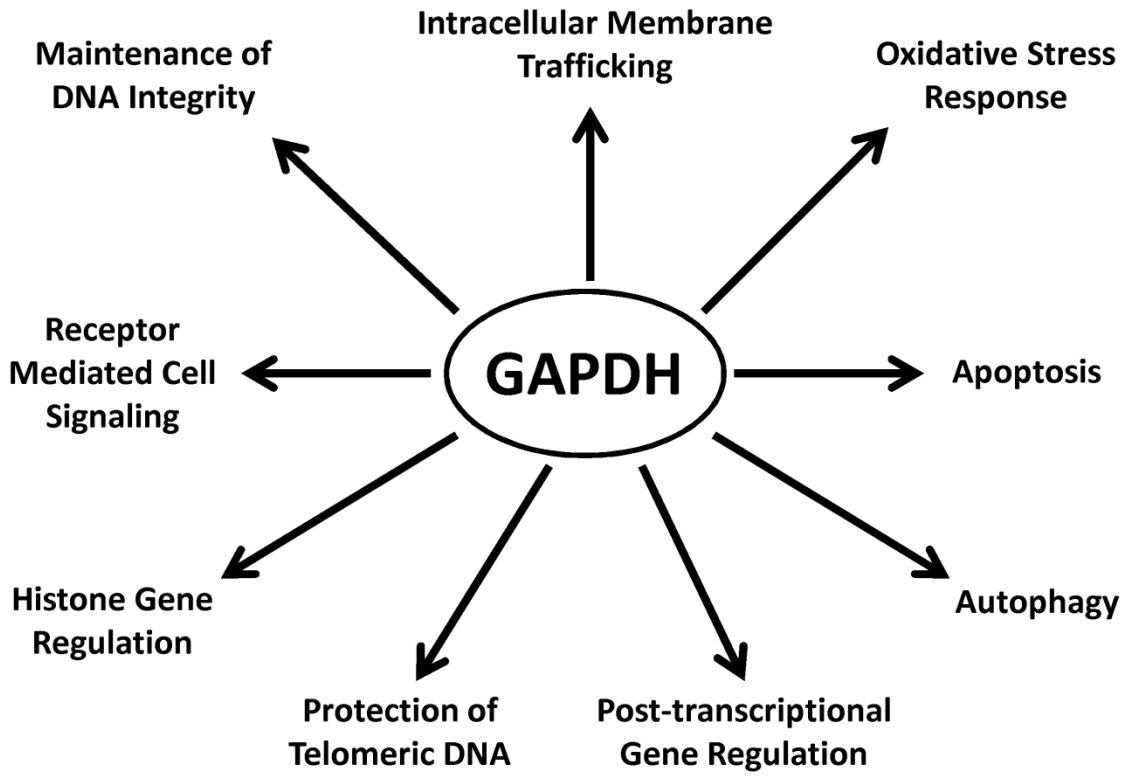

Figure 7. Functional pathways in which GAPDH is involved.

Amino acid	Position	Post-translational modification	Functional property
Lysine	117	Acetylation	Nuclear localization
Lysine	227	Acetylation	Nuclear localization
Lysine	251	Acetylation	Nuclear localization
Threonine	227	O-linked N-acetyl glucosamine	Nuclear localization
Threonine	237	Phosphorylation	Nuclear localization
Cysteine	149	Nitrosylation	Heme metabolism
Cysteine	149	Nitrosylation	Apoptosis
Cysteine	149	Oxidation	Nuclear Localization
Lysine	160	Acetylation	Apoptosis
Tyrosine	41	Phosphorylation	Membrane trafficking
Serine	N.D.	Phosphorylation	Membrane trafficking

Table I. Post-translational modifications of GAPDH residues associated to the enzyme activities.

2.4 Irradiation of HeLa living cells: preliminary experiments

The first step of the project consisted in the inspection of the potential of femtosecond UV laser pulses in inducing protein-protein cross-linking. To this purpose, living HeLa cells (resuspended in PBS at a concentration of $4x10^4$ cells/mL) were exposed to UV laser using different combinations of laser pulses energy (E_{pulse}), pulse repetition rate (f_{rate}) and total irradiation time (T_{irr}), as indicated in Table II.

Since a previous study on *in vitro* cross-linking of peptides [Leo G et al, 2013] revealed that cross-linking is effective when the total irradiation energy (**D**), calculated as

$$D = E_{pulse} \times T_{irr} \times f_{rate}$$

is in the range between 1.2 J and 13.0 J, we tested several experimental conditions within this range.

In Table II the experimental conditions tested, numbered from 1 to 16, are reported.

After UV laser exposition, irradiated and not irradiated (control sample) HeLa cells were lysed in PBS containing 1% NP40 and protease inhibitors (see Material and Methods section). Following the determination of the total protein content by the Bradford assay, cell lysates, corresponding to $2x10^5$ cells, were analysed by 10% polyacrylamide denaturing gel electrophoresis (SDS-PAGE), followed by Coomassie blue staining (Figures 8 A and B) and by Western blotting (Figures 8 C and D) using anti-GAPDH specific antibodies.

Western blot analyses revealed that, besides the presence of the monomeric form of GAPDH (37 kDa), additional immunopositive protein bands were present in most of the irradiated samples (Figures 8 C, lanes 3-5 and 9, and 7 D, lanes 4-7). Among these, a protein species with a molecular mass of about 90 kDa was the most evident. This species was not detected in control cells (lane 2). This suggested that UV laser irradiation induced cross-linking between GAPDH and its protein partners and/or between GAPDH subunits. In either case, this represents a very promising starting point for further studies aimed at investigating the potential of this methodology in different environments.

Further, Coomassie blue staining revealed no significant differences between the protein pattern of the control (Figures 8 A and B, lane 2) and that of irradiated samples (lanes 3-10), indicating that irradiation does not significantly alter cell protein profile. However, it is evident that, at very high energy values, aggregation and/or precipitation of almost all cellular proteins is caused, as shown in lane 7 of Figure 8 A and lane 3 of Figure 8 B.

From the comparison between Coomassie blue staining and Western blots, we selected condition 11 of Table II as the one which allows the major recovery of cross-linking products combined with low protein precipitation (Figures 8 B and D, lane 5).

On the basis of these preliminary results, we concluded that the exposure of intact living cells to UV laser induces the formation of covalent adducts inside the cells and that the phenomenon can be modulated, since the responses are function of the time of the exposure, the intensity of the laser beam and the repetition rate of the pulses.

Condition #	Total energy (J)	Repetition rate (kHz)	Pulse energy (µJ)	Irradiation time (s)
1	2.88	0.2	120	120
2	2.88	2.0	120	12
3	1.2	2.0	50	12
4	1.2	0.2	50	120
5	12.0	2.0	50	120
6	12.0	2.0	50	40
7	5.76	2.0	120	24
8	8.64	2.0	120	36
9	12.0	2.0	100	60
10	2.4	2.0	50	24
11	3.6	2.0	50	36
12	4.8	2.0	50	48
13	6.0	2.0	50	60
14	7.2	2.0	50	72
15	8.4	2.0	50	84
16	9.6	2.0	50	96

Table II: The first set of irradiation conditions tested.

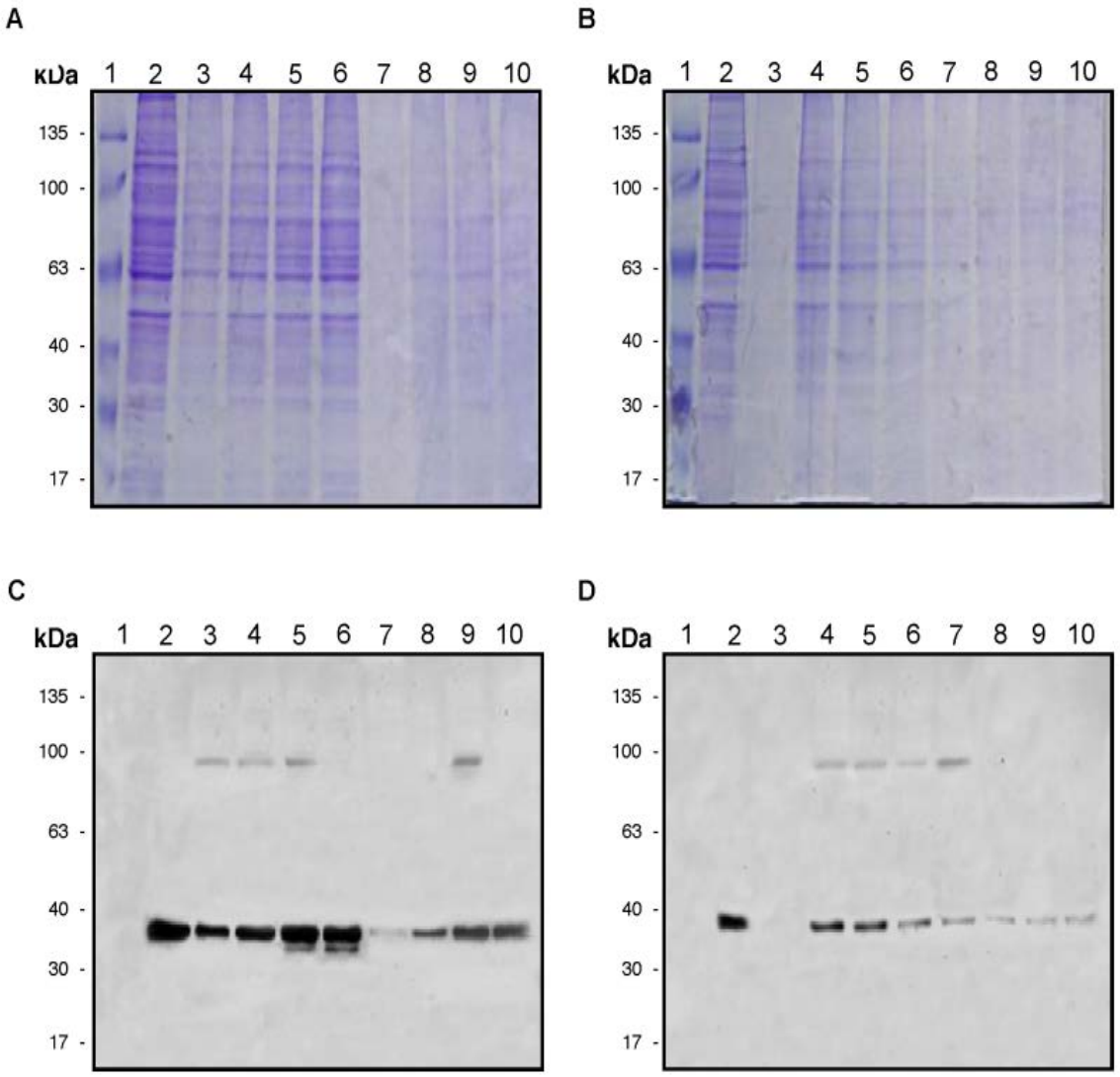

Figure 8. SDS-PAGE analyses of proteins extracted from control and irradiated cells following the experimental conditions described in Table II.

A and B, Coomassie blue staining; C and D, Western blots
A and C, lane1, molecular weight markers
lane 2, not irradiated sample
lanes 3-10, samples irradiated in conditions 1-8
B and D, lane1, molecular weight markers
lane 2, not irradiated sample
lanes 3-10, samples irradiated in conditions 9-16

The analyses described above demonstrated that condition #11, with a f_{rate} of 2 kHz, E_{pulse} of 50 µJ and T_{irr} of 36 seconds, is the best irradiation condition among those tested (Table II).

In order to optimize the cross-linking efficiency, a second set of irradiation conditions was tested (see Table III). By modulating the irradiation time, a range of energy values, spanning from higher to lower values with respect to condition #11, was inspected.

Following the experimental procedure described above, SDS-PAGE analysis of protein extracts followed by Coomassie blue staining and Western blotting were performed (Figures 9 A and B). The Western blot confirmed the presence of immunopositive protein bands corresponding to species with a molecular weight higher than that of monomeric GAPDH, with the protein species of ~90 kDa molecular mass as the most abundant. A comparative analysis of the data let us to establish that the best condition for living cells irradiation was #19, corresponding to 2 kHz of repetition rate, 50 µJ of pulses energy and 40 seconds of irradiation time (Figures 9 A and B, lane 6).

.

Condition #	Total energy (J)	Repetition rate (kHz)	Pulse energy (µJ)	Irradiation time (s)
11	**3.6**	**2.0**	**50**	**36**
17	2.8	2.0	50	28
18	3.2	2.0	50	32
19	4.0	2.0	50	40
20	4.4	2.0	50	44

Table III: The second set of irradiation conditions tested: effects of the increase of total energy on cross-linking efficiency. In red, condition #11 (Table II) as a reference.

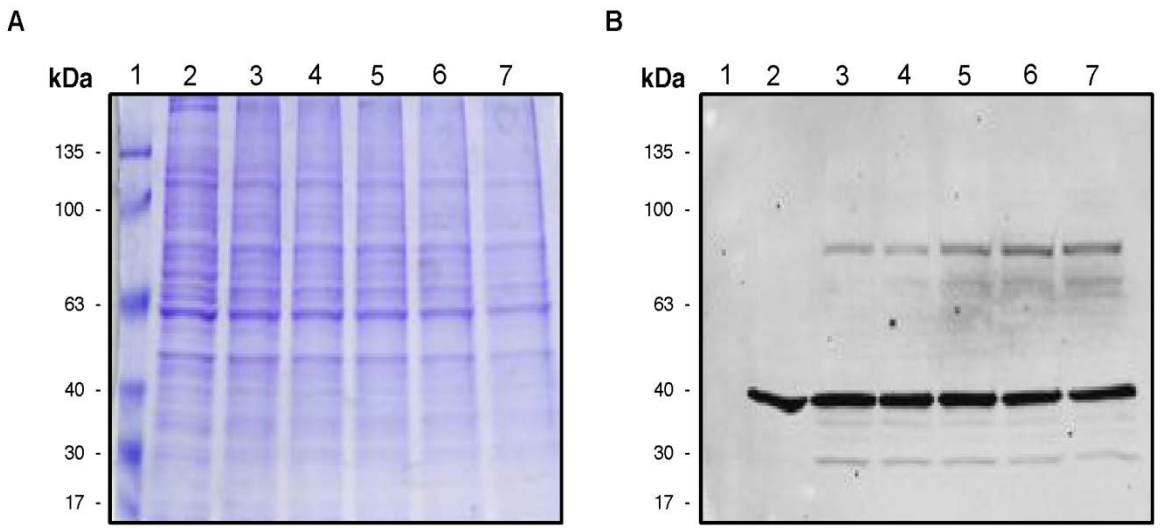

Figure 9. SDS–PAGE analysis of proteins extracted from cells before and after exposure to UV laser following the experimental conditions described in Table III. Coomassie blue staining (A) and Western blot (B)

Lane1, molecular weight markers
Lane 2, not irradiated sample
Lanes 3, 4, 6 and 7, samples irradiated in condition #17, 18, 19 and 20, respectively
Lane 5, sample irradiated in condition #11

2.5 - Irradiation parameters and their influence on protein-protein cross-linking *in vivo*: tuning the procedure

In order to optimize the efficiency of UV laser induced protein–protein cross-linking, we analysed the influence of three physical parameters, i.e. f_{rate}, E_{pulse} and T_{irr}, on the cross-linking yield. It is worth noticing that, in place of the pulse energy, we should better consider the laser intensity, **I** [Boyd RW, 2008], proportional to E_{pulse} and defined as

$$I \approx \frac{E_{pulse}}{S \times \tau_{pulse}}$$

where **S** is the laser beam section onto the target and τ_{pulse} the laser pulse duration. Typically, **I** is expressed in W/cm^2 and corresponds to the peak intensity of a single ultra-short laser pulse. In our case, S and τ_{pulse} were fixed to ~0.3 cm^2 and ~250 femtosec, respectively, [Valadan M et al, 2015] in all the experimental conditions tested. Thus, in the following, we shall refer to E_{pulse}, rather than **I**, being varied between 30 and 70 µJ, that implies 4.0×10^8 W/cm^2 $\leq I \leq$ 9.3×10^8 W/cm^2.

Therefore, three different sets of experiments (indicated in Table IV as A, B and C) were carried out at constant total irradiation energy, set at 4.0 J. Through the experiments, each of the three parameters, i.e. repetition rate, pulse energy and irradiation time, was kept constant, while the other two were varied. In particular, in the case of set A (conditions A_1 to A_5), the repetition rate was kept constant (2 kHz) and both the irradiation time and energy pulses were modulated; in set B (conditions B_1 to B_5), the irradiation time was kept constant (40 s) and both energy pulses and repetition rate were modulated; in set C (conditions C_1 to C_5), energy pulses was kept constant (50 µJ) and both repetition rate and irradiation time were modulated.

Using this scheme, E_{pulse} was scanned between 30 and 70 µJ, T_{irr} was varied between 30 and 70 s, and f_{rate} was tested between 1 and 6 kHz, as shown in Table IV.

For each set of experiments, the cross-linking yield was determined as follows. Upon UV laser irradiation of HeLa living cells, total proteins were extracted and analysed by Western blotting using anti-GAPDH specific antibodies (Figure 10). The relative intensities of the two main protein bands recognized by the antibody, corresponding to monomeric GAPDH (37 kDa) and to cross-linked species (~90 kDa band), were determined by densitometric analyses, normalized to the total protein amount of each sample and expressed as percentage of total GAPDH amount (monomers + complexes = 100 %). The results are reported in the contour plot frame of Figure 10, where pulse energy and irradiation time are reported on x- and y-axes, respectively, whereas the color code refers to laser repetition rate reported in the third dimension.

Interestingly, we found that in all the tested conditions the relative amounts of GAPDH monomer and cross-linked products remain substantially unvaried, being the percentage of GAPDH cross-linked species (~90 kDa) nearly stable at ~10 % (inset in Figure 11), independently on E_{pulse}, T_{irr} and f_{rate}.

According to these results, we can assume that the phenomenon can be easily modulated and that the cross-linking yield is a linear function of the total irradiation energy, since the yield of the process depends upon E_{pulse}, T_{irr} and f_{rate} only through the total irradiation energy.

Condition #	Total energy (J)	Repetition rate (kHz)	Pulse energy (μJ)	Irradiation time (s)
A_1	4.0	2.0	50	40
A_2	4.0	2.0	40	50
A_3	4.0	2.0	60	34
A_4	4.0	2.0	70	29
A_5	4.0	2.0	30	67
B_1	4.0	2.5	40	40
B_2	4.0	2.0	50	40
B_3	4.0	1.7	60	40
B_4	4.0	1.5	70	38.7
B_5	4.0	3.4	30	40
C_1	4.0	1.0	50	80
C_2	4.0	3.0	50	26.6
C_3	4.0	4.0	50	20
C_4	4.0	5.0	50	16
C_5	4.0	6.0	50	13.3
D_1	2.4	2.0	50	24
D_2	2.6	2.0	50	26
D_3	2.8	2.0	50	28
D_4	3.0	2.0	50	30
D_5	3.2	2.0	50	32
D_6	3.4	2.0	50	34
D_7	3.6	2.0	50	36
D_8	3.8	2.0	50	38
D_9	4.2	2.0	50	42
D_{10}	4.4	2.0	50	44

Table IV. Panel of experimental conditions tested. In each group of tests (from A to C), at a constant total energy (4.0 J), one the three parameters, repetition rate, pulse energy and irradiation time, was kept constant, while the other two were varied. In group D, the energy dose was tested by varying total irradiation time.

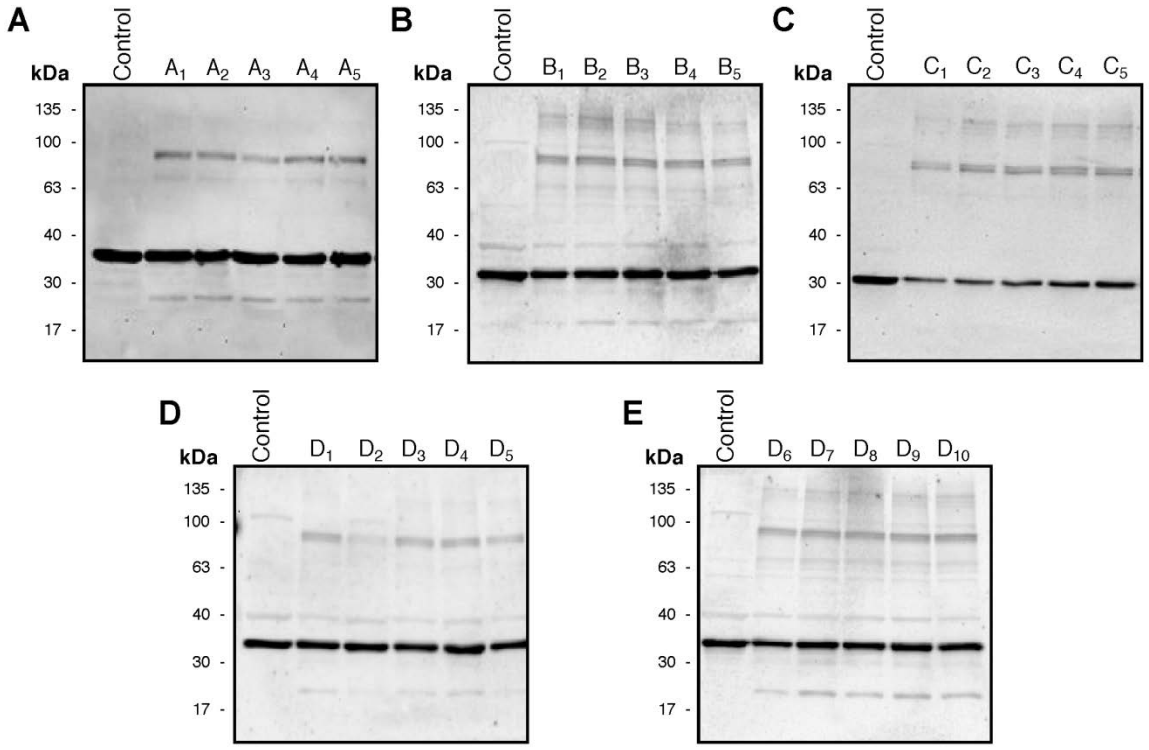

Figure 10. Western blot analyses of total proteins extracted from samples irradiated in the conditions listed in Table IV using anti-GAPDH antibodies.

Control: protein extract from not irradiated cells.
Lanes from A_1 to D_{10}: extracts from cells irradiated in conditions from A_1 to D_{10} (see Table IV), respectively.

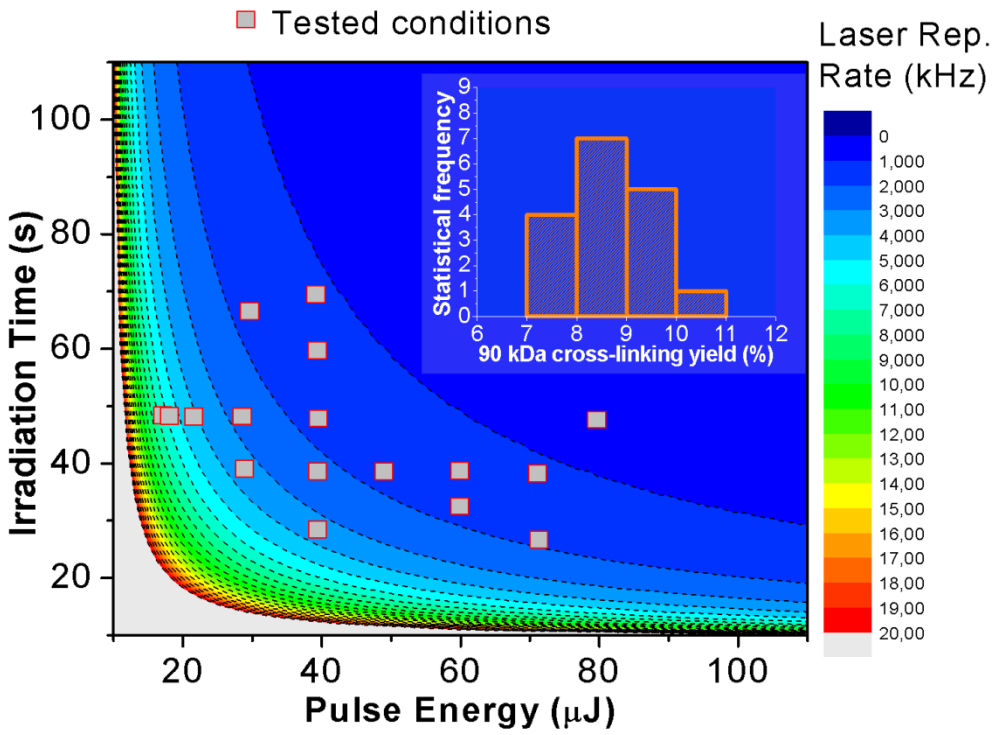

Figure 11. 3D representation of the laser parameter space as a contour plot, being the pulse energy and the irradiation time reported on the x- and y-axis, respectively, and the color code representing in the third dimension the laser repetition rate. In the plot, the experimental conditions tested (rectangles) refer to the selected constant energy dose of 4.0 J. The ~90 kDa cross-linked species yield (%) at a constant energy dose of 4.0 J is reported in the inset.

We then analysed the effects of the energy dose in order to maximize cross-linking efficiency. We set f_{rate} and E_{pulse} at 2 kHz and 50 µJ, respectively, while the T_{irr} was varied from 24 to 44 s to reach a dose comprised in the 2.4 – 4.4 J range, as shown in Table IV (conditions from D_1 to D_{10}).

The experiments were performed as previously described. From the results of Western blots reported in Figure 10, the densitometric percentage of monomeric GAPDH and of cross-linked species was calculated and reported in Figure 12, as a function of total irradiation energy. Obtained results showed a double linear correlation between the total irradiation dose and the depletion of the 37 kDa monomeric GAPDH species (from 98 to 92 %), with the consequent formation of ~90 kDa molecular weight complexes (from 3 to 8 %). The Pearson's R coefficients of the linear best-fit in Figure 11 were found to be 0.97 and 0.96, respectively, thus confirming the goodness of linearity in the investigated range of laser dose. It is noteworthy that, by delivering a total irradiation energy lower than 2.4 J, significantly less efficient cross-linking occurs, while at higher energy doses total protein amount appeared to be dramatically lower, although no significant changes in protein pattern were observed. This suggests that, at high energy doses, too extensive and uncontrolled cross-linking occurred in the overcrowded conditions of the intracellular environment generating insoluble protein aggregates, removed by centrifugation prior to electrophoresis.

These experiments demonstrated that protein–protein cross-linking efficiency can be modulated, since the phenomenon is a linear function of the total energy released to the target.

By this way, we were able to define as optimal irradiation conditions 42 s of irradiation time, 50 µJ of pulse energy, 2 kHz of repetition rate and 4.2 J of total irradiation energy, as these conditions maximize cross-linked GAPDH signals without perturbing cell proteome. Under these conditions, we observed high reproducibility of the cross-linked species yield (10% ± 1, n = 30 independent experiments). Moreover, the linear correlation observed also suggests that the process is triggered by the absorption of a single UV laser photon by side chains of aromatic amino acids. In this hypothesis, it is possible to define the value of the energy required to induce protein–protein cross-linking as approximately the energy associated to a single 257 nm photon (4.81 eV).

This makes the molecular mechanism of the process basically different from that occurring in the case of protein-DNA photo-induced cross-linking, where the reaction proceeds in two steps: 1. bi-photonic UV light absorption [Nikogosyan DN,1990] and excitation of the DNA bases, in the nano-, pico- or even femto-sec time scale; 2. cross-linking with proteins interacting with the DNA excited site and therefore lying nearby (zero-length cross-linking), which is completed in less than 1 millisec [Altucci C et al, 2012].

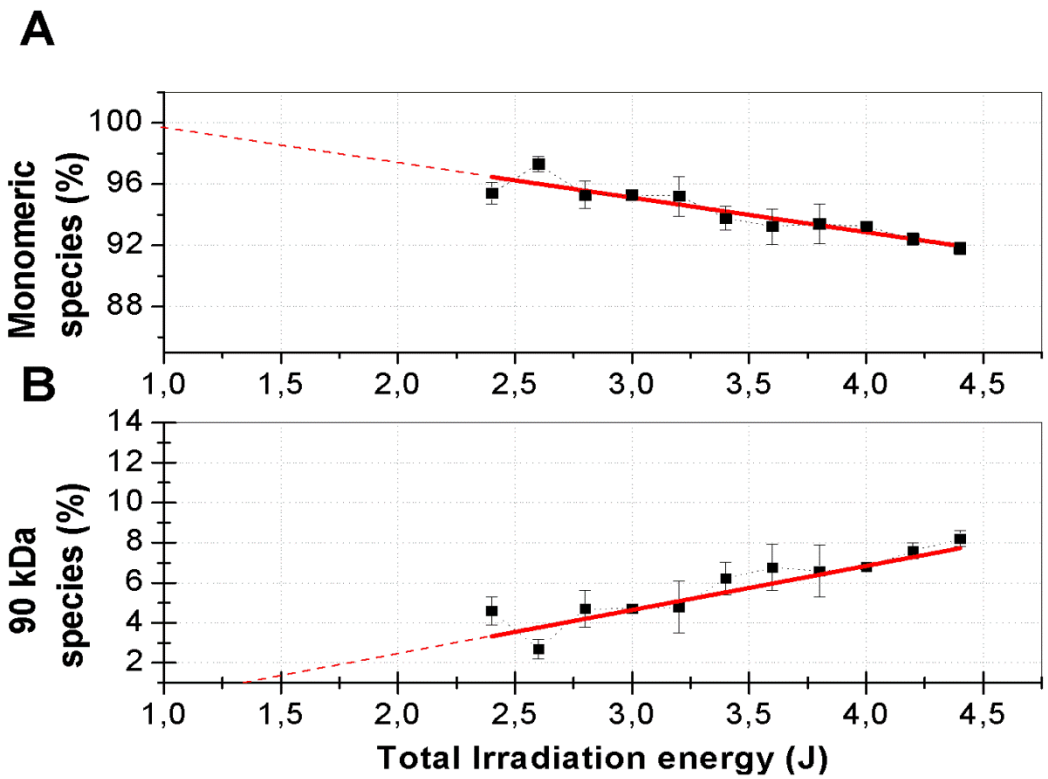

Figure 12. The percentage of monomeric GAPDH (A) and of the ~90 kDa species (B), with GAPDH monomers + GAPDH complexes equal to 100 %, is reported as a function of total irradiation energy. The latter was varied by increasing the irradiation time between 24 and 44 s, while keeping constant the pulse energy at 50 µJ and the repetition rate at 2 kHz.

CHAPTER 3

IDENTIFICATION OF UV LASER INDUCED GAPDH CROSS-LINKED SPECIES

3.1 Electrophoretic analysis and Western blotting

In order to identify GAPDH cross-linked species induced by UV laser irradiation, MALDI-MS analyses of total proteins extracted from irradiated cells were performed in collaboration with Prof. Leila Birolo (Dept. of Chemical Sciences, University of Naples Federico II). As it is known, protein identification by mass spectrometry (MS) can be performed using sequence-specific peptide fragmentation [Aebersold R & Goodlett DR, 2001].

The standard approach to identify proteins includes separation of proteins by denaturing gel electrophoresis, protein digestion *in situ* with sequence-specific endoproteases, analysis of the generated peptides by LC–MS/MS and protein identification by a suitable software [Aebersold R & Mann M, 2003].

To our purpose, $2x10^6$ HeLa cells were exposed to UV laser using the optimal irradiation parameters previously set up (see Chapter 2, para. 2.5). Proteins extracted from irradiated and control (not irradiated) samples were analysed by SDS-PAGE, followed by Western blotting or Coomassie blue staining (Figures 13 A and B). By superimposition of Western blot (Figure 13 B) to the Coomassie blue stained gel (Figure 13 A), the gel area corresponding to the immunopositive signal of ~90 kDa species was localized (Figure 13 A, lane 2), excised from gel and treated as described in the ‘‘Materials and methods’’ section. As control, the corresponding gel section of the not irradiated sample was excised (Figure 13 A, lane 1).

In agreement with the immunopositive signal revealed by the Western blot analysis, LC–MS/MS analysis indicated the presence of GAPDH in the ~90 kDa protein band, based on the identification of 8 peptides covering 35% of GAPDH sequence (data not shown). This suggests the formation of GAPDH-containing cross-linked species upon living cells irradiation.

Interestingly, beside GAPDH, MS analyses showed the presence of other proteins which are known to interact with GAPDH, such as phosphoglycerate kinase 1 (PGK), actin and L-lactate dehydrogenase [Walsh JL & Knull HR, 1988; Tomokuni Y et al, 2010; Tristana C et al, 2011; Clarke FM & Morton DJ, 1982]. All these proteins have a molecular mass much lower than 90 kDa. Hence, their presence should be due to the formation, upon exposure to UV laser, of covalent adducts between interacting proteins inside the cells. Future extensive analyses will be performed to assess the identity of these complexes and, consequently, the potential of our approach in elucidating protein interactions in their natural context.

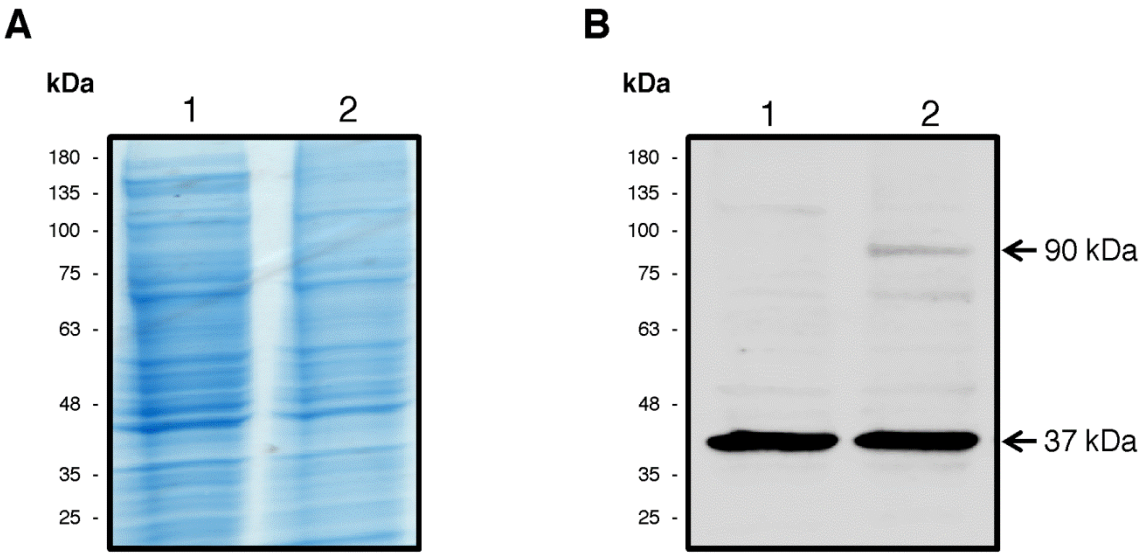

Figure 13. SDS–PAGE analysis followed by Coomassie blue staining (A) or Western blotting (B) of cell lysates from irradiated and control samples.

Lanes 1, extract from not irradiated cells
Lanes 2, extract from irradiated cells

3.2 Two-dimensional gel electrophoresis analysis

In order to identify GAPDH cross-linked species, further experiments were carried out. HeLa cells ($2x10^6$) were exposed to UV laser using the optimized irradiation parameters. The resulting total protein extract was fractionated by two-dimensional gel electrophoresis (2D gel) and analysed by MALDI-MS experiments, in collaboration with Prof. Leila Birolo (Dept. of Chemical Science, University of Naples Federico II). The same procedure was applied to control (not irradiated) cells.

The 2D gel is a two-step process able to separate proteins according to two independent properties: the first-dimension corresponds to an isoelectric focusing (IEF), which separates proteins according to their isoelectric points (pI); the second-dimension corresponds to SDS-PAGE, which separates proteins according to their molecular mass.

The resulting gels were either stained with colloidal Coomassie blue (Figures 14 A and B, for control and irradiated cells, respectively) or analysed by Western blotting with anti-GAPDH specific antibodies (Figures 14 C and D, for control and irradiated cells, respectively). As shown in Figure 14, a high molecular mass protein spot (spot 1), with the same pI as monomeric GAPDH (spot 2), was recognized by anti-GAPDH antibodies in the irradiated sample, migrating as a ~90 kDa species. This protein spot was found to be absent in control cells. By superimposition of 2D blot and 2D gel of the irradiated sample, we localized the protein spots of interest that were excised from gel and *in situ* digested with trypsin as described in the ‘‘Materials and Methods’’ section. As control, the corresponding spots were excised from the gel of the not irradiated sample.

The resulting peptide mixtures were analysed by nanoLC-MS/MS experiments and, in agreement with the results obtained by immuno-staining, the high molecular mass protein spot of irradiated sample was found to contain GAPDH.

Most interestingly, no other proteins were identified in the same spot, thus suggesting that the cross-linked species corresponds to a covalently linked GAPDH oligomer.

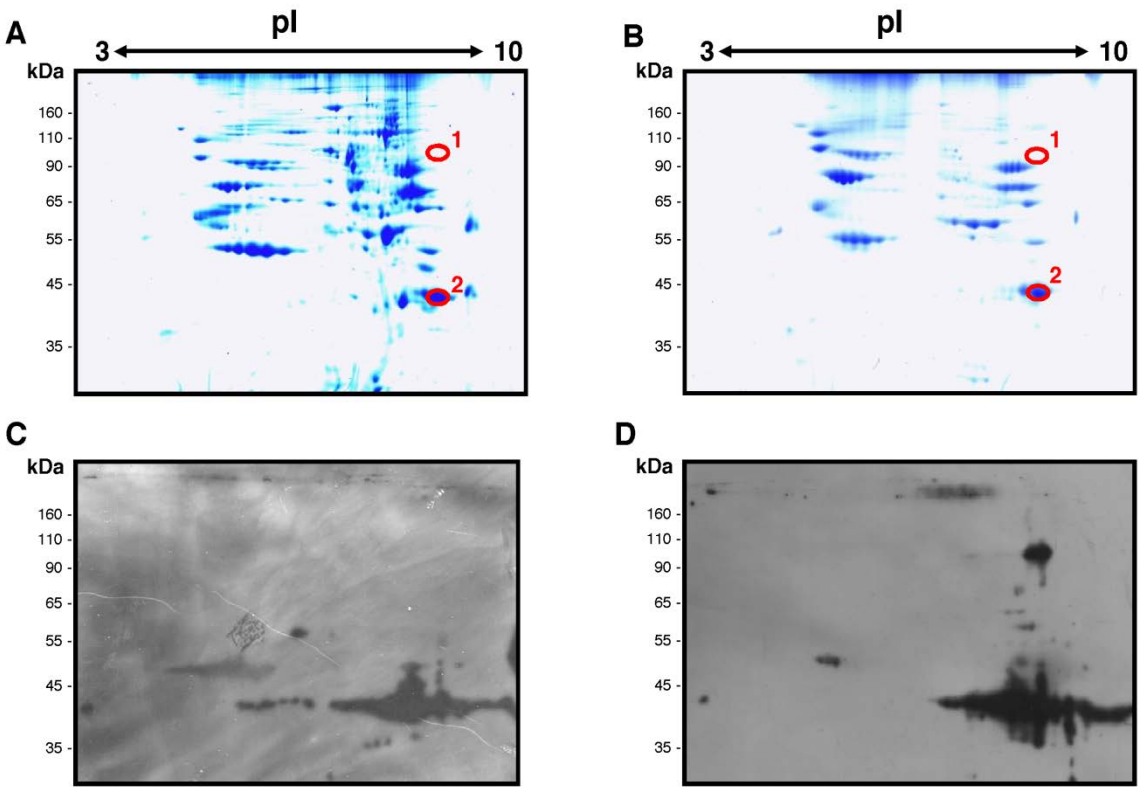

Figure 14. Two-dimensional electrophoresis of total proteins extracted from HeLa cells, untreated (A, C) or exposed to UV laser irradiation (B, D). Duplicate samples of each total protein extract were fractionated in parallel by two-dimensional gel electrophoresis, and analysed by colloidal Coomassie blue staining (A, B), or transferred onto a PVDF membrane (C, D) and immunoblotted with anti-GAPDH antibodies. Circles on Coomassie blue stained gels correspond to spots that were excised for subsequent analyses.

3.3 Immunoprecipitation assays

To further analyse the cross-linked species, an immunoprecipitation experiment was performed by using anti-GAPDH specific antibodies, aimed at isolating the high molecular weight products.

To this purpose, HeLa cells ($3x10^6$) were exposed to UV laser irradiation using the previously selected optimal irradiation condition and then lysed as described in "Materials and Methods" section. The protein extract was incubated with anti-GAPDH specific antibodies and then the immuno-complexes were selected by the addition of protein G-Sepharose resin. After incubation, the mixture was centrifuged to remove the unbound protein species (supernatant). Since unspecific protein interactors could have been still selected by the procedure, multiple washings with PBS were performed. The same procedure was applied to control cells.

The immuno-selected proteins were then eluted by the addition of a reducing and denaturing buffer (8% SDS, 40% glycerol in 0.5 M Tris-HCl pH 6.8) and analysed by SDS-PAGE, followed by colloidal Coomassie blue staining or by Western blotting using anti-GAPDH specific antibodies (Figure 15).

As shown in Figure 15, in both the immuno-selected samples, i.e. control and irradiated, the presence of monomeric, uncross-linked GAPDH (37 kDa, Figure 15 A), immunopositive to its specific antibody (Figures 15 B and C), was observed. Instead, the immunopositive species of about 90 kDa was found to be selectively present in the irradiated sample (Figure 15 C).

It should be noted that in Figure 15 A additional bands are present, having molecular weight of about 50 and 25 kDa, respectively. As determined by MS analyses, these protein bands correspond to the heavy and light chains of GAPDH antibody, respectively, which have been used in the immunoprecipitation procedure.

From gels of control and irradiated samples, stained with colloidal Coomassie, 12 slices were excised (Figure 15 A) and analysed by nanoLC-MS/MS, as previously described. The comparative analysis of the proteins identified confirmed the presence of GAPDH in slice 12, corresponding to 37 kDa molecular mass. Interestingly, only in the irradiated sample, but not in control cells, GAPDH was also present as a ~90 kDa species (slice 5) and at even higher molecular mass (slices 2–4).

Since, beside GAPDH, no other proteins were found to be present, these results clearly confirmed that UV laser irradiation is able to covalently link *in vivo* GAPDH subunits in a stable oligomeric structure, therefore fixing a physiological interaction occurring in a natural environment.

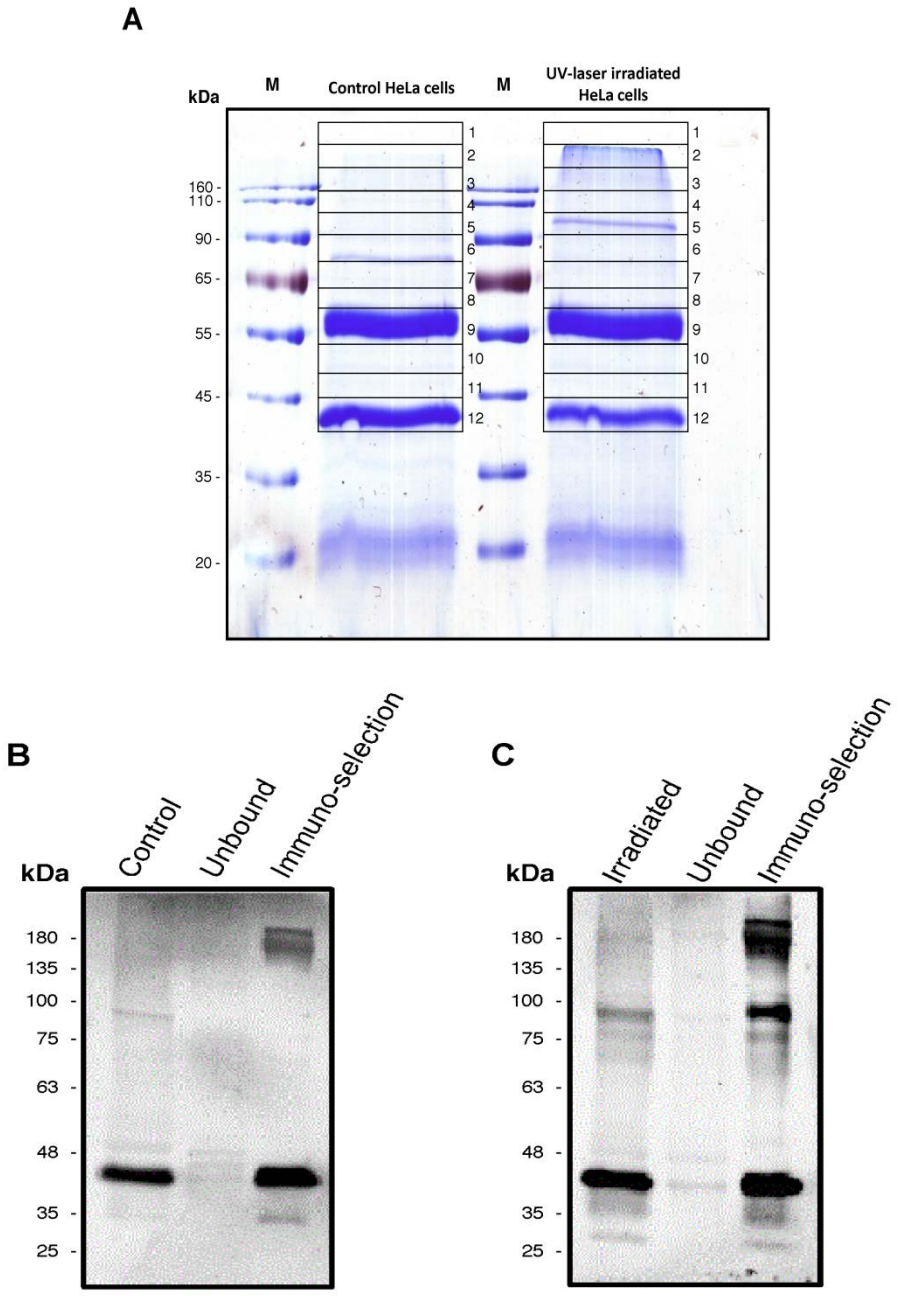

Figure 15. SDS-PAGE analysis of UV laser irradiated and control HeLa cell extracts after immuno-selection by anti-GAPDH antibodies. (A) Colloidal Coomassie staining of control and irradiated samples; (B and C) Western blot of control (B) and irradiated (C) samples. In B and C, the unbound and immuno-selected fraction of extracts are shown.

3.4 *In vitro* and *in silico* analyses

First, we performed a comparative analysis of the cross-linked species generated in *in vitro* and *in vivo* experiments by UV laser irradiation, in order to add knowledge to our results on GAPDH subunit-subunit cross-linking. For *in vitro* experiments, we used pure GAPDH, isolated from rabbit muscle (95% identity with human GAPDH).

To irradiate *in vitro* pure GAPDH (65 µM) the following conditions were selected: 5 s irradiation time, 100 µJ pulse energy, 2 kHz repetition rate and 1.0 J total irradiation energy. These experimental conditions were inspired by previous *in vitro* studies [Leo G. et al, 2013].

The resulting cross-linked products were then analysed by SDS-PAGE followed by Western blotting, using anti-GAPDH specific antibodies (Figure 15). The electrophoretic mobilities of GAPDH immonopositive products were compared to those of the immunopositive species obtained upon irradiation of HeLa living cells.

As shown in Figure 16, lanes 1 and 2, a species with an apparent molecular mass of ~90 kDa, as that generated by GAPDH cross-linking in living cells, was found to be present in the *in vitro* irradiated sample.

Thus, the *in vitro* cross-linking test supports our experimental findings *in vivo*, i.e. that oligomeric GAPDH is the main protein species formed upon UV laser irradiaton.

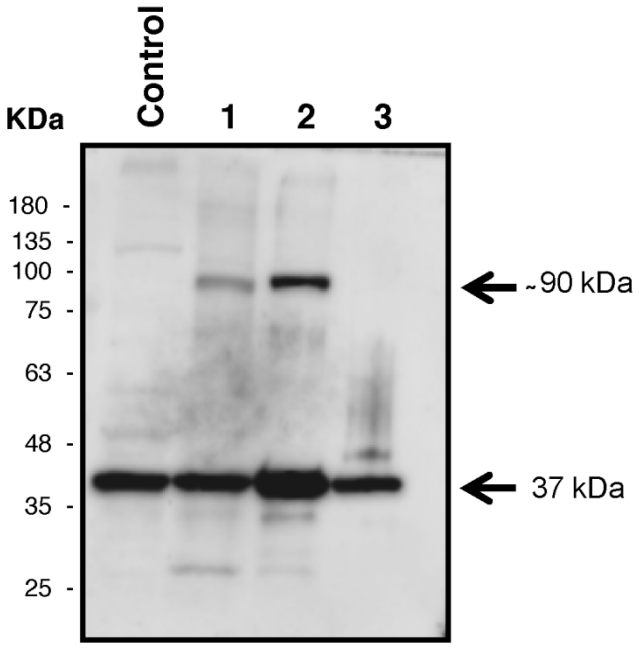

Figure 16. Comparative Western blot analysis of *in vitro* irradiated commercial GAPDH from rabbit muscle and endogenous GAPDH from irradiated cells.

Control, extract from not irradiated cells
Lane 1, extract from irradiated cells
Lane 2, commercial GAPDH after *in vitro* irradiation
Lane 3, commercial GAPDH before *in vitro* irradiation

Then, to provide a structural basis to our experimental results, in collaboration with Prof. Angelina Lombardi (Dept. of Chemical Science, University of Naples Federico II), we analysed the high-resolution crystal structure of human GAPDH (1.75 Å), solved by Jenkins JL & Tanner JJ [Jenkins JL & Tanner JJ, 2006] (Figure 17). The protein is a D_2-symmetric homo-tetramer in its functional form, with three independent interfaces.

Being aromatic residues the main target of UV laser irradiation, we analysed their cross-distance in the GAPDH crystal structure. The results are shown in the matrix in Figure 18 where distances are reported in angstroms and are highlighted in a heat map (blue/close, red/far).

This analysis suggested possible cross-linking sites. In particular, only one interface (the so-called R interface) presents aromatic residues prone to cross-link. In Figure 17, the four subunits are labeled as O, P, Q and R. In particular, W196 from P subunit is in close proximity with three tyrosine residues (Y42, Y45, Y49) from the nearby Q subunit.

Hence, given the one-photon excitation mechanism of this technique, we infer that the formation of a covalent GAPDH homo-dimer upon photochemical cross-coupling involves W196 and one of the three tyrosine residues in its proximity. As these residues lie on the symmetric interface between two subunits of the tetrameric structure, a dimer is the sole product expected to be generated by light excitation. These results demonstrate that proteins directly interacting one to each other in their cellular environment can be easily cross-linked by UV laser irradiation.

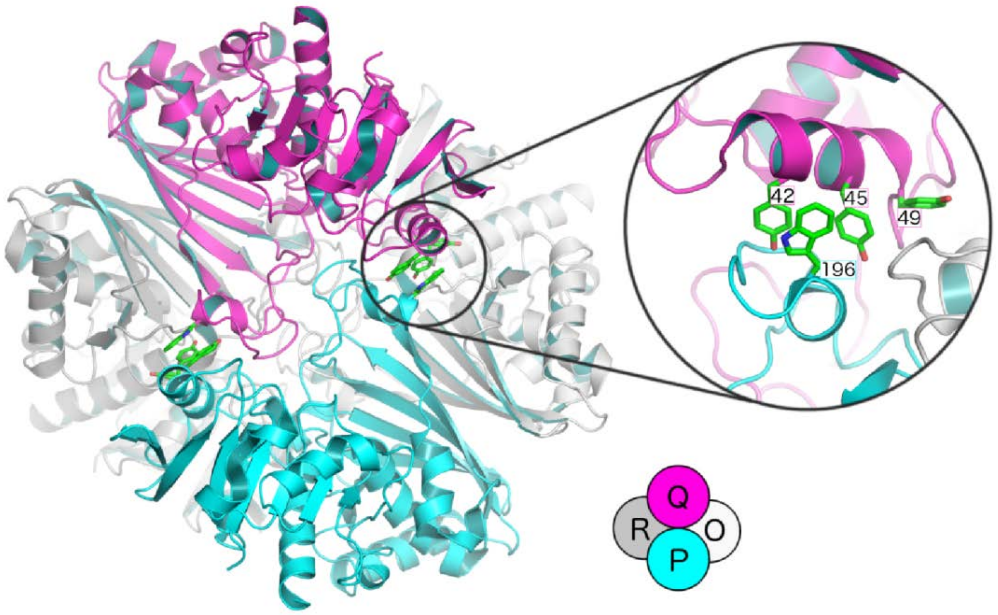

Figure 17. Human GAPDH crystal structure (PDB ID 1U8F). The four symmetry-related subunits are specified as in the bottom balloons. W196 from P subunit, and Y42, Y45, Y49 from Q subunit are showed as green sticks. This Figure was generated by using the PyMOL molecular graphics system, by Delano Scientific (*www.pymol.org*).

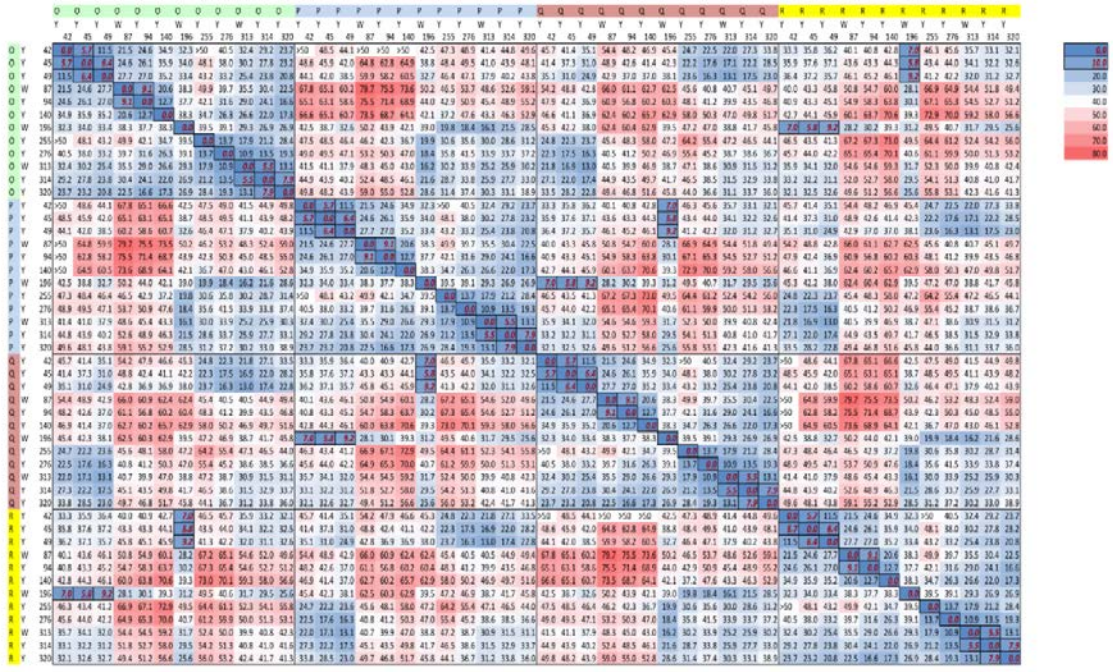

Figure 18. Aromatic residues distance matrix as measured from human GAPDH crystal structure (PDB ID 1U8F). Distances are reported in angstroms, and are highlighted in a heat map (blue/close, red/far).

3.5 Spectroscopic analyses

To analyse the involvement of aromatic residues in the intersubunit cross-linking, we performed a spectroscopic characterization of the irradiated GAPDH from rabbit muscle *in vitro*, using the irradiation conditions described above.

Multiple analyses were performed, consisting in: UV-Vis absorption performed in the 200-800 nm spectral range (Figure 19 A); intrinsic fluorescence spectra recorded in the 300-450 nm region and in the 360-500 nm region with excitation wavelengths of 280 and 340 nm, respectively (Figure 19 B); far-UV and aromatic region circular dichroism (CD) spectra recorded in the 190-250 nm (far-UV) and 255-375 nm (Soret) regions (Figures 19 C and D, respectively).

UV–Vis spectrum of irradiated sample clearly showed a new band centred around 330 nm (Figure 19 A), which can be interpreted as a conjugated aromatic chromophore [Williams TJ et al, 2014], whereas the absorption intensity of the 280 nm band remains substantially unchanged, with a slight increase in the 250–270 nm region. Tryptophan intrinsic fluorescence analyses of the irradiated GAPDH showed only a decrease in intensity (Figure 19 B), without any difference in the emission maximum wavelength, suggesting a quenching of the fluorescence probably due to a higher solvent exposure, or a decrease in the number of fluorophores that are excited at 280 nm. The latter hypothesis was further supported by a concomitant increase of emission at 420 nm, upon 340 nm excitation, thus indicating that a fraction of aromatic residues was involved in the red-shifted fluorescence. CD spectra in the far-UV (Figure 19 C) were typical of an α/β protein, in good agreement with previously published GAPDH CD analyses [Pappenberger G et al, 1997; He RQ et al, 1995]. Irradiated sample showed only slight spectral differences in this region with respect to control GAPDH, indicating that the secondary structure content is almost unaltered. Spectral differences between irradiated and control samples in the near-UV region (Figure 19 D) were more evident, in agreement with fluorescence and absorption data. Global profiles of the spectra remained unaltered, with bands centered at the same wavelengths. However, we found a significant decrease of the molar ellipticity of the minimum at 280 nm in the case of the irradiated sample.

Overall, these results strongly confirm that the formation of specific cross-linked species induced by UV laser irradiation is mainly based on the involvement of aromatic residues.

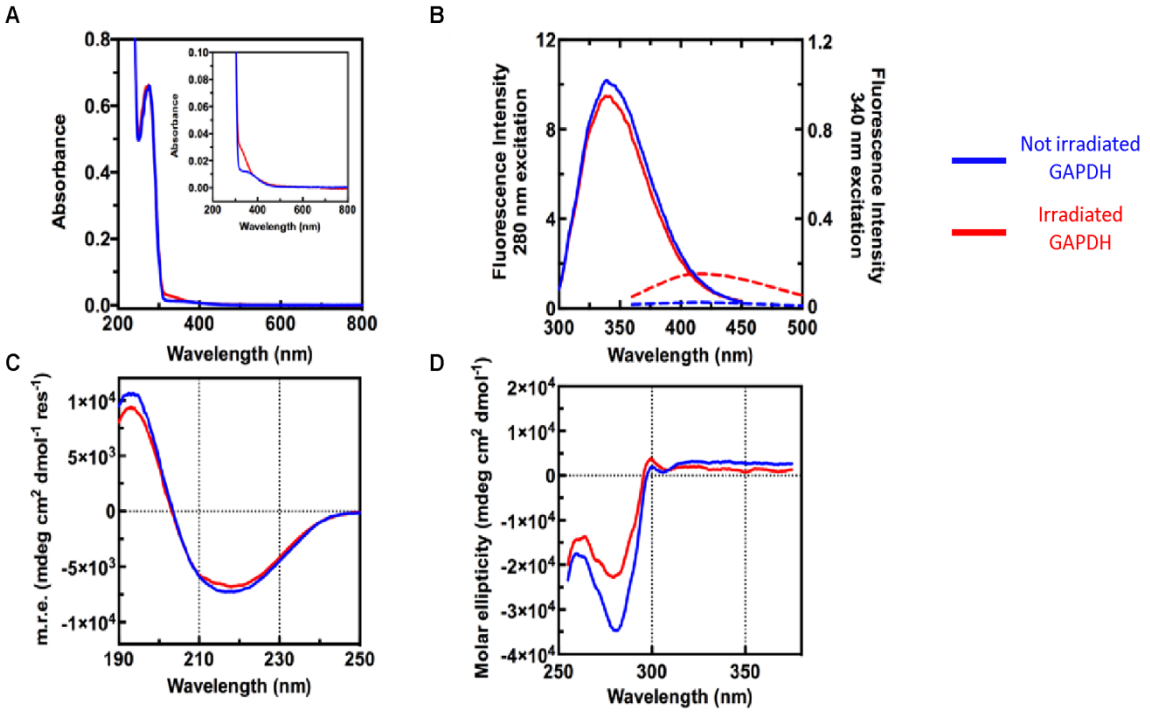

Figure 19. Spectroscopic characterization of *in vitro* irradiated *vs* non-irradiated GAPDH from rabbit muscle by UV-Vis absorption (A), intrinsic fluorescence analysis (B), far-UV and aromatic spectral region circular dichroism (C, D).

CHAPTER 4

FLIM-FRET APPROACH TO STUDY PPIs SPATIO-TEMPORAL DYNAMICS

This chapter concerns the setting-up of a FLIM-FRET methodology to validate and to analyse molecular details of PPIs "fixed" in living cells by UV laser irradiation. The ultimate goal is to apply the methodology to GAPDH cross-linked species in living cells, in order to elucidate PPIs spatio-temporal dynamics. To this purpose, we believe that combined FRET (Fluorescence Resonance Energy Transfer) and FLIM (Fluorescence Lifetime Imaging Microscopy) methodologies may be used to study transient and/or stable PPIs. In fact, FRET analyses detect interactions based on physical distance by energy transfer from an excited fluorophore (donor) to an acceptor one. Hence, once detected, interactions may be analysed by TR-FRET (Time-Resolved FRET) or by FRET-FLIM.

By FAST-FLIM technique, interactions can be detected and spatially localized within living cells [Padilla-Parra S & Tramier M, 2012], thus allowing to map formation and dissolution of protein complexes. Hence, FLIM-FRET and anisotropy experiments may allow the analysis of protein binding in living cells and the estimation of intermolecular distances on an Angström scale. By this experimental approach, PPIs spatial information may be acquired by a non-invasive procedure. In this scenario, it may be possible to set-up a general protocol to study the interaction pattern of any protein of interest with its partners, leading to significant progresses with respect to conventional strategies.

This part of the research work was carried out during my research experience in the "Unitè de Trafic membranaire et Pathogenèse" at Institut Pasteur, Paris (France) and in the "Département de Biologie Cellulaire et Developpement" at University of Rennes 1, Rennes (France).

To set-up the FLIM-FRET procedure, we used a cholesterol fluorescent probe and focused on the measurement of its lifetime, in order to analyse the membrane environment in different epithelial cell lines. Once acquired this information, the same probe was used as a fluorescent donor to perform FLIM-FRET experiments by using glycosylphosphatidylinositol-anchored proteins (GPI-APs) as acceptors.

4.1 FRET methodology

During the last 40 years, Fluorescence Resonance Energy Transfer (FRET) has been used to study a great variety of molecular interactions, both *in vitro* and *in vivo*. This powerful technique took also advantage of advances in different photonic imaging techniques and in the development of novel fluorescent probes and proteins [Tsien RY, 1998; Shaner NC et al, 2005].

FRET is a collision-free and distance-dependent photo-physical process where a transfer of energy occurs from an excited donor fluorophore to a suitable acceptor protein or fluorophore *via* long-range dipole–dipole coupling mechanism. Donor absorbs energy at shorter wavelength, whereas the acceptor absorbs energy

at longer wavelength [Förster T, 1965; Shrestha D et al, 2015]. FRET occurs over interatomic distances due to resonance-based interaction between chromophores. No transmission of photons from donor to acceptor species occurs. In particular, FRET can occur when the emission spectrum of the donor fluorophore significantly overlaps (>30%) with the absorption spectrum of the acceptor (Figure 20), as long as dipoles of both fluorophores are in favorable mutual orientation.

Since energy transfer efficiency is inversely correlated to the sixth power of the distance between donor and acceptor fluorophores, the distance over which FRET may occur is limited among 1 and 10 nm. Hence, when these criteria are satisfied, donor excitation results in sensitized fluorescence emission by the acceptor. This will be an evidence that tagged proteins under study are located at a distance lower than 10 nm.

The interpretation of intensity-based FRET measurements is intricate and limited by experimental conditions. Artefacts may be observed due to signal cross-contamination, variations in fluorochromes concentration and labeling efficiency, variations in excitation intensity and exposure duration, and photobleaching. To overcome these limitations, several approaches have been developed. Among these, the Fluorescence Lifetime Imaging Microscopy (FLIM) could be a suitable alternative technique [Padilla-Parra S et al, 2009].

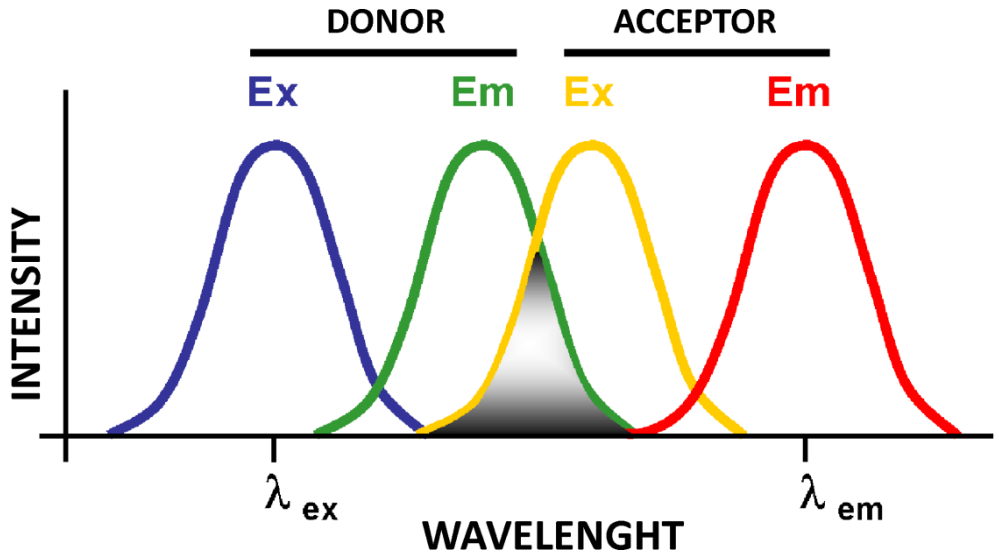

Figure 20. Schematic diagram showing FRET occurrence. Donor and acceptor excitation spectra are reported in blue and yellow, respectively. Donor and acceptor emission spectra, instead, are reported in green and red, respectively. The overlap between donor and acceptor excitation spectrum is shown in grey.

4.2 FLIM-FRET methodology

Fluorescence lifetime (τ) is the exponential decay following the excitation of a fluorescent probe. In more detail, it is the average time that a molecule spends in the excited state before returning to the ground state, typically accompanied by the emission of a photon. The lifetime of a fluorophore (in the absence of non-radiative processes) is an intrinsic property of the fluorophore, which provides information about probe's local microenvironment [Sun Y et al, 2011].

Excited-state lifetime measurements are independent from excitation light intensity, probe concentration and light scattering, but are highly dependent from fluorophore local environment, since FRET occurrence is sensitive to variations in pH and temperature.

The combination of lifetime measurement and FRET (FLIM-FRET) provides information on spatio-temporal dynamics of the interactions between biomolecules [Bacskai BJ et al, 2003; Elangovan M et al, 2002; Krishnan RV et al, 2003]. When acceptor molecules are located within donor local environment, energy transfer is permitted and will influence donor fluorescence lifetime. Hence, by measuring donor lifetime in the presence and in the absence of the acceptor molecule, it is possible to deeply analyse and quantify FRET occurrence.

FLIM-FRET has been used in several applications, such as the analysis of protein-protein interactions with high temporal resolution in living cells, ion concentration imaging, as well as in measuring oxygen concentration in medical applications [Bastiaens PI & Squire A, 1999; Van Munster EB & Gadella TW Jr, 2004].

In the case of PPIs analysis in living cells, FLIM represents a very suitable system, since it allows the determination of the minimal fraction of donor undergoing FRET (mf_D) independently from FRET efficiency (E). By this way, it is possible to determine the percentage of interacting proteins in a given population, with a spatio-temporal resolution higher than that of other approaches based on longer acquisition times [Padilla-Parra S et al, 2008].

4.3 GPI-anchored proteins

Glycosylphosphatidylinositol-anchored proteins (GPI-APs) are a class of lipid-anchored proteins widely expressed in eukaryotes. GPI-APs are almost exclusively localized on the cell surface, where they are confined to the outer leaflet of the bilayer. They are involved in different cell processes, such as membrane protein transportation, cell adhesion, cell wall synthesis and cell surface protection. Some of these anchored proteins are antigens, such as human carcinoembryonic antigen (CEA), which is used as a cancer marker [Imjeti NS et al, 2011]. Positioned at the C-terminus of many eukaryotic proteins, the GPI anchor is a post-translational modification that anchors the modified protein in the outer leaflet of the cell membrane. The GPI anchor is a complex structure comprising a phosphoethanolamine linker, a glycan core and a phospholipid tail (Figure 21) [Ikezawa H, 2002; McConville MJ & Menon AK, 2000; Orlean P & Menon AK, 2007].

In particular, GPI-APs use their GPI anchor to associate to specific membrane domains called rafts, which are lipid-ordered membrane micro-domains enriched in

cholesterol and sphingolipids. These rafts are involved in many cell functions, such as protein sorting, endocytosis and virus budding [Imjeti NS et al, 2011].

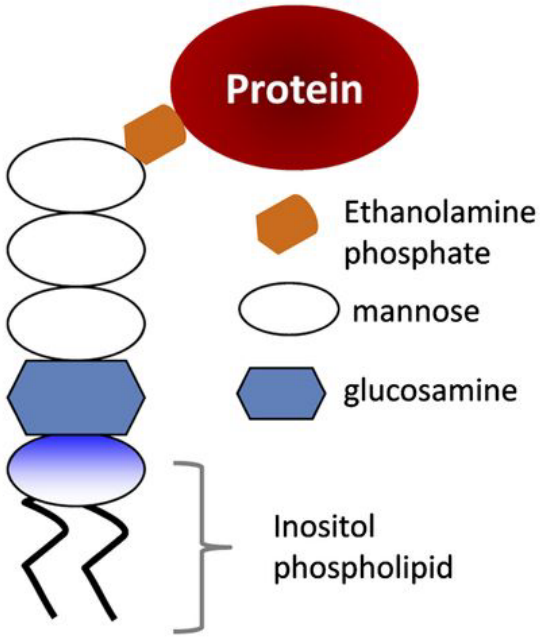

Figure 21. Core structure of the GPI anchor. The phosphatidylinositol (PI) is anchored to plasma membrane lipid bilayer. The glycan core consists of one molecule of *N*-glucosamine, three mannose molecules and one molecule of ethanolamine phosphate. GPI anchored proteins are linked at their carboxy-terminus through a phosphodiester linkage to phosphoethanolamine attached to a trimannosyl-nonacetylated glucosamine (Man3-GlcN) core.

4.4 Plasma membrane labeling

One specific characteristic of GPI-APs is to be selectively sorted to the apical plasma membrane in polarized epithelial cells. Interestingly, recent evidences indicated that the organization of GPI-APs in fully polarized epithelial cells is different from fibroblasts. Indeed, at the apical membrane of polarized epithelial cells, GPI-APs are organized in small clusters of single GPI-AP species (named homo-clusters), which are independent from cholesterol. These complexes, but not monomeric GPI-APs, coalesce into larger cholesterol-dependent clusters formed by multiple GPI-APs species, called hetero-clusters [Paladino S et al, 2014]. Interestingly, this hetero-clustered organization of GPI-APs is achieved only when they are properly sorted to the apical plasma membrane in fully polarized cells, thus correlating Golgi GPI-APs sorting to their surface organization. Indeed, prior to their apical sorting, GPI-APs form cholesterol-dependent homo-clusters in the Golgi [Paladino S et al, 2004]; once having reached the apical surface, these homo-clusters coalesce in hetero-clusters. This interdependence between GPI-APs sorting in the Golgi and their plasma membrane organization is critical for epithelial cells, since this will allow GPI-APs to exert their specific functions only at the apical surface.

Moreover, these data suggest that intrinsic differences exist in the organization of GPI-APs between epithelial cells and fibroblasts, where GPI-APs are delivered as monomers to the plasma membrane and their further hetero-cluster organization is independent from pre-homo-clustering in the Golgi apparatus, but solely depends on cholesterol [Paladino S et al, 2014; Paladino S et al, 2015].

Hence, while cholesterol appears to be critical for GPI-APs clustering at the plasma membrane of both epithelial and fibroblastic cells, recent findings showed that in fibroblasts GPI-AP clusters also depend on cortical actin [Goswami D et al, 2008]. Indeed, it has been demonstrated that both cholesterol and actin perturbation affect GPI-APs cluster organization in fibroblasts and that actomyosin contractility is also required for their formation [Goswami D et al, 2008]. Interestingly, it has been shown that cholesterol depletion impacts on the organization of cortical actin [Chubinskiy-Nadezhdin VI et al, 2013; Kwik J et al, 2003]. However, the mechanistic link between cholesterol and actin in GPI-APs organization is unknown, and possible involved molecules have not yet been identified. Furthermore, it will be interesting to investigate the role of actin cytoskeleton in GPI-AP organization in polarized cells, since actin cytoskeleton rearrangement occurs during epithelial cells polarization.

In order to investigate the relationship between cholesterol and actin cytoskeleton in apical GPI-APs organization, a cholesterol probe, i.e. BODIPY (TopFluorcholesterol), was used to measure membrane cholesterol lifetime in Madin-Darby canine kidney epithelial cells (MDCK cells) and in Chinese hamster ovary cells (CHO cells).

The TopFluorcholesterol fluorophore is used to fluorescently label sterol in living cells. It is characterized by high absorption coefficient, high fluorescence quantum and high photochemical stability.

First, cells were incubated with TopFluorcholesterol for different time intervals, in order to define the experimental conditions to efficiently label plasma membrane (PM). To this purpose, MDCK cells were plated and, following an incubation of three days at 37°C, thus allowing surface polarization, they were treated with TopFluorcholesterol for 10, 25 or 60 min. In the case of CHO cells, incubation with TopFluorcholesterol was performed for 5,10 or 15 min.

As shown in Figure 22, fluorescence microscopy analyses revealed that, in the case of MDCK cells, 25 min of incubation are sufficient to efficiently label PM (Figure 22 A), whereas, in the case of CHO cells, 5 min of incubation were selected as optimal condition for PM labeling (Figure 22 B).

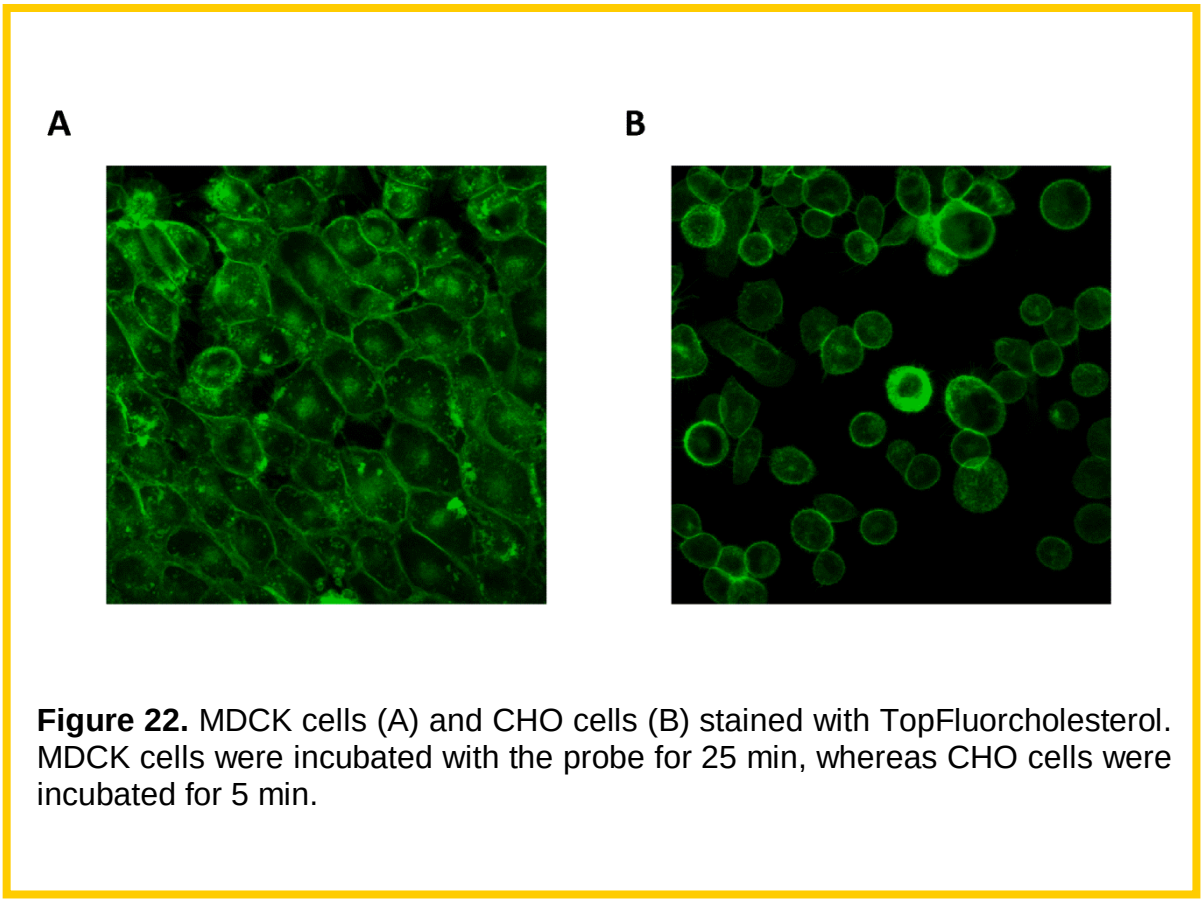

Figure 22. MDCK cells (A) and CHO cells (B) stained with TopFluorcholesterol. MDCK cells were incubated with the probe for 25 min, whereas CHO cells were incubated for 5 min.

4.5 FLIM analysis

It has been postulated that, in the case of fibroblasts and normal rat kidney cells, plasma membranes are compartmentalized and that actin plays an essential role in proteins confinement. In fact, it has been demonstrated that transmembrane proteins interact with actin fibers and this contributes to the establishment of membrane compartments in which proteins are able to diffuse [Morone N et al, 2006; Murase K et al, 2004].

To define the putative role of actin cytoskeleton in the organization of raft-associated proteins, the integrity of actin meshwork was perturbed by using latrunculin A, which prevents actin polymerization [Morton W et al, 2000]. To demonstrate this, we stained F-actin with phalloidin-rhodamine in polarized MDCK cells and in CHO cells, in the absence or in the presence of latrunculin A (60 min of incubation). We demonstrated that cell treatment with lantrunculin A drastically affects actin cytoskeleton and cell integrity. By contrast, following an incubation of 5 min with latrunculin A, cell integrity was preserved. Hence, this incubation time was selected for all the experiments aimed at the evaluation of TopFluorcholesterol fluorescence decay in the presence or in the absence of actin perturbation.

In particular, CHO and polarized MDCK cells were treated with latrunculin A and then labeled with TopFluorcholesterol, as previously described. Following staining, analyses were performed by using FLIM methodology to measure probe fluorescence decay.

As shown in Figure 23, TopFluorcholesterol lifetime was found to be 5.23 ns ± 0.09 at the apical surface of control polarized MDCK cells and 4.08 ns ± 0.23 in control CHO cells, hence revealing a different cholesterol environment in the two cell lines. In the case of CHO cells, TopFluorcholesterol lifetime is drastically reduced upon actin perturbation, from 4.08 ns ± 0.23 to 3.87 ns ± 0.17. At the apical surface of epithelial cells, instead, probe lifetime appears unchanged upon actin perturbation (5.25 ns ± 0.04). This result highlights that membrane organization is different in the two cell types, as well as the relationship between actin and cholesterol.

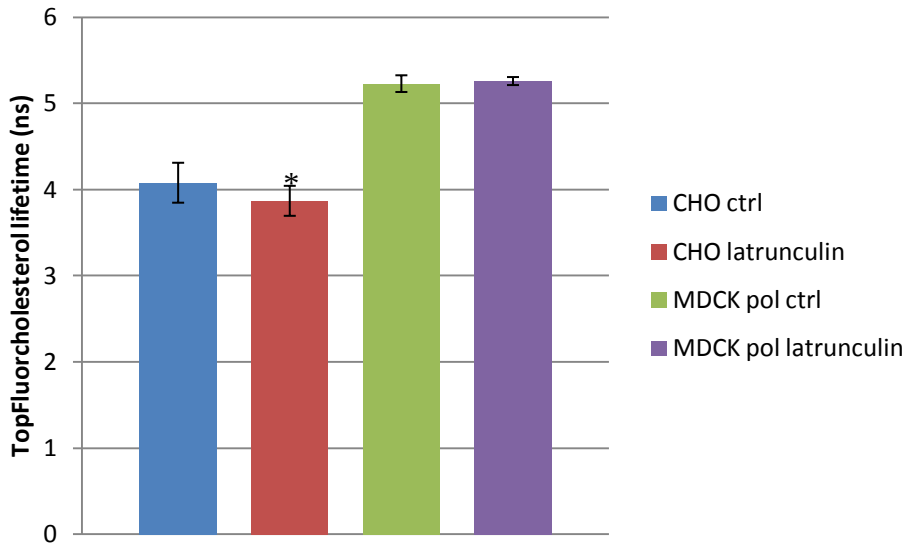

Figure 23. MDCK and CHO cells were treated with Latrunculin A for 5 min and then stained with TopFluorcholesterol for 25 min and 5 min, respectively. TopFluorcholesterol lifetime (ns) was measured and reported in histograms. CHO cells (blue and red bars) and polarized MDCK cells (green and purple bars) were analysed either in control conditions (blue and green bars) or after lantrunculin treatment (red and purple bars).
Experiments were performed three times (n>35). Error bars indicate the standard deviation (SD). * P<0.0001, Student's t-test.

4.6 FLIM-FRET analysis

We then set up a FLIM-FRET approach, in order to measure donor fluorescence decay in the presence or in the absence of a putative acceptor. Donor lifetime decrease, in the presence of an acceptor, reveals fluorescence energy transfer (FRET) between the two molecules, indicating close proximity.

FLIM-FRET analyses were performed on CHO cells using TopFluorcholesterol as a donor and placental alkaline phosphatase (PLAP), a GPI-anchored protein which is apically sorted in epithelial cells, as an acceptor.

To this purpose, $3x10^5$ CHO cells were plated and, following 24 h of incubation, they were transiently transfected with a recombinant plasmid encoding PLAP fused to mCherry. Following an incubation of 36 h, CHO cells were either treated with latrunculin A or directly labeled with TopFluorcholesterol, as previously described. Cells were then analysed by fluorescence lifetime imaging microscopy (FLIM).

As shown in Figure 24, in control cells (not transfected) the mean TopFluorcholesterol lifetime was 4.08 ns ± 0.23. This value significantly decreased up to 3.8 ns ± 0.03 when cells were transfected with mCherry-PLAP (as acceptor), revealing FRET occurrence between TopFluorcholesterol and the apical GPI-AP.

Following treatment with latrunculin A, FRET occurrence was found to be drastically reduced. Figure 23 C shows that the mean probe lifetime was 3.87 ns ± 0.17 in control CHO cells treated with lantrunculin A, whereas lifetime decreased to 3.75 ns ± 0.05 when cells were transiently transfected with mCherry-PLAP and then treated with lantrunculin A.

These results strongly confirmed the conclusion that GPI-APs organization/compartmentation is strongly influenced by actin cytoskeleton in fibroblasts.

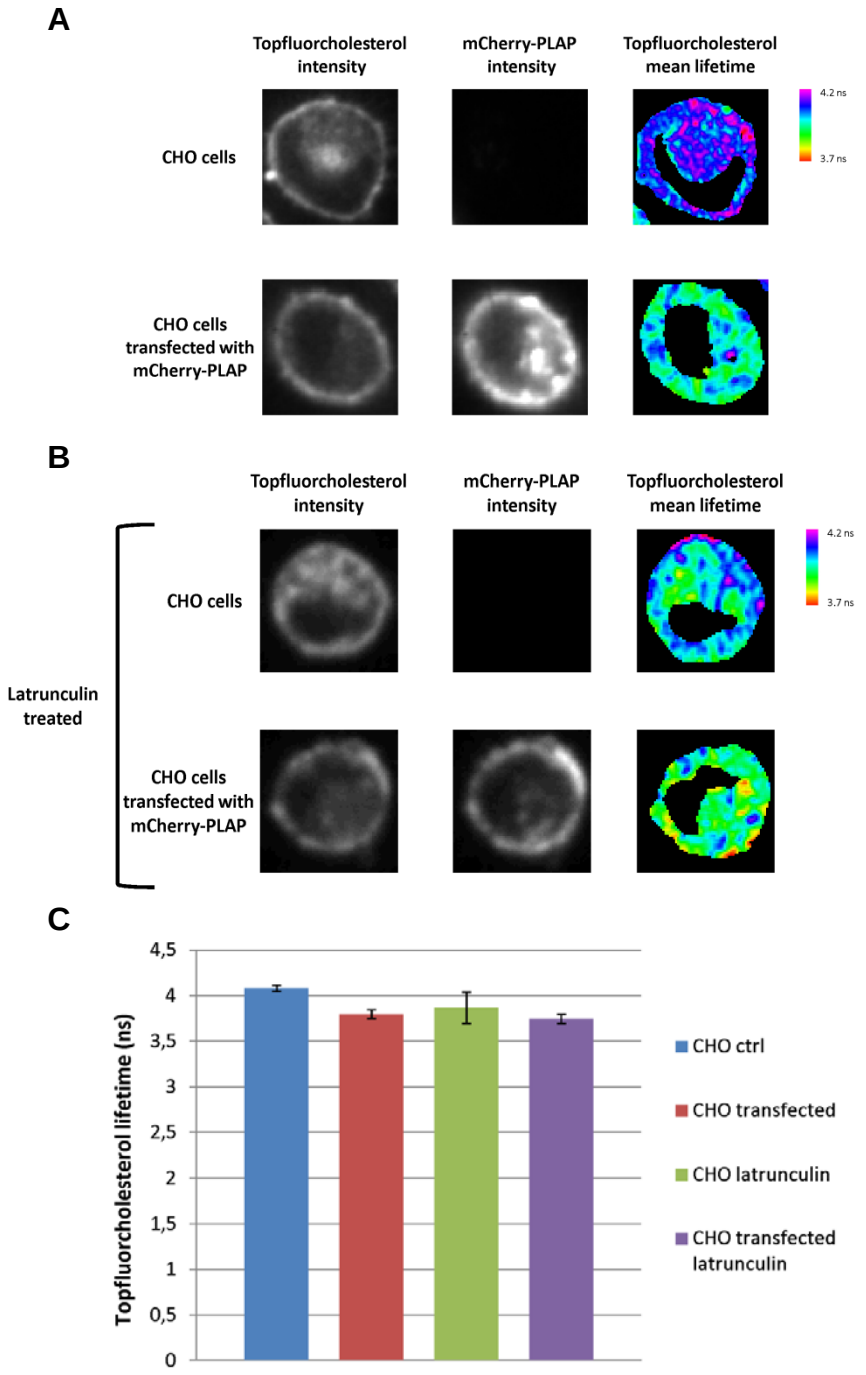

Figure 24. FLIM-FRET analyses. (A) Mean fluorescence lifetime maps of TopFluorcholesterol in the absence or in the presence of mCherry-PLAP in control CHO cells. (B) Mean fluorescence lifetime maps of TopFluorcholesterol in the absence or in the presence of mCherry-PLAP in CHO cells treated with latrunculin A.
(C) Histograms representing TopFluorcholesterol lifetime (ns) in control CHO cells in the absence (blue bar) or in the presence of mCherry-PLAP (red bar). The same analysis was performed in the presence of lantrunculin A (green bar, control CHO cells; violet bar, transfected CHO cells).
Experiments were performed three times (n>35 cells). Error bars indicate the standard deviation (SD). * P<0.0001, Student's t-test.

CHAPTER 5

MATERIALS AND METHODS

5.1 Materials

All reagents were purchased from Sigma-Aldrich, unless differently specified. Protein G Sepharose was from GE Healthcare. The chemiluminescence detection system (SuperSignal® West Pico) was purchased from Pierce. Protease inhibitors cocktail was from Roche. Mouse monoclonal anti-GAPDH antibody was from Ambion; rabbit polyclonal anti-GAPDH was from ProteinTech; anti-mouse and anti-rabbit secondary antibodies conjugated to horseradish peroxide enzyme (HRP) were from Thermo Scientific.

5.2 Cell culture

HeLa, MDCK and CHO cells were purchased from American Type Cuture Collection (ATCC). HeLa cells were cultured in DMEM (Dulbecco's Modified Eagle's Medium), supplemented with 10% fetal bovine serum (FBS) (HyClone), 4 mM L-glutamine, 1 mM sodium pyruvate and penicillin-streptomycin (50 U/mL), in a 5% CO_2 humidified atmosphere at 37ºC. To perform experiments, cells were detached with trypsin-EDTA for about 5 min at RT and then diluted in serum containing medium.

MDCK cells were cultured in DMEM supplemented with 5% FBS, while CHO cells were cultured in HAM's F12 medium supplemented 10% FBS, in a 5% CO_2 humidified atmosphere at 37ºC.

CHO cells were transiently transfected with cDNA encoding mCherry-PLAP (cloned by PCR in pcDNA3.1 vector carrying hygromycin resistance) by using lipofectamine (Invitrogen), as described in the manufacturer instructions.

5.3 UV laser irradiation of living HeLa cells

To irradiate HeLa living cells, a powerful source of UV radiation, a custom-made version of the PHAROS laser system (Light Conversion Ltd., Vilnius, Lithuania, see the company web site at http://www.lightcon.com/) was used. This is a very compact femtosecond amplified laser source – a single-unit integrated system, combining up-to-millijoule pulse energies and high average output power. This system, based on the new Yb:KGW lasing medium and on a very compact Chirped Pulse Amplification scheme, emits 1.3 mJ, 170 femtosec pulses, centred at 1030 nm, at a repetition rate of 2 kHz, corresponding to an average power of 2.5–2.6 W. The repetition rate can be increased up to 200 kHz, where the average output power reaches nearly 7 W. The IR pulse is then frequency up-converted into a harmonic generator stage (HIRO) where II (515 nm), III (343 nm), and VI (257 nm) harmonic pulses, lasting about 250 femtosec, are obtained. The system is equipped with a

sophisticated pulse picker, which allows one to separately select any possible repetition rate, from single-shot to 200 kHz.

For UV laser irradiation, HeLa cells were detached by trypsin-EDTA and suspended in phosphate buffer (PBS 1X) at a density of $4x10^5$ cells/mL. Cells were then placed in a cuvette containing a magnetic stirrer to ensure continuous agitation of the cell suspension during irradiation and uniform irradiation conditions.

5.4 UV laser irradiation of GAPDH *in vitro*

In vitro cross-linked GAPDH was prepared by irradiating the protein isolated from rabbit muscle (65 µM, 500 µL total volume). To this purpose, lyophilized GAPDH was dissolved in 50 mM phosphate buffer pH 7.5 and placed in a cuvette containing a magnetic stirrer. Irradiation was then performed under the following conditions: 5 s irradiation time, 100 µJ pulse energy, 2 kHz repetition rate and 1.0 J total irradiation energy.

5.5 Cells lysis

Following irradiation, HeLa cells were centrifuged at 5,000 rpm for 5 min. To analyse intracellular proteins, the cell pellet was dissolved ($1x10^4$ cells/µL) in 1% NP-40 in PBS containing protease inhibitors cocktail (Roche, Germany). Upon 30 min incubation on ice, lysates were obtained by centrifuging samples at 14,000 g for 30 min at 4°C. Soluble protein concentration was then determined by the Bradford assay.

5.6 Gel electrophoresis under denaturing conditions

Gel electrophoresis under denaturing conditions (SDS-PAGE) was performed as described by Laemmli (1970) using 10% polyacrilamide gels. Protein samples, dissolved in loading buffer (0.125 M Tris-HCl pH 6.8 containing 2% SDS, 10% glycerol, 0.02% bromophenol blue and 5% 2-mercaptoethanol) were boiled for 2 min, centrifuged and loaded on the gel. At the end of the electrophoretic run, performed at 150 V, the gel was treated as follows:

a) Coomassie staining: the gel was stained with a Coomassie blue solution (20% isopropanol, 10% acetic acid, 0.1% Coomassie blue) by incubation for 30 min under gentle shaking. The gel was destained with extensive washes in a solution containing 20% Ethanol and 7% acetic acid. This solution was replaced by ultra pure water when protein bands were detected.

b) Western blotting analyses: the proteins were transferred by electroblotting (25 V) onto a PVDF membrane at 4°C for 16 h. The membrane was incubated on a shaker in 10 mL of blocking solution (0,1% Tween-20, 5% BSA in PBS) at 25°C for 1 h and was then incubated with anti-GAPDH monoclonal antibody (dilution 1:10,000) on a shaker at RT for 1 h. After extensive washing with PBS containing 0.1% Tween-20, the membrane was incubated with a goat anti-mouse secondary antibody conjugated to HRP (dilution 1:10,000). Membranes were then washed with PBS containing 0.1% Tween-20. The detection of immunopositive species by enzyme-linked chemiluminescence (enhanced chemiluminescence: ECL) was performed

according to the manufacturer's instructions (Super Signal®West-Pico Chemiluminescent Substrate, Pierce), using a Chemidoc (Biorad).

5.7 Immunoprecipitation

For immunoprecipitation (IP) experiments, protein extracts (300 µg), obtained as described before, were diluted in PBS containing 0.01% Tween-20 (1 µg/µL final concentration) and incubated with rabbit polyclonal anti-GAPDH specific antibodies (3 µg) over-night at 4 °C on a shaker. After incubation with protein G Sepharose (60 µL) for 1.5 h at RT, the sample was centrifuged, washed, and bound proteins eluted in 0.125 M Tris-HCl, pH 6.8 containing 2% SDS and 10% glycerol. Selected proteins were then analysed by Western blotting with anti-GAPDH monoclonal antibodies.

5.8 Two-dimensional gel electrophoresis

Protein extracts were obtained as described above. For each sample, 200 µg of proteins were precipitated using the 2D Clean-Up Kit (GE Healthcare). After precipitation, the pellet was mixed with 125 µL of rehydration buffer (6 M urea, 2 M tiourea, 0.4% CHAPS, 1% bromophenol blue), 3 µL of 1 M DTT and 2.5 µL of pH 3-10 NL IPG buffer (GE Healthcare). Samples were loaded in duplicates onto 7 cm Immobiline™DryStrip gels strips (GE Healthcare) with a non-linear pH range of 3–10 using an isoelectric focusing system (EttanIPGphoreIII). Strips were rehydrated (20 °C, 16 h) and isoelectric focused (500 V for 1 h, 1000 V for 1 h, 5000 V for 3 h, held at 5000 V, 6000 V for 3 h, and held at 6000 V for 5 h to reach 15000 V total energy). The maximum current was maintained at 50 µA per strip. Strips were subsequently reduced and alkylated twice (15 min each) in equilibration buffer (50 mM Tris-HCl pH 8.8, 6 M urea, 30% (v/v) glycerol, 2% (w/v) SDS, and 0.03% bromophenol blue) containing 65 mM DTT and 135 mM iodoacetamide. Strips were subjected to the second dimensional separation (Ettan DALTsix) using a SDS-polyacrylamide gel (12.5%). SDS-PAGE was carried out by standard methods with a constant voltage (180 V) at RT. A set of samples was then stained with colloidal Coomassie Brilliant Blue, while a second set of samples was electroblotted for Western blot analysis.

5.9 Protein identification

Protein identification by mass spectrometry was performed on Coomassie Blue stained spots from 2D gels and on bands excised from monodimensional gels. Excised spots/bands were destained by repetitive washes with 0.1 M NH_4HCO_3, pH 7.5 and acetonitrile. Enzymatic digestion was carried out with 100 ng of proteomic grade trypsin (Sigma) in 10 mM NH_4HCO_3 buffer, pH 7.5. Samples were incubated for 2 h at 4 °C, then trypsin solution was removed and a fresh trypsin solution was added and samples were incubated for 18 h at 37 °C. Peptides were then extracted by washing the gel spots/bands with acetonitrile and 0.1% formic acid at RT and then were filtered using 0.22 µm PDVF filters (Millipore) following the recommended procedure.

The resulting peptide mixtures were analysed by nanoLC-MS/MS, on a CHIP MS 6520 QTOF equipped with a capillary 1200 HPLC system and a chip cube

(Agilent Technologies, Palo Alto, Ca). After sample loading, the peptide mixture was first concentrated and washed at 4 µL/min in 40 nL enrichment column (Agilent Technologies chip), containing 0.1% formic acid in 2% acetonitrile. The sample was then fractionated on a C18 reverse-phase capillary column (75 µm x 43 mm in the Agilent Technologies chip) at a flow rate of 400 nL/min, with a linear gradient of eluent B (0.1% formic acid in 95% acetonitrile) in A (0.1% formic acid in 2% acetonitrile) from 7 to 60% in 50 min. Peptide analysis was performed using data-dependent acquisition of one MS scan (mass range from 300 to 2000 m/z) followed by MS/MS scans of the five most abundant ions in each MS scan. MS/MS spectra were automatically measured when the MS signal surpassed the threshold of 50,000 counts. Double and triple charged ions were preferably isolated and fragmented. Each LC-MS/MS analysis was preceded and followed by blank runs to avoid carryover contamination.

5.10 Data handling

The acquired MS/MS spectra were transformed in *Mascot Generic* format (.mgf) and used to query the SwissProt database 2015_01 (547,357 sequences; 194874700), with taxonomy restriction to *Human* (142,140 sequences), for protein identification with a licensed version of MASCOT software (www.matrixscience.com) version 2.4.0. Mascot search parameters were: trypsin as enzyme; 3, as allowed number of missed cleavages; carboamidomethylation of cysteines as fixed modification; 10 ppm MS tolerance and 0.6 Da MS/MS tolerance; peptide charge from +2 to +3. Possible oxidation of methionine and the formation of pyroglutamic acid from glutamine residues at the N-terminal position of peptides were considered as variable modifications. Peptide score threshold provided from MASCOT software to evaluate quality of matches for MS/MS data was 10. Individual ion score threshold provided by MASCOT software to evaluate the quality of matches in MS/MS data was 22. Only proteins presenting two or more peptides were considered as positively identified.

5.11 UV, Fluorescence and CD spectroscopies

The spectroscopic characterization was carried out with commercially available GAPDH from rabbit muscle in 50 mM phosphate buffer pH 7.5, at a final concentration of 65 µM (ε_{280} = 29910 $M^{-1}cm^{-1}$). All acquired spectra were conveniently subtracted from blank contribution. The UV-Vis absorption spectra were recorded in 0.33 cm path length quartz cuvette. Wavelength scans were performed in the 200-800 nm range, with a 300 nm/min scan rate, 1.0 nm data interval and an average time of 0.0125 s, with the temperature set at 25 °C.

Fluorescence experiments were performed on a Horiba Jobin Yvon Fluoromax-4 fluorimeter. The spectra were recorded with a reduced volume quartz cuvette with a 1.0 cm path length. Temperature of 25 °C was kept costant by the peltier unit with 2 nm slits. Spectra were recorded in the 300-450 nm region and in the 360-500 nm region with excitation wavelengths of 280 and 340 nm, respectively. Fluorescence spectra were smoothed adopting a Savitzky-Golay filter with a 15 points window.

CD experiments were performed on a Jasco J-815 circular dichroism spectropolarimeter, calibrated for intensity with ammonium [D_{10}] camphorsulfonate ([$\theta_{290.5}$] = 7910 deg cm^2 $dmol^{-1}$). Depending on the observed region, the cell path length was 0.01 or 0.33 cm. CD spectra were recorded in the 190-250 nm (far-UV) and 255-375 nm (Soret) regions, at 0.2 nm intervals, with a 20 nm/min scan rate, 1.0 nm bandwidth and a 16 s response. In order to improve the signal to noise ratio, 3 accumulations were collected for the near-UV region. Spectra in the far-UV region are reported in terms of mean residue ellipticity, calculated by dividing the total molar ellipticity by the number of amino acids in the molecule, whereas spectra in the near-UV region are reported in terms of molar ellipticity.

5.12 Cytoskeleton meshwork perturbation

To perturb actin cytoskeleton, cells were incubated for 5 or 60 min at 37 °C with latrunculin A (Molecular probes, Invitrogen) diluted in complete medium to 6 µM as final concentration.

5.13 Topfluorcholesterol staining

CHO and MDCK cells were plated on matek culture dishes ($3x10^5$ cells/dish) in the appropriate medium. After 72 h, MDCK cells were incubated with Topfluorcholesterol (Avanti) for 10, 25 or 60 min, whereas CHO cells were incubated for 5,10 or 15 min. Cells were then washed and maintained in PBS solution for fluorescence analyses.

5.14 Confocal microscopy analyses

50-frame time images series were acquired with a Zeiss LSM 510 META microscope equipped with a Plan Apo 63× oil-immersion (numerical aperture (NA) 1.4) objective lens by using the following settings: 488-nm argon laser, 0.05 mW of output power, 505- to 550-nm emission, gain less than or equal to 900, offset 0.1, digital gain 1. The scanning parameters were as follows: 512 × 512 frame window, 25.61 µs per pixel dwell time, no average, zoom 6×, ROI (x, y) 256 × 64, pinhole corresponding to 1-µm optical slice. Images were acquired with a resolution of 70 nm per pixel. All the measurements were performed on cells displaying comparable levels of fluorescence signal intensity.

5.15 FLIM measurements

The FRET-FLIM apparatus combines multifocal multiphoton excitation (TriMscope, LaVisionBiotec, Bielefeld, Germany) connected to an inverted microscope (IX 71, Olympus, Tokyo, Japan) and a fast-gated charge-coupled device (CCD) camera (Picostar, LaVisionBiotec, Bielefeld, Germany). A mode-locked Ti:Sa laser at 950 nm for the excitation of GFP (Spectra Physics, France) is split into 2–64 beams by using a 50/50 beam splitter and mirrors. A line of foci is then created at the focal plane, which can be scanned across the sample. A filter wheel of spectral filters

(535AF45 for GFP) is used to select the fluorescence imaged onto a fast-gated light intensifier connected to a CCD camera. The gate of the intensifier (adjusted at 2 ns) is triggered by an electronic signal coming from the laser. A programmable delay box was used to acquire a stack of five time-correlated images of the 10-ns fluorescence decay window. The acquisition time of the CCD camera was adjusted considering the fluorescence signal level (between 3 and 5 s). Instrumentation is controlled by Imspector software developed by LaVision Biotec. ROIs of 140 × 140 pixels (4–6 cells) were acquired.

Data analysis was performed by using ImageJ software (Rasband, WS, ImageJ, US National Institutes of Health, Bethesda, Maryland, USA, http://rsb.info.nih.gov/ij/). The five images coming from a time-gated stack were first smoothened by a 3 × 3 mask to decrease the noise, and to recover mean lifetime, $< \tau >$, by applying the following equation:

$$< \tau >= \sum_{i=1}^{5} \Delta t_i / \sum_{i=1}^{5} I_i$$

where $\Delta t_i = 2i - 1$ corresponds to the time delay after the laser pulse of the ith image acquired, and I_i corresponds to the pixel intensity map in the ith image.

CONCLUDING REMARKS

The study of protein-protein interactions (PPIs) is one of the key topics for the development and the progress of systems biology. Primary challenges associated with the study of biological systems include identification of protein interactions and measurement of topological/structural features of protein interactions *in vivo*. However, current state-of-the-art technologies do not allow definition of interaction mechanisms between key biomolecules in their natural context, such as living cells.

In this scenario, UV laser cross-linking may offer a potentially powerful tool to investigate PPIs. In particular, this PhD project was aimed at the development of an innovative UV laser based system able to “weld” protein surfaces which come in direct contact one to each other without perturbing their physiological environment, by establishing cross-links at zero-length.

Indeed, crosslinking induced by ultra-short laser pulses has two main advantages: (i) it binds only species that are in proximity (“zero length” covalent bond) of the absorbed photons, thus filtering the direct interactions from the indirect ones, and (ii) it only operates within the inducing pulse duration, thus paving the way for time-resolved studies of transient interactions with high temporal resolution.

Moreover, previous studies performed *in vitro* on peptides demonstrated that a radical mechanism is at the basis of the phenomenon as, upon absorption of UV-light, aromatic side chains produce radicals able to react and generate covalent bonds with nearby residues [Leo G et al, 2013]. Hence, reactive groups belong to the interacting proteins themselves, without the need of introducing reagents, which may alter the protein natural environment. This represents a great advantage of the methodology. Even though the aromatic amino acids occurrence on protein surface is clearly lower than that of polar residues, Phe, Trp, Tyr are strong contact formers and hot spots of PPIs frequently contain Trp, Arg and Tyr. Moreover, due to their presence in almost all proteins, this procedure can be applied, in principle, to any protein-protein complex.

Furthermore, cross-linking intermediates have a short half-life (nano- or microsec), which is important to minimize non-specific cross-linking and to monitor interaction events with a flexible temporal resolution ranging in the millisec time scale.

By using HeLa cells as a cell system and endogenous GAPDH (37 kDa) as a model protein, we demonstrated, for the first time, that femtosecond UV laser irradiation of living cells is able to weld GAPDH complexes of high molecular mass, among which we focused on species of about 90 kDa for protein identification. We demonstrated that the phenomenon can be easily modulated, since we defined a wide energy range (from 2.4 J to 4.4 J) in which the yield of cross-linking is a linear function of total irradiation energy with no apparent perturbation of cell proteome. Indeed, by delivering a total irradiation energy lower than 2.4 J no efficient cross-linking occurs, while at higher energy dose (>4.4 J) an extensive and uncontrolled cross-linking occurred.

Within this range, we set up optimal conditions to induce cross-linking by UV laser irradiation of living cells, *i.e.* 2 kHz repetition rate, 50 µJ pulse energy and 42 seconds irradiation time, as these parameters maximize cross-linked GAPDH signals.

By immunological, 2D-electrophoretic and mass spectrometric analyses, we demonstrated that UV laser irradiation of HeLa living cells induces cross-linking between two GAPDH subunits, generating cross-linked dimers. Analysis of the high-resolution GAPDH crystal structure [Jenkins JL & Tanner JJ, 2006] provides a structural basis to our experimental results. A detailed structure analysis of the distances between aromatic residues shows that W196 and Y42, Y45, Y49 form the most important set of aromatic interaction sites between the two subunits. Given the one-photon excitation mechanism of the here proposed technique, it is likely to hypothesize that the covalent GAPDH homo-dimer formation upon photochemical cross-coupling involves W196 and one of the three tyrosine residues in its proximity, both tryptophan and tyrosine being indeed amino acid residues amongst the most involved in excitation mechanisms induced by UV-C light (200–280 nm) [Pattison DI, 2011]. Most notably, these aromatic residues lie at the C2 symmetric R-interface of GAPDH natural tetramer, thus a dimer is the sole product expected to be generated by light excitation, as experimentally found both in living cells and *in vitro*.

Spectroscopic analyses, performed on rabbit muscle GAPDH irradiated *in vitro*, clearly support the involvement of aromatic residues in the covalent cross-linking between two subunits. Taken together, all the spectroscopic data suggest that a new chromophore, absorbing around 330 nm, is produced upon laser irradiation. Concomitant changes were detected in both UV-Vis and fluorescence spectra. In particular, fluorescence emission registered upon 340 nm excitation can be attributed to the presence of highly conjugated aromatic moieties, in agreement with literature data [Williams TJ et al, 2014]. Aryl substituted tryptophan in position 2 have been previously synthesized *via* Pd-catalyzed Suzuki–Miyaura cross-coupling [Williams TJ et al, 2014]. Taking these unnatural amino acids as a model for a tyrosyl-tryptophan cross-coupling product, their UV-Vis and fluorescence spectral features fairly correlate with our results, thus suggesting that a cross-coupled aromatic moiety is produced upon laser irradiation.

CD analyses gave further insights into the molecular mechanism occurring after cross-coupling. The lower intensities of the positive and negative bands in the far-UV region, upon laser irradiation, can be related to a decrease in the secondary structure content, or to a change in the oligomerization state, as already reported for GAPDH [Pappenberger G et al, 1997; He RQ et al, 1995]. A more evident decrease in spectrum amplitude is observed in the near-UV region, further confirming that aromatic residues are involved in the cross-coupling event. The observed CD variations are generally interpreted as a partial transition to a molten globule state [Fasman GD, 1996], which in the case of the GAPDH has been correlated with a lower oligomerization state [Pappenberger G et al, 1997; He RQ et al, 1995]. It can be argued that the observed changes in the CD signals are related to degenerative oxidative processes, triggered by the laser *in vitro*, differently from what observed in living cells. The decrease of the near-UV signal amplitude has been indeed reported for GAPDH, after exposure to chemical oxidative stress [Nakajima H et al, 2009] and it has been related to non-native amyloid-like aggregates. In that case, differently from our results, such a decrease in the near-UV region was accompanied by an increased signal amplitude in far-UV region. Our results well fit with a mechanism of tetramer destabilization upon covalent dimer formation. In conclusion, the results herein reported strongly confirm the formation of specific cross-linked species through aromatic residues triggered by laser irradiation.

Since this novel methodology needs to be validated and deeply characterized, the second part of the project was aimed at the setting up of an experimental system

based on FLIM-FRET microscopy suitable to support and to perform a spatio-temporal characterization of the interactions weld by UV laser irradiation. This experimental system was set up by performing experiments on membrane cholesterol distribution in two different cell lines in collaboration with Prof. Chiara Zurzolo, Institut Pasteur, Paris.

By measuring the lifetime of a cholesterol fluorescent probe, *i.e.* TopFluorcholesterol, in the presence or in the absence of actin perturbation, we demonstrated that the membrane environment of epithelial cells and fibroblasts are significantly different. Indeed, FLIM experiments clearly indicate that, in the case of fibroblasts, cholesterol probe lifetime significantly decreases upon actin perturbation. This was not observed in the case of polarized epithelial cells.

Moreover, we used this probe as the fluorescent donor to perform FLIM-FRET experiments with glycosylphosphatidylinositol-anchored proteins (GPI-APs) as acceptors, *i.e.* mCherry-PLAP. By this technique, it is possible to accurately monitor FRET occurrence between the donor- and acceptor-labeled proteins by measuring the donor lifetime in the presence and absence of the acceptor. By this way, we observed FRET occurrence between membrane cholesterol and mCherry-PLAP in fibroblasts. Moreover, this interaction was found to be affected by actin perturbation, since FRET occurrence was found to significantly decrease upon latrunculin treatment.

Our aim is that of using this technique to validate and spatio-temporally characterize PPIs that will be “photo-fixed” by our innovative system. The UV laser procedure herein proposed is a fast, reproducible and controlled process. It is fast, as the time needed for cross-linking induction is much shorter (seconds) than that required for conventional methodologies applied to living cells. It is a reproducible and controlled process, as the energy dose can be modulated accurately to optimize cross-linking in a given experimental system.

The linear response of protein-protein cross-linking in living cells to the laser intensity let us to highlight that the cross-linking event is triggered by the absorption of a single UV laser photon by aromatic side chains. This makes the process basically different from that occurring in the case of protein-DNA photoinduced cross-linking, from a microscopic point of view. For DNA-protein cross-linking, in fact, the reaction proceeds in two steps: 1. bi-photonic UV light absorption [Nikogosyan DN, 1990] and excitation of the DNA bases, in the nanosec-, picosec- or even femtosec-time scale; 2. cross-linking with proteins interacting with the DNA excited site and therefore lying nearby (zero-length cross-linking), which is completed in less than 1 millisec [Nikogosyan DN, 1990].

It is also important underlying the reproducibility and high cross-linking efficiency of this novel technique as compared to many of the presently available alternatives, based on the use of chemicals. The yield of the cross-linked products was found to be about 10%, suggesting that 10% of total GAPDH chains are cross-linked as dimers upon UV laser irradiation. Based on this observation, our method turns out to be approximately 5 times more efficient than that typically obtained with conventional formaldehyde cross-linking [Valadan M et al, 2015], and it is comparable to the efficiency of recently developed single-molecular-interaction sequencing (SMI-seq) technology for *in vitro* analyses [Gu L et al, 2014]. Therefore, the impact of this novel methodology will be relevant both in the generation of scientific knowledge and insight as well as in practical applications. It has the potentiality to become a universal technique to photo-fix protein interactions, as in

principle it may be applicable to any biological context, such as the intracellular milieu of living cells, to unveil protein-protein interactions in a native context.
Due to the ultra-short time scale of UV laser induced cross-linking, this technique might allow to unveil transient interactions between proteins in a native context, differently from most of the methods based on the chemical induction of bonds between partners. Hence, this approach might have a great impact in terms of elucidation of fundamental biological processes and identification of potential key targets of biotechnological relevance.

REFERENCES

Aebersold R & Goodlett DR, **Mass spectrometry in proteomics**. (2001) Chem Rev. 101 (2): 269-295.

Aebersold R & Mann M, **Mass spectrometry-based proteomics**. (2003) Nature. 422 (6928): 198-207.

Alexander P & Moroson H, **Cross-linking of deoxyribonucleic acid to protein following ultra-violet irradiation different cells**. (1962) Nature. 194: 882-883.

Altucci C et al, **Nonlinear protein – nucleic acid crosslinking induced by femtosecond UV laser pulses in living cells**. (2012) Laser Phys Lett. 9: 234-239.

Angelov D et al, **Solution study of the NF-kappaB p50-DNA complex by UV laser protein-DNA cross-linking**. (2003) Photochem Photobiol. 77 (6): 592-596.

Ashmarina LI et al, **Phosphorylation of D-glyceraldehyde-3-phosphate dehydrogenase by Ca2+/calmodulin-dependent protein kinase II**. (1988) FEBS Lett. 231 (2): 413-416.

Bacskai et al, **Fluorescence resonance energy transfer determinations using multiphoton fluorescence lifetime imaging microscopy to characterize amyloid-beta plaques**. (2003) J Biomed Opt. 8 (3): 368-3675.

Bastiaens PI & Squire A, **Fluorescence lifetime imaging microscopy: spatial resolution of biochemical processes in the cell**. (1999) Trends Cell Biol. 9 (2): 48-52.

Baxi MD & Vishwanatha JK, **Uracil DNA-glycosylase/glyceraldehyde-3-phosphate dehydrogenase is an Ap4A binding protein**. (1995) Biochemistry. 34 (30): 9700-9707.

Berry MD, **Glyceraldehyde-3-phosphate dehydrogenase as a target for small-molecule disease-modifying therapies in human neurodegenerative disorders**. (2004) J Psychiatry Neurosci. 29 (5): 337-345.

Boeri Erba E et al, **Combining a NHS ester and glutaraldehyde improves crosslinking prior to MALDI MS analysis of intact protein complexes**. (2015) J Mass Spectrom. 50 (10): 1114-1119.

Boyd RW, **Nonlinear optics**. (2008) Elsevier Academic Press.

Bryksin AV & Laktionov PP, **Role of glyceraldehyde-3-phosphate dehydrogenase in vesicular transport from golgi apparatus to endoplasmic reticulum**. (2008) Biochemistry (Mosc). 73 (6): 619-625.

Buser C & McDonald K, **Correlative GFP-immunoelectron microscopy in yeast**. (2010) Methods Enzymol. 470: 603-618.

Carr A & Biggin MD, **An in vivo UV crosslinking assay that detects DNA binding by sequence-specific transcription factors**. (1999) Methods Mol Biol. 119: 497-508.

Chowdhury SM et al, **Identification of cross-linked peptides after click-based enrichment using sequential collision-induced dissociation and electron transfer dissociation tandem mass spectrometry**. (2009) Anal Chem. 81 (13): 5524-5532.

Chu F et al, **Isotope-coded and affinity-tagged cross-linking (ICATXL): an efficient strategy to probe protein interaction surfaces**. (2006) J Am Chem Soc. 128 (32): 10362-10363.

Chuang DM et al, **Glyceraldehyde-3-phosphate dehydrogenase, apoptosis, and neurodegenerative diseases**. (2005) Annu Rev Pharmacol Toxicol. 45: 269-290.

Chubinskiy-Nadezhdin VI et al, **Functional impact of cholesterol sequestration on actin cytoskeleton in normal and transformed fibroblasts**. (2013) Cell Biol Int. 37 (6): 617-623.

Clarke FM & Morton DJ, **Glycolytic enzyme binding in fetal brain-the role of actin**. (1982) Biochem Biophys Res Commun. 109 (2): 388-393.

Davies MJ et al, **Electron spin resonance and pulse radiolysis studies on the spin trapping of sulphur-centered radicals**. (1987) Chem Biol Interact. 61 (2): 177-188.

Dimitrov SI & Moss T, **UV laser-induced protein-DNA crosslinking**. (2001) Methods Mol Biol. 148: 395-402.

Elangovan et al, **Dynamic imaging using fluorescence resonance energy transfer**. (2002) Biotechniques. 32 (6): 1260-1262, 1264-1265.

Elion EA, **Detection of protein-protein interactions by coprecipitation**. (2006) Curr Protoc Mol Biol. Chapter 20: Unit 20.5.

Engel M et al, **Glyceraldehyde-3-phosphate dehydrogenase and Nm23-H1/nucleoside diphosphate kinase A. Two old enzymes combine for the novel Nm23 protein phosphotransferase function**. (1998) J Biol Chem. 273 (32): 20058-20065.

Fasman GD, **Circular dichroism and the conformational analysis of biomolecules**. (1996) Springer Science & Business Media, New York.

Förster T, (1965). **Modern Quantum Chemistry**. Sinanoglu O Ed. New York and London: Academic Press. 93–137.

Goswami et al, **Nanoclusters of GPI-anchored proteins are formed by cortical actin-driven activity**. (2008) Cell. 135 (6): 1085-1097.

Greenberg JR, **Ultraviolet light-induced crosslinking of mRNA to proteins**. (1979) Nucleic Acids Res. 6 (2): 715-732.

Gu L et al, **Multiplex single-molecule interaction profiling of DNA-barcoded proteins**. (2014) Nature. 515 (7528): 554-557.

Guerrero C et al, **An integrated mass spectrometry-based proteomic approach: quantitative analysis of tandem affinity-purified in vivo cross-linked protein complexes (QTAX) to decipher the 26 S proteasome-interacting network**. (2006) Mol Cell Proteomics. 5: 366–378.

Guerrero C et al, **Characterization of the proteasome interaction network using a QTAX-based tag-team strategy and protein interaction network analysis**. (2008) Proc Natl Acad Sci U S A. 105 (36): 13333-13338.

Hara MR et al, **GAPDH as a sensor of NO stress**. (2006) Biochim Biophys Acta. 1762 (5): 502-509.

He RQ et al, **Inactivation and conformation changes of the glycated and non-glycated D-glyceraldehyde-3-phosphate dehydrogenase during guanidine-HCl denaturation**. (1995) Biochim Biophys Acta. 1253: 47–56.

Huber G et al. **Solid-state lasers: status and future**. (2010) J Opt Soc America. 27 (11): B93.

Ikezawa H, **Glycosylphosphatidylinositol (GPI)-anchored proteins**. (2002) Biol Pharm Bull. 25 (4): 409-417.

Imjeti NS et al, **N-Glycosylation instead of cholesterol mediates oligomerization and apical sorting of GPI-APs in FRT cells**. (2011) Mol Biol Cell. 22 (23): 4621-4634.

Ishikawa-Ankerhold HC et al, **Advanced fluorescence microscopy techniques--FRAP, FLIP, FLAP, FRET and FLIM**. (2012) Molecules. 17 (4): 4047-4132

Jenkins JL &Tanner JJ, **High-resolution structure of human D-glyceraldehyde-3-phosphate dehydrogenase**. (2006) Acta Crystallogr D Biol Crystallogr. 62 (Pt 3): 290-301.

Jones S & Thornton JM, **Principles of protein-protein interactions**. (1996) Proc Natl Acad Sci U S A. 93 (1): 13-20.

Kaake RM et al, **Profiling of protein interaction networks of protein complexes using affinity purification and quantitative mass spectrometry**. (2010) Mol Cell Proteomics. 9 (8): 1650-1665.

Kaake RM et al, **A new in vivo cross-linking mass spectrometry platform to define protein-protein interactions in living cells**. (2014) Mol Cell Proteomics. 13 (12): 3533–3543.

Kocher T & Superti-Furga G, **Mass spectrometry-based functional proteomics: from molecular machines to protein networks**. (2007) Nat Methods. 4 (10): 807-815.

Krishnan RV et al, **Quantitative imaging of protein-protein interactions by multiphoton fluorescence lifetime imaging microscopy using a streak camera**. (2003) J Biomed Opt. 8 (3): 362-367.

Kwik J et al, **Membrane cholesterol, lateral mobility, and the phosphatidylinositol 4,5-bisphosphate-dependent organization of cell actin**. (2003) Proc Natl Acad Sci U S A. 100 (24): 13964-13699.

Lander ES et al, **Initial sequencing and analysis of the human genome**. (2001) Nature. 409 (6822): 860-921.

Leinisch F et al, **Evaluation of the Forrester-Hepburn mechanism as an artifact source in ESR spin-trapping**. (2011) Chem Res Toxicol. 24 (12): 2217-2226.

Leitner A et al, **Probing native protein structures by chemical cross-linking, mass spectrometry, and bioinformatics**. (2010) Mol Cell Proteomics. 9 (8): 1634-1649.

Lejnine S et al, **Crosslinking of proteins to DNA in human nuclei using a 60 femtosecond 266 nm laser**. (1999) Nucleic Acids Res. 27 (18): 3676-3684.

Leo G et al, **Ultraviolet laser-induced cross-linking in peptides**. (2013) Rapid Commun Mass Spectrom. 27 (14): 1660-1668.

Lind C et al, **Studies on the mechanism of oxidative modification of human glyceraldehyde-3-phosphate dehydrogenase by glutathione: catalysis by glutaredoxin**. (1998) Biochem Biophys Res Commun. 247 (2): 481-486.

Liu BA et al, **High-throughput analysis of peptide-binding modules**. (2012) Proteomics. 12 (10): 1527-1546.

McConville MJ & Menon AK, **Recent developments in the cell biology and biochemistry of glycosylphosphatidylinositol lipids**. (2000) Mol Membr Biol. 17 (1): 1-16.

Meisenheimer KM & Koch TH, **Photocross-linking of nucleic acids to associated proteins**. (1997) Crit Rev Biochem Mol Biol. 32 (2): 101-140.

Mizdrak J et al, **Tryptophan-derived ultraviolet filter compounds covalently bound to lens proteins are photosensitizers of oxidative damage**. (2008) Free Radic Biol Med. 44 (6): 1108-1119.

Morone N et al, **Three-dimensional reconstruction of the membrane skeleton at the plasma membrane interface by electron tomography**. (2006) J Cell Biol. 174 (6): 851-862.

Morton W et al, **Latrunculin alters the actin-monomer subunit interface to prevent polymerization**. (2000) Nat Cell Biol. 2: 376–378.

Moss T et al, **UV-laser crosslinking of proteins to DNA**. (1997) Methods. 11 (2): 225-234.

Murase K et al, **A membrane-anchored protein kinase involved in Brassica self-incompatibility signaling**. (2004) Science. 303 (5663): 1516-1519.

Nakagawa K, **Direct observation of laser generated free radicals from a myocardium target site**. (1992) Free Radic Biol Med. 12 (3): 241-242.

Nakagawa K, **Pulsed UV laser generated short-lived free radicals from biological samples**. (1993) Free Radic Res Commun. 18 (4): 223-227.

Nakajima H et al, **Glyceraldehyde-3-phosphate dehydrogenase aggregate formation participates in oxidative stress-induced cell death**. (2009) J Biol Chem. 284 (49): 34331-34341.

Nikogosyan DN, **Two-quantum UV photochemistry of nucleic acids: comparison with conventional low-intensity UV photochemistry and radiation chemistry**. (1990) Int J Radiat Biol. 57 (2): 233-299.

Nooren IM & Thornton JM, **Diversity of protein-protein interactions**. (2003) EMBO J. 22 (14): 3486-3492.

Orlean P & Menon AK, **Thematic review series: lipid posttranslational modifications. GPI anchoring of protein in yeast and mammalian cells, or: how we learned to stop worrying and love glycophospholipids**. (2007) J Lipid Res. 48 (5): 993-1011.

Padilla-Parra S et al, **Quantitative FRET analysis by fast acquisition time domain FLIM at high spatial resolution in living cells**. (2008) Biophys J. 95 (6): 2976-2988.

Padilla-Parra S et al, **Quantitative comparison of different fluorescent protein couples for fast FRET-FLIM acquisition**. (2009) Biophys J. 97 (8): 2368-2376.

Padilla-Parra S & Tramier M, **FRET microscopy in the living cell: different approaches, strengths and weaknesses**. (2012) Bioessays. 34 (5): 369-376.

Paladino S et al, **Protein oligomerization modulates raft partitioning and apical sorting of GPI-anchored proteins**. (2004) J Cell Biol. 167 (4): 699-709.

Paladino S et al, **Golgi sorting regulates organization and activity of GPI proteins at apical membranes**. (2014) Nat Chem Biol. 10 (5): 350-357.

Paladino S et al, **Trafficking and Membrane Organization of GPI-Anchored Proteins in Health and Diseases**. (2015) Curr Top Membr. 75: 269-303.

Panchaud A et al, **xComb: a cross-linked peptide database approach to protein-protein interaction analysis**. (2010) J Proteome Res. 9 (5): 2508-2515.

Pappenberger G et al, **Disruption of an ionic network leads to accelerated thermal denaturation of D-glyceraldehyde-3-phosphate dehydrogenase from the hyperthermophilic bacterium Thermotoga maritima**. (1997) J Mol Biol. 274: 676–683.

Paschotta R, **Field Guide to Lasers**. (2008) SPIE Press.

Patterson RL et al, **Inositol 1,4,5-trisphosphate receptor/GAPDH complex augments Ca2+ release via locally derived NADH**. (2005) Proc Natl Acad Sci U S A. 102 (5): 1357-1359.

Pattison DI et al, **Photo-oxidation of proteins**. (2012) Photochem Photobiol Sci. 11 (1): 38-53.

Piston DW & Kremers G, **Fluorescent protein FRET: the good, the bad and the ugly**. (2007) Trends Biochem Sci. 32 (9): 407-414.

Rinner O et al, **Identification of cross-linked peptides from large sequence databases**. (2008) Nat Methods. 5 (4): 315-318.

Rotili D et al, **A photoreactive small-molecule probe for 2-oxoglutarate oxygenases**. (2011) Chem Biol. 18 (5): 642-654.

Russmann C et al, **Crosslinking of progesterone receptor to DNA using tuneable nanosecond, picosecond and femtosecond UV laser pulses**. (1997) Nucleic Acids Res. 25 (12): 2478-2484.

Russmann C et al, **Two wavelength femtosecond laser induced DNA-protein crosslinking**. (1998) Nucleic Acids Res. 26 (17): 3967-3970.

Shaner NC et al, **A guide to choosing fluorescent proteins**. (2005) Nat Methods. 2 (12): 905-909.

Shrestha D et al, **Understanding FRET as a research tool for cellular studies**. (2015) Int J Mol Sci. 16 (4): 6718-6756.

Sinz A, **Chemical cross-linking and mass spectrometry to map three-dimensional protein structures and protein-protein interactions**. (2006) Mass Spectrom Rev. 25 (4): 663-682.

Sioud M & Jespersen L, **Enhancement of hammerhead ribozyme catalysis by glyceraldehyde-3-phosphate dehydrogenase**. (1996) J Mol Biol. 257 (4): 775-789.

Sirover MA, **New insights into an old protein: the functional diversity of mammalian glyceraldehyde-3-phosphate dehydrogenase**. (1999) Biochim Biophys Acta. 1432 (2): 159-184.

Sirover MA, **Structural analysis of glyceraldehyde-3-phosphate dehydrogenase functional diversity**. (2014) Int J Biochem Cell Biol. 57: 20-26.

Solomon MJ et al, **Mapping protein-DNA interactions in vivo with formaldehyde: evidence that histone H4 is retained on a highly transcribed gene**. (1988) Cell. 53 (6): 937-947.

Stumpf MP et al, **Estimating the size of the human interactome**. (2008) Proc Natl Acad Sci U S A. 105 (19): 6959-6964.

Subbotin RI & Chait BT, **A pipeline for determining protein-protein interactions and proximities in the cellular milieu**. (2014) Mol Cell Proteomics. 13 (11): 2824-2835.

Suchanek M et al, **Photo-leucine and photo-methionine allow identification of protein-protein interactions in living cells**. (2005) Nat Methods. 2 (4): 261–267.

Sun G et al, **DNA-protein cross-linking: model systems for pyrimidine-aromatic amino acid cross-linking**. (2006) Org Lett. 8 (4): 681-683.

Sun Y et al, **Investigating protein-protein interactions in living cells using fluorescence lifetime imaging microscopy**. (2011) Nat Protoc. 6 (9): 1324-1340.

Sutherland BW et al, **Utility of formaldehyde cross-linking and mass spectrometry in the study of protein-protein interactions**. (2008) J Mass Spectrom. 43 (6): 699-715.

Tarze A et al, **GAPDH, a novel regulator of the pro-apoptotic mitochondrial membrane permeabilization**. (2007) Oncogene. 26 (18): 2606-2620.

Tomokuni Y et al, **Loose interaction between glyceraldehyde-3-phosphate dehydrogenase and phosphoglycerate kinase revealed by fluorescence resonance energy transfer-fluorescence lifetime imaging microscopy in living cells**. (2010) FEBS J. 277 (5): 1310-1318.

Tristana C et al, **The diverse functions of GAPDH: views from different subcellular compartments**. (2011) Cell Signal. 23 (2): 317-323.

Tsien RY, **The green fluorescent protein**. (1998) Annu Rev Biochem. 67:509-544.

Valadan M et al, **Temporal and spectral characterization of femtosecond deep-UV chirped pulses**. (2015) Laser Phys Lett 12 (2): 025302.

Van Munster EB & Gadella TW Jr, **phiFLIM: a new method to avoid aliasing in frequency-domain fluorescence lifetime imaging microscopy**. (2004) J Microsc. 213 (Pt 1): 29-38.

Vidal M & Fields S, **The yeast two-hybrid assay: still finding connections after 25 years**. (2014) Nat Methods. 11 (12): 1203-1206.

Volker KW & Knull H, **A glycolytic enzyme binding domain on tubulin**. (1997) Arch Biochem Biophys. 338 (2): 237-243.

Walsh JL & Knull HR, **Heteromerous interactions among glycolytic enzymes and of glycolytic enzymes with F-actin: effects of poly(ethylene glycol)**. (1988) Biochim Biophys Acta. 952 (1): 83-91.

Walzthoeni T et al, **False discovery rate estimation for cross-linked peptides identified by mass spectrometry**. (2012) Nat Methods. 9 (9): 901-903.

Weisbrod CR et al, **In vivo protein interaction network identified with a novel real-time cross-linked peptide identification strategy**. (2013) J Proteome Res. 12 (4): 1569-1579.

Williams TJ et al, **A mild and selectivePd-mediated methodology for the synthesis of highly fluorescent 2-arylated tryptophans and tryptophan-containing peptides: a catalytic role for Pd(0) nanoparticles?** (2014) Chem Commun (Camb). 50: 3052–3054.

Wong SS & Jameson DM, **Chemistry of protein and nucleic acid and cross-linking and conjugation**. (2012) 2nd edition. Taylor & Francis.

Yang B et al, **Identification of cross-linked peptides from complex samples**. (2012) Nat Methods. 9 (9): 904-906.

Zhang H et al, **Identification of protein-protein interactions and topologies in living cells with chemical cross-linking and mass spectrometry**. (2009) Mol Cell Proteomics. 8(3): 409-420.

Zhang L et al**, Detecting DNA-binding of proteins in vivo by UV-crosslinking and immunoprecipitation**. (2004) Biochem Biophys Res Commun. 322 (3): 705-711.

Zheng L et al, **S phase activation of the histone H2B promoter by OCA-S, a coactivator complex that contains GAPDH as a key component**. (2003) Cell. 114 (2): 255-266.

APPENDIX

List of Pubblications:

- Fulgione D, Trapanese M, Maselli V, Rippa D, Itri F, Avallone B, Van Damme R, Monti DM & Raia P, **Seeing through the skin: dermal light sensitivity provides cryptism in moorish gecko**. (2014) J Zool. 294 (2): 122-128.

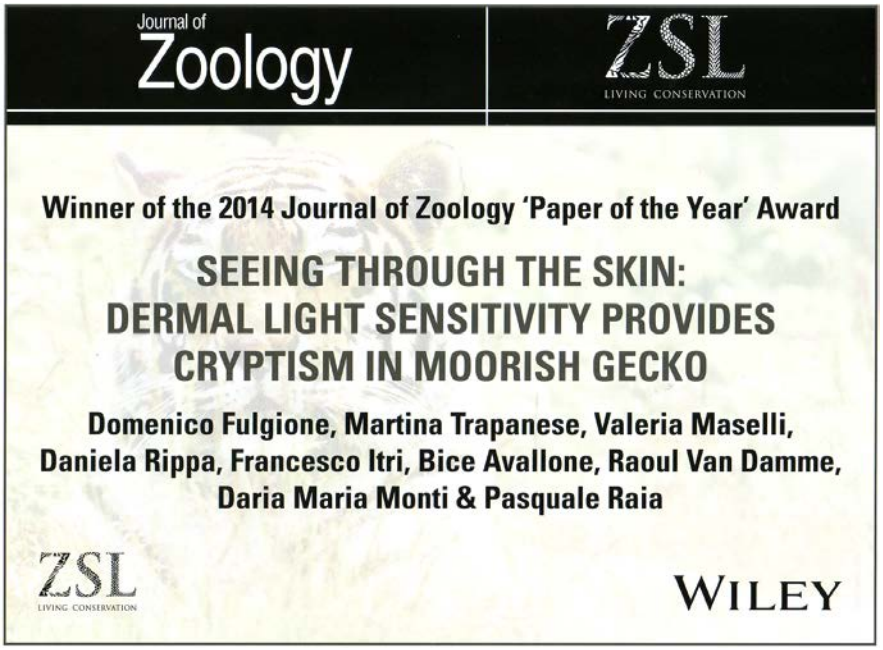

- Itri F, Monti DM, Della Ventura B, Vinciguerra R, Chino M, Gesuele F, Lombardi A, Velotta R, Altucci C, Birolo L, Piccoli R, Arciello A, **Femtosecond UV-laser pulses to unveil protein-protein interactions in living cells**. (2015) Cell Mol Life Sci. 73 (3): 637-648.

- Del Giudice R, Arciello A, Itri F, Merlino A, Monti M, Buonanno M, Penco A, Canetti D, Petruk G, Monti SM, Relini A, Pucci P, Piccoli R, Monti DM, **Protein conformational perturbations in hereditary amyloidosis: Differential impact of single point mutations in ApoAI amyloidogenic variants**. (2015) Biochim Biophys Acta. 1860 (2): 434-444.

List of Communications:

- Del Giudice R, Monti DM, Arciello A, Itri F, Piccoli R, **A comparative analysis of two amyloidogenic variants of ApoA-I**. (Naples 2014) Biophysics of Amyloids and Prions.

- Fulgione D, Trapanese M, Maselli V, Rippa D, Itri F, Avallone B, Van Damme R, Monti DM, Raia P, **Seeing through the skin: dermal light sensitivity provides cryptism in moorish gecko**. (Pisa, 2014) FISV, Federazione Italiana Scienze della Vita.

- Itri F, Del Giudice R, Arciello A, Piccoli R, Monti DM, **Structural perturbations in hereditary amyloidosis: the case of two variants of apoA-I**. (Pisa, 2014) FISV, Federazione Italiana Scienze della Vita.

- Gaglione R, Itri F, Pane K, Cafaro V, Piccoli R, Notomista E, Arciello A, **Identification and characterization of novel cryptic cationic antimicrobial peptides from human ApoB**. (Urbino, 2015) SIB, 58th National Meeting of th Italian Society of Biochemistry and Molecular Biology.

Research activity in scientific Institutions abroad

From September 15th to October 15th, 2015, the research activity of Dr. Itri has been carried out at the Institut Pasteur, Paris (France), in the laboratory of the "Unitè de Trafic membranaire et Pathogenèse". The work was supervised by Prof. Zurzolo.

From October 16th to December 15th, 2015, the research activity of Dr. Itri has been carried out at the University of Rennes 1, Rennes (France), in the laboratory of the "Département Biologie Cellulaire et Developpement". The work was supervised by Prof. Tramier.

Institut Pasteur

Unité Postulante de Trafic
Membranaire et Pathogenèse

This is to certify that Mr. Francesco Itri, Researcher at University of Naples "Federico II" (Italy) carried out research at Institut Pasteur, Paris (France), in the "Unitè de Trafic membranaire et Pathogenèse" Laboratory for the period from 15/09/2015 to 15/10/2015.

During his time at Institut Pasteur he worked in the lab of Professor Chiara Zurzolo.

Date

02 February 2016

Sincerely,

Chiara ZURZOLO

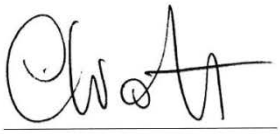

Département Biologie cellulaire
et Infection

25-28, Rue du Docteur Roux
75724 Paris Cedex 15
Téléphone: +33 (0)1 45 68 82 77
Télécopie: +33 (0)1 40 61 32 38

UMR 6290 CNRS – UR1
igdr.univ-rennes1.fr
Faculté de Médecine
2 avenue du Professeur Léon Bernard
CS 34317, 35043 Rennes cedex, France
marc.tramier@univ-rennes1.fr
T. +33 (0)2 23 23 54 87
F. +33 (0)2 23 23 44 78

Francesco Itri certificate

This is to certify that Mr. Francesco Itri, Researcher at University of Naples "Federico II" (Italy) carried out research at Rennes (France) for the period from 15/10/2015 to 15/12/2015, in the "Institut de Génétique et Développement de Rennes" supported by CNRS and Université de Rennes 1.

During his time at University of Rennes 1 he worked in my lab.

Rennes, January 27th 2016.

Marc Tramier
PI « Microscopie de Fluorescence Quantitative » team

Sous la tutelle de

ACKNOWLEDGMENTS

First of all, I would like to thank my supervisor, Prof. Renata Piccoli. She has been a fundamental and essential guide during my work experience in her lab.

I wish to express my gratitude to Prof. Chiara Zurzolo and Prof. Marc Tramier to give me the opportunity to work in their laboratories.
Moreover, I would like to thank Dr. Stéphanie Lebreton to support me during my experience in France with her knowledge and advices.

I extend special thanks to Dr. Angela Arciello and to Dr. Daria Maria Monti who always supported and encouraged me with their precious teachings since my master degree.

I would like to thank all my old and new lab colleagues, especially Rosa and Anna, for the time spent together during these years. In particular, I wish to thank Dr. Rita Del Giudice who helped me since my first day in the laboratory.

Special thanks are due to the head of the PhD school in Biotechnology, Prof. Giovanni Sannia, as he motivated all the PhD students to do their best.

Finally, I wish to express my special thanks to my family and all my friends for supporting me at all times.

Journal of Zoology

Journal of Zoology. Print ISSN 0952-8369

Seeing through the skin: dermal light sensitivity provides cryptism in moorish gecko

D. Fulgione[1], M. Trapanese[1], V. Maselli[1], D. Rippa[1], F. Itri[2], B. Avallone[1], R. Van Damme[3], D. M. Monti[2] & P. Raia[4]

1 Department of Biology, University of Naples Federico II, Naples, Italy
2 Department of Chemical Sciences, University of Naples Federico II, Naples, Italy
3 Department of Biology, University of Antwerp, Antwerp, Belgium
4 Department of Earth Science, Environment and Resources, University of Naples Federico II, Naples, Italy

Keywords
cryptism; moorish gecko; body colouration; reptile; dermal photosensitivity; opsin; camouflage.

Correspondence
Domenico Fulgione, Department of Biology, University of Naples Federico II, Via Cinthia MSA, Naples, Italy. Email: fulgione@unina.it

Editor: Mark-Oliver Rödel

Received 14 May 2014; revised 30 May 2014; accepted 31 May 2014

doi:10.1111/jzo.12159

Abstract

Concealment by means of colour change is a pre-eminent deceptive mechanism used by both predators and prey. The moorish gecko *Tarentola mauritanica* is able to blend into the background by either darkening or paling according to the substrate darkness. Here we examined the functioning of background perception in moorish gecko. We experimentally excluded the involvement of melanophore-stimulating hormone in camouflage. Blindfolded individuals change their colour consistently with the background. Surprisingly, individuals with covered flanks were not able to change colour, no matter whether they were allowed to see the substrate or not. Accordingly, we found high levels of opsin transcript and protein in the flank region of the gecko. These observations suggest that *T. mauritanica* skin melanophores are able to activate a process of colour change autonomously. This study yields the first evidence of crypsis mediated by dermal light sensitivity in amniotes.

Introduction

It has long been recognized that camouflage through background colour matching is an important adaptation that helps prey to evade predators and predators to ambush prey (Cott, 1940; Darwin, 1974; Wallace, 1985; Stevens & Merilaita, 2011). Although animals living in stable and uniform habitats can achieve concealment by fixed colours or colour patterns, a more flexible camouflage system is better suited when background colours exhibit spatial or temporal heterogeneity, or when concealment conflicts with other functions of integumentation, such as communication, or thermoregulation (Stuart-Fox & Moussalli, 2009). Many animals change their own body colour in response to ontogenetic or seasonal variation in the environment. Yet, the most spectacular examples of camouflage occur in species that modify their body colour within minutes or even seconds. Famous examples include octopuses, which alter their colour pattern within fractions of a second (Hanlon, Forsythe & Joneschild, 1999; Hanlon *et al*., 2009) as well as in fiddler crabs (Thurman, 1988; Llandres *et al*., 2013). Rapid colour change, serving social display, was reported in African dwarf chameleons (Stuart-Fox, Whiting & Moussalli, 2006; Stuart-Fox & Moussalli, 2008).

Although 'fixed' concealment colours could be explained by simple fixation of particular colour patterns by means of natural selection (Norris & Lowe, 1964), rapid camouflage requires that the animal somehow perceives its environment and adequately adjusts its colour. In previous experiments, we showed that the moorish gecko *Tarentola mauritanica* adjusts its skin darkness to match the substrate tone, and requires light to achieve this goal (Vroonen *et al*., 2012). Light triggering possibly acts directly on skin melanophores, or indirectly through autonomic or humoral responses (Cooper & Greenberg, 1992; Oshima, 2001). However, the scientific literature is quiet on which stimuli and perceptual systems are involved in the assessment of background colouration, particularly in lizards.

Darkening in moorish gecko might be a general response involving the activation of melanophores via alpha-melanophore-stimulating hormone (α-MSH), or under nervous control as in chameleons (Stuart-Fox, Moussalli & Whiting, 2008). Alternatively, darkening might be a local response exerted directly by melanophores (i.e. without any involvement of either the nervous or endocrine system). The perception of background shade change should have an almost instantaneous effect if the nervous system is involved, whereas colour change mediated by either the endocrine system or local cell response happens within minutes to hours (Fujii, 2000; Ban *et al*., 2005). Which of these systems, or combination of, affects melanophores functioning in the moorish gecko is unknown.

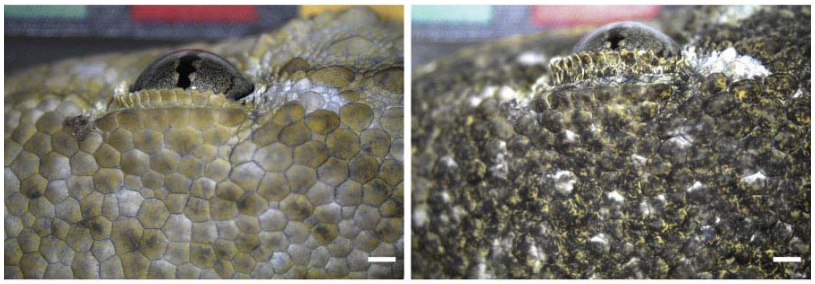

Figure 1 Change in colour of moorish gecko's skin surface. Images show the same spot of the gecko on light substrate (left) and on dark substrate (right). Scale bar = 1 mm.

Here, we address the question of how the moorish gecko obtains and processes information on background shading to modify its body colour. We specifically tested the contribution of the eyes, the central nervous system and the endocrine system in detection of light reflectance by the substrate.

Our results suggest that moorish gecko uses a previously unreported system based on dermal light sensitivity to perceive background coloration.

Material and methods

Sampling

We caught 40 *T. mauritanica* individuals by noose near Cilento, Italy (40°15′N, 14°54′E). During field work, we repeatedly observed the presence of barn owl *Tyto alba* as well as other predators that usually affect gecko population (Costantini *et al.*, 2005; Roulin & Dubey, 2012).

After experimentation, 30 individuals were released at the point of capture and 10 individuals were sacrificed for tissue analysis.

The animals were collected with the permissions from the county authorities (Cilento, Vallo di Diano and Alburni National Park prot. 0010678/ 2013). The animals were kept according to ministerial authorization (prot. 165/2006). The experiment was approved by the Ethical Committee for Animal Experiments University of Naples Federico II (ID: 2013/0096988) and according to Italian law (DL 116/92).

Skin reflectance

The animals' body colouration was determined by spectrophotometry on 15 individuals (Avantes, AvaSpec – 2048-USB2-UA-50, 250–1000 nm). The measurement probe was held perpendicular to the body surface. The diameter of the spectrophotometer hole probe end covers an area (0.2 mm) smaller than the surface of a single scale (see Fig. 1).

A reference percentage tile (R%) was assayed among each individual. Geckos' dorsal skin coloration was measured by the reflectance at six positions: (1) on the head; (2) between the forelimbs; (3) mediosagital; (4) mediolateral left and (5) right; and (6) between the hind limbs. Reflectance for wavelengths was considered between 300 and 700 nm (according to Vroonen *et al.*, 2012). The average of the integrals subtended the reflectance curve within the range of wavelength considered was assumed to be representative of the whole back.

Enzyme-linked immunosorbent assay (ELISA) detection of α-MSH

To test the idea that darkening in the moorish gecko involves the activation of melanine production in melanophores by α-MSH (i.e. via the endocrine system), we determined hormonal variation in individual geckos before and after the experimental induction of skin darkening. α-MSH levels in gecko sera were determined by ELISA assay, as described in Monti *et al.* (2013). For α-MSH assay, a blood sample of *c.* 50 μL was taken from the tail vein. Each sample was fractionated by centrifugation at 2300 g. for 15 min. The individual variation in α-MSH levels under the two light conditions was compared by means of paired *t*-test.

Testing light sensitivity of different body regions

We tested different body regions for light sensitivity. At the beginning of each trial, the gecko individual was placed in a small terrarium (15.5 × 25 × 18 cm). The bottom and adjacent sides of the terrarium were covered with either black or white paper (white or black box, substrate colour treatment). The top side was left transparent. The terrarium was then placed in a large incubator (Mir253; Sanyo, Bensenville, IL, USA) at 30°C. After 3 h, the gecko was removed from the incubator and its dorsal skin reflectance was measured immediately. Geckos were handled as little as possible to avoid colour changes due to stress: spectrophotometric measurements were collected in less than a minute.

To assess the contribution of the eyes to the perception of background colour, we performed experimental trials with blindfolded animals. In particular, for every gecko tested, measurements were performed in the absence of bandages, by bandaging the gecko's eyes or by covering the animal's thorax (body treatment). On each gecko the experiment was performed at least twice. Fifteen different *T. mauritanica* individuals were tested overall.

Gene expression of photosensitive protein SWS1 in gecko

We tested for gene expression of photosensitive protein SWS1 in gecko. In many vertebrates, the perception of substrate colour via the skin (rather than the eyes) was found to be local (i.e. based on direct action of the melanophores, Bagnara, 1957; Van Der Lek *et al.*, 1958; Oshima *et al.*, 1998). In the eye tissue of other gekkonids (i.e. tokay gecko, *Gekko gecko*), photosensitive pigments such as SWS1 (short wavelength-sensitive opsin) were observed (Kojima *et al.*, 1992; Loew, 1994). SWS1 opsin is sensitive to short wavelengths and is therefore expected to be present in *T. mauritanica* eyes. In order to measure the amount of SWS1 opsin present in each analysed tissue sample, we performed a semi-quantitative reverse transcriptase polymerase chain reaction (RT-PCR) on SWS1 mRNA. To obtain specific primers to be used in the RT-PCR, SWS1 gene, *exon* 4, was aligned among homologous sequences of *G. gecko* (accession number AY024356), *Anolis carolinensis* (exon 4 accession number ACSWSOPS3) and *Iguana iguana* (accession number AB626972). Primers were designed using the Geneious tools, Primer3 v.0.4.0 (Untergrasser *et al.*, 2012) and used to amplify and sequence the 177 base pairs (bp) of the codogenic SWS1 exon 4 in moorish gecko. The PCR reaction was performed in a DNA thermal cycler (Perkin Elmer Life Science, Waltham, MA, USA) as follows: 1 cycle at 45°C for 45 min for the reverse transcription followed by 2 min at 95°C; 40 cycles, each including 30 s at 94°C, 1 min at 60°C and 2 min at 68°C. After the last cycle, samples were kept for 7 min at 68°C and then stored at 4°C. Amplified PCR products were sequenced using Big Dye Terminator 1.1 (Applied Biosystems, Foster City, CA, USA). Sequence analysis was performed using Geneious Basic program 5.5.3 (created by Biomatters; available from https://www.geneious.com). Homologous primers for the RT-PCR were then designed. Primers were forward, 5′-CGGGAG GTGTCCCGGATGGT-3′; reverse, 5′-GTAGATGATG GGGTTGTAGA-3′ (moorish gecko SWS1 mRNA, GenBank accession number KF803233). Endogenous actin was used as housekeeping gene for normalizing RNA expression; primer sequences were forward, 5′-ATCACT ATTGGCAACGAGC-3′; reverse, 5′-GGTCTTTACGG ATGTCAACG-3′.

Tissues from belly, flank, back, eyes and heart from 10 geckos were sampled and lysed with RNeasy mini kit (Qiagen Turnberry Lane, Valencia, CA) to isolate total RNA as described by the manufacturer. Total RNA was resuspended in 80 μL of RNase-free water, quantified using a NanoDrop 1000 (Thermo Scientific Inc., Waltham, MA USA) and 200 ng was reverse transcribed using Access RT-PCR System kit (Promega Fitchburg, WI, USA). Cycling parameters included a single-step cycle at 45°C for 45 min followed by 95°C for 2 min. Afterwards, we performed a semi-quantitative PCR using 30 cycles at 94°C 30 s, 60°C 1 min and 68°C 2 min. A final extension step was performed at 68°C for 7 min. PCR products were visualized by 1.5% agarose gel electrophoresis.

Western blot analyses

SWS1 opsin expression was analysed on 10 individuals by Western blotting of proteins obtained from tissue samples taken from the belly, flank, back, eyes and from the heart. The tissues were resuspended in radioimmunoprecipitation assay buffer containing protease inhibitors (Roche, Sandhofer Straße Mannheim, Germany) and lysed on ice by homogenization (200 strokes per sample) and sonication (2 min). Lysates were obtained by centrifugation at 14 000 *g* for 30 min at 4°C. Following the determination of protein content by the Bradford assay (Sigma Aldrich St. Louis, MO, USA), 100 μg of total proteins was analysed by 15% polyacrylamide sodium dodecyl sulfate polyacrylamide gel electrophoresis, followed by Western blotting with anti-opsin antibodies (1:1000 dilution) (Thermo Scientific). Only in the case of eye's sample, the total amount of protein analysed was 20 μg. For each sample, the protein intensity level was normalized to endogenous actin using anti-actin polyclonal antibodies (1:1000 dilution) (Sigma Aldrich).

Immunohistochemistry

Skin pigmentation in reptiles depends on melanophores, which synthesize and/or store pigments or light reflecting structures (Leclercq, Taylor & Migaud, 2009). We analysed the skin of geckos to detect the morphology of melanophores and their relationship with the opsin photosensitive protein. All skin samples (belly, flank, back) were fixed in Lillie's solution for 48 h, which acts also as decalcifier. Samples were embedded in paraffin and sliced into 5 μm thick sections. Some of the slides were stained with haematoxylin-eosin to look at their morphology while other serial slides, after deparaffinization, were subjected to decolourization of the melanin in 10% H_2O_2 for 48 h. The latter slides were processed in 10 mM sodium citrate (pH 6.0) for heat-induced epitope retrieval. Slides were then rinsed in 0.05% Tween 20 (Sigma Aldrich) in 0.1 M phosphate buffered saline (PBS) pH 7.4 (PBS-T20) for 30 min and incubated for 15 min in PBS with 3% H_2O_2 to block endogenous peroxidases. After blocking in 2% goat serum in PBS-T20 with 1% bovine serum albumin (BSA), sections were incubated with polyclonal anti-opsin antibody (1:800 dilution in PBS-T20 with 1% BSA; Thermo Scientific) at 4°C overnight. Sections were then washed twice in PBS-T20 and incubated with a peroxidase-conjugated secondary antibody (IgG anti-rabbit, 1:300 diluted in PBS-T20 with 1% BSA; Sigma Aldrich) for 1 h. Binding sites were revealed by 4-chloro-1-naphthol reaction according to the manufacturer instructions. Finally, slides were mounted with Aqua-Mount mounting medium (ThermoFisher Scientific, Hudson, NH, USA).

Results

α-MSH determination

According to the literature, skin darkening in lizard can be imputable to plasmatic α-MSH (Raia *et al.*, 2010; Monti *et al.*, 2013). As a consequence, we first tested the correlation

between the plasma level of this hormone and skin reflectance of either black or white geckos. Individuals treated in the laboratory to darken their skin colour show no significant increase in α-MSH concentration (paired sample *t*-test, $P = 0.332$).

Light sensitivity of different body regions

The gecko's ability to change colour in the presence of different substrates was observed (Fig. 1) and estimated by spectrophotometry (Figs 2 and 3). As shown in Fig. 2, geckos without bandages adjusted their body colour to the black substrate on which they had resided for 3 h (see also Vroonen *et al.*, 2012). When blindfolded, the geckos retained the ability to adjust their colour to the black box, although no appreciable change in skin reflectance was observed when the thorax was covered (Fig. 2).

Therefore, we measured the skin reflectance of geckos after 3 h in white or black boxes under three different experimental conditions: without any bandages, blindfolded and with the

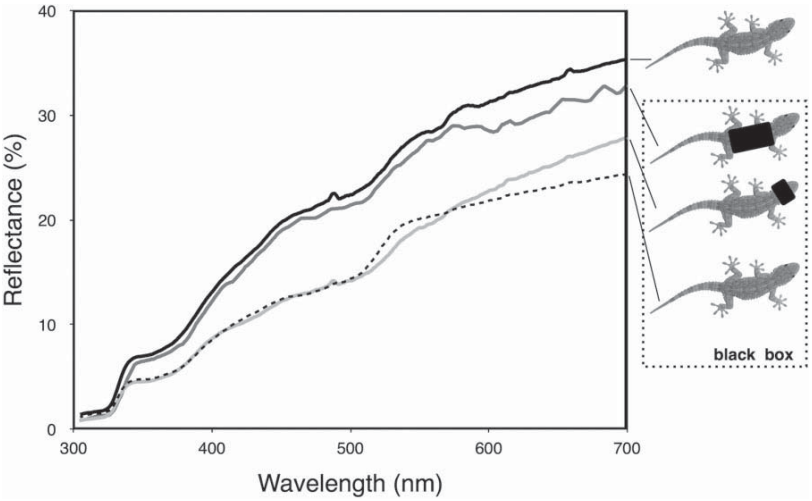

Figure 2 Mean reflectance spectra (%) of *Tarentola mauritanica* under different experimental conditions. From the top: pale gecko (just caught), covered thorax, bandaged eyes and without bandages (the last three measurements were performed after 3 h of immersion in a black box).

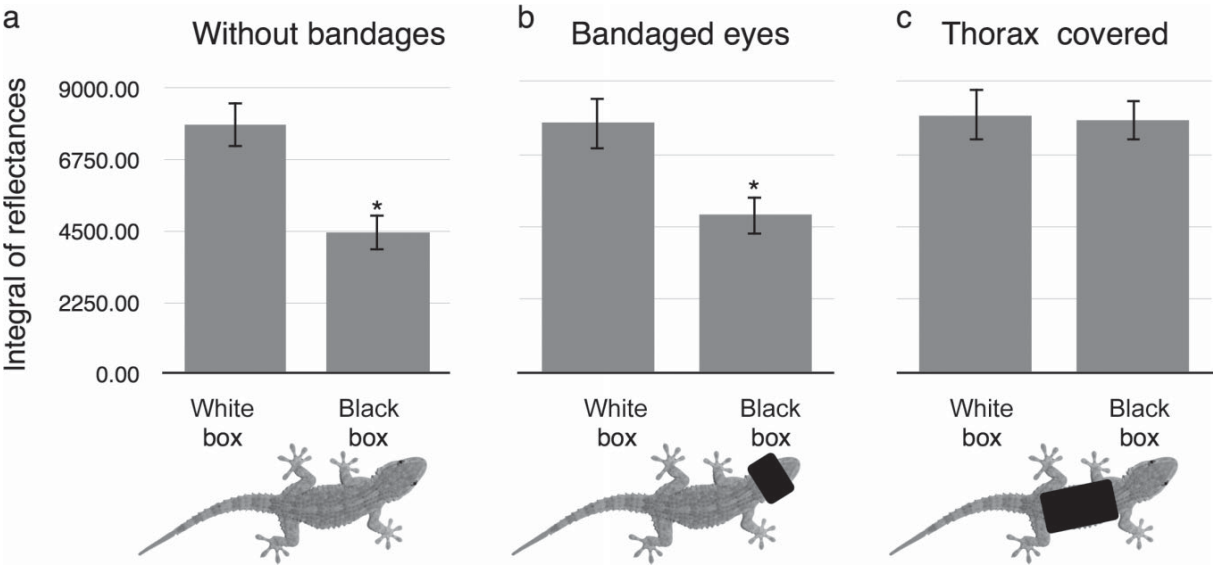

Figure 3 Spectrophotometric analysis of moorish gecko. Reflectance spectra were measured on geckos without bandages (a), with bandaged eyes (b) and with the thorax covered (both flanks and undersides) (c). Reflectance after 3 h of immersion in white and black boxes is reported. Histograms represent the mean values of the mathematical integrals under the spectrophotometric curves (significant differences were assessed using paired sample *t*-test; * indicates $P < 0.001$).

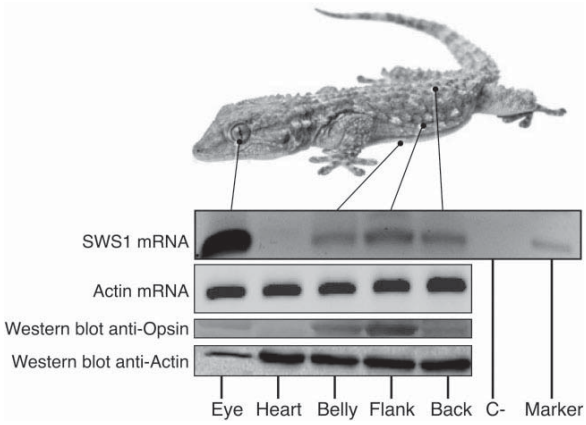

Figure 4 Opsin expression in moorish gecko. Reverse transcriptase polymerase chain reaction (RT-PCR; upper panels) and Western blot analysis (lower panels) of opsin SWS1 gene and protein expression, respectively. C-, negative control of the RT-PCR. For both RT-PCR and Western blot analyses, endogenous actin was used as an internal standard. Western blot was performed using anti-opsin and anti-actin antibodies. Total eye's proteins loaded in the Western blot were five times lower than in the other samples.

thorax covered. We observed that average skin reflectance of geckos without bandages was much higher after the animals had been exposed to white substrate than when kept on black one [Fig. 3a; paired sample *t*-test; $t = 15.6$, degrees of freedom (d.f.) = 14, $P < 0.001$]. A similar response was observed when the animals were blindfolded (Fig. 3b; paired sample *t*-test; $t = 8.07$, d.f. = 14, $P < 0.001$). Interestingly, no difference in reflectance between substrate treatments was observed when geckos had their thorax covered (Fig. 3c; paired sample *t*-test; $t = 0.47$, d.f. = 14, $P = 0.646$).

Expression of SWS1 opsin and immunohistochemistry of melanophores

As SWS1 opsin is sensitive to short wavelengths and is therefore expected to be present in *T. mauritanica* eyes, we performed a semi-quantitative RT-PCR analysis and observed a strong expression of the SWS1 opsin gene in geckos eyes (Fig. 4). Yet, SWS1 mRNA was also observed in skin tissues taken from belly, back and flanks. Heart tissue samples were used as negative controls for SWS1 RNA expression. In keeping with RT-PCR, Western blot analysis showed that opsin protein was present in eyes, as well as in skin cells of the trunk (belly, flank and back). In particular, we observed distinctively higher levels of opsin protein in the flanks than elsewhere (Fig. 4). As expected, no trace of either SWS1 mRNA or related protein was present in the heart. This important result was further borne out by immunohistochemistry analysis. Melanophores in the skin are rich in melanin (Fig. 5). Importantly, they are sensitive to opsin antibody. This suggests that the moorish gecko's melanophores are light sensitive and can therefore be held responsible for skin darkening.

Discussion

Non-fixed body colouration accrues to a number of species and body parts. Many of them serve the goal of concealment from predators or from vigilant prey, which is known as cryptism. Colour change in animals may involve either the nervous or endocrine system (a secondary response), or directly light-sensible cells in the outer layer of the organism, a primary response (Oshima *et al.*, 1998). The adaptive significance of such changes, whether it is cryptism or any feasible alternative, is little known in many cases. Cryptic colour change triggered by dermal light perception (i.e. based on direct action of the melanophores) has been noted in several non-amniotes, but seems to be quite rare in other vertebrates (Bagnara, 1957; Van Der Lek *et al.*, 1958; Lythgoe, Shand & Foster, 1984; Oshima *et al.*, 1998; Ban *et al.*, 2005; Kasai & Oshima, 2006). It has been demonstrated that in tilapia's (*Oreochromis niloticus*) skin multiple types of visual pigments are present, suggesting that dermal colour and pattern changes for camouflage and communication are regulated at the level of the integument (Ban *et al.*, 2005; Chen, Robertson & Hawryshyn, 2013). Recently, the expression of opsin in the skin and its putative role in 'distributed sensing' and camouflage has been reported in cuttlefish (Mäthger, Roberts & Hanlon, 2010). Tail darkening in hypophysectomized tadpoles held under dark conditions has an obvious cryptic function (Bagnara, 1957). Although few pioneering experiments (e.g. Parker, 1938; reviewed in Cooper & Greenberg, 1992) showed that this might be true for some lizards as well, little or no in-depth analysis of the mechanisms involved was surprisingly developed until now, despite the obvious importance of understanding cryptism as an anti-predatory strategy in amniotes (Meunier *et al.*, 2011). In a previous study, we demonstrated that the moorish gecko adjusts its skin darkness to match the substrate. This change in color only happens in daylight (Vroonen *et al.*, 2012). We started the present study thinking that the moorish gecko represents an ideal model to answer to some questions about colour perception and change. With this in mind, we investigated features involved in the sensorial dimension (visual) of this lizard, in order to clarify the mechanism and evolutionary constraints that induced its cryptism. The evidences we gathered in the present study (such as the coverage effects on substrate matching, the performance and the tissue-dependent opsin expression) indicate that background brightness is perceived by skin receptors, irrespective of circulating levels of α-MSH. In particular, we experimentally proved that the eye is not determinant in *T. mauritanica* skin colour change, as it is able to change colour even when blindfolded. Interestingly, we observed that the slow process of accommodation of the skin colour does not work when the thorax was completely obscured, suggesting that colour perception is mediated by this region of the body. Accordingly, we showed evidence for opsin expression in the skin, both at mRNA and

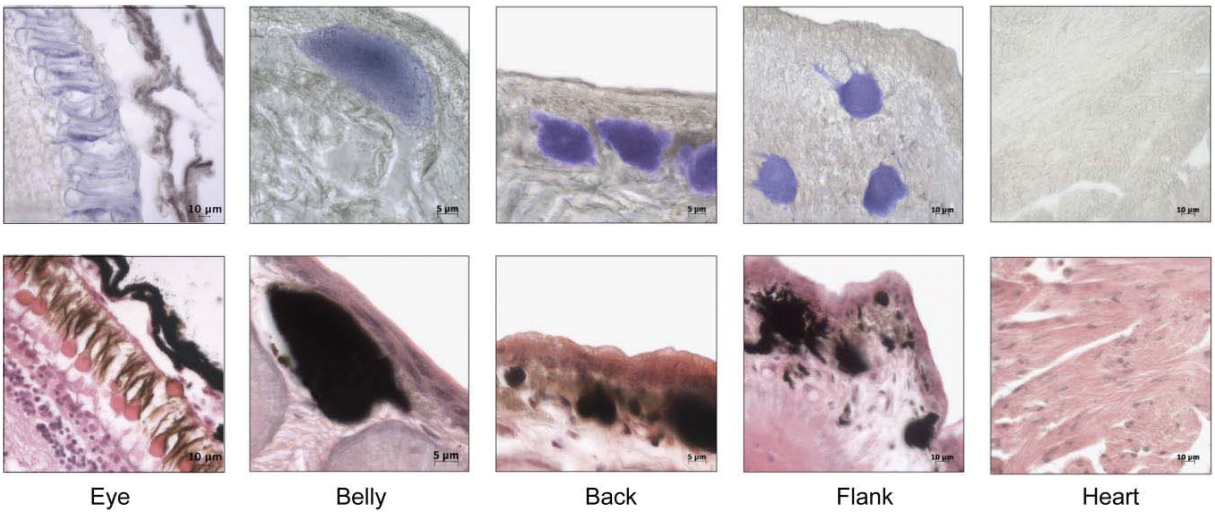

Figure 5 Sample sections in moorish gecko's eye, skin (belly, back and flank) and heart. Top: immunoreactivity with anti-opsin antibody shows the presence of opsin (blue) in cells of the eye and skin, but not in heart; bottom: haematoxylin–eosin analysis shows from left to right, retina with cone in eyes, skin (belly, back and flank) with brown melanophore and heart tissue.

protein levels. Histological analysis also showed the presence of opsin in the dermis, strongly linked to the melanophores. Our findings indicate that the gecko's skin acts as both a receptor and effector of skin darkening, independently from visual inputs. In other words, the gecko's skin is photosensitive, similar to that of other non-amniotes, and melanophores are able to activate skin darkening autonomously.

These results open room to further scientific questions, such as how the light brightness information, which is mainly processed at the level of the flanks, is transmitted to the back of the trunk, where colour change most prominently appears (Vroonen *et al.*, 2012).

Acknowledgements

We are grateful to *Cilento Vallo di Diano e degli Alburni National Park* for granting permits to conduct this study.

References

Bagnara, J.T. (1957). Hypophysectomy and the tail darkening reaction in *Xenopus*. *Exp. Biol. Med.* **94**, 572–575.

Ban, E., Kasai, A., Sato, M., Yokozeki, A., Hisatomi, O. & Oshima, N. (2005). The signaling pathway in photoresponses that may be mediated by visual pigments in erythrophores of Nile tilapia. *Pigment Cell Res.* **18**, 360–369.

Chen, S.-C., Robertson, R.M. & Hawryshyn, C.W. (2013). Possible involvement of cone opsins in distinct photoresponses of intrinsically photosensitive dermal chromatophores in tilapia *Oreochromis niloticus*. *PLoS ONE* **8**, e70342.

Cooper, W.E. Jr. & Greenberg, N. (1992). Reptilian coloration and behavior. In *Biology of the Reptilia*: 298–422. Gans, C. & Crews, D. (Eds). Chicago, IL: University of Chicago Press.

Costantini, D., Casagrande, S., Di Lieto, G., Fanfani, A. & Dell'Omo, G. (2005). Consistent differences in feeding habits between neighbouring breeding kestrels. *Behaviour* **142**, 1409–1421.

Cott, H.B. (1940). *Adaptive coloration in animals*. London: Methuen & Co. Ltd.

Darwin, E. (1974). *Zoonomia or the laws of organic life*. London: J. Johnson.

Fujii, R. (2000). The regulation of motile activity in fish chromatophores. *Pigment Cell Res.* **13**, 300–319.

Hanlon, R.T., Forsythe, J.W. & Joneschild, D.E. (1999). Crypsis, conspicuousness, mimicry and polyphenism as antipredator defences of foraging octopuses on Indo-Pacific coral reefs, with a method of quantifying crypsis from video tapes. *Biol. J. Linn. Soc.* **66**, 1–22.

Hanlon, R.T., Chiao, C.-C., Mäthger, L.M., Barbosa, A., Buresch, K.C. & Chubb, C. (2009). Cephalopod dynamic camouflage: bridging the continuum between background matching and disruptive coloration. *Philos. Trans. R. Soc. Lond. B. Biol Sci.* **364**, 429–437.

Kasai, A. & Oshima, N. (2006). Light-sensitive motile iridophores and visual pigments in the neon tetra, *Paracheirodon innesi*. *Zoolog. Sci.* **23**, 815–819.

Kojima, D., Okano, T., Fukada, Y., Shichida, Y., Yoshizawa, T. & Ebrey, T.G. (1992). Cone visual pigments are present in gecko rod cells. *PNAS* **89**, 6841–6845.

Leclercq, E., Taylor, J.F. & Migaud, H. (2009). Morphological skin colour changes in teleosts. *Fish Fish.* **11**, 159–193.

Llandres, A.L., Figon, F., Christidès, J.-P., Mandon, N. & Casas, J. (2013). Environmental and hormonal factors controlling reversible colour change in crab spiders. *J. Exp. Biol.* **216**, 3886–3895.

Loew, E.R. (1994). A third, ultraviolet-sensitive, visual pigment in the Tokay gecko (*Gekko gecko*). *Vision Res.* **34**, 1427–1431.

Lythgoe, J.N., Shand, J. & Foster, R.G. (1984). Visual pigment in fish iridocytes. *Nature* **308**, 83–84.

Mäthger, L.M., Roberts, S.M. & Hanlon, R.T. (2010). Evidence for distributed light sensing in the skin of cuttlefish, *Sepia officinalis*. *Biol. Lett.* **6**, 600–603.

Meunier, J., Figueiredo Pinto, S., Burri, R. & Roulin, A. (2011). Eumelanin-based coloration and fitness parameters in birds: a meta-analysis. *Behav. Ecol. Sociobiol.* **65**, 559–567.

Monti, D.M., Raia, P., Vroonen, J., Maselli, V., Van Damme, R. & Fulgione, D. (2013). Physiological change in an insular lizard population confirms the reversed island syndrome. *Biol. J. Linn. Soc.* **108**, 144–150.

Norris, K.S. & Lowe, C.H. (1964). An analysis of background color-matching in amphibians and reptiles. *Ecology* **45**, 565–580.

Oshima, N. (2001). Direct reception of light by chromatophores of lower vertebrates. *Pigment Cell Res.* **14**, 312–319.

Oshima, N., Nakata, E., Ohta, M. & Kamagata, S. (1998). Light-induced pigment aggregation in xanthophores of the medaka, *Oryzias latipes*. *Pigment Cell Res.* **11**, 362–367.

Parker, G.H. (1938). The color changes in lizards, particularly in *Phrynosoma*. *J. Exp. Biol.* **15**, 48–73.

Raia, P., Guarino, F.M., Turano, M., Polese, G., Rippa, D., Carotenuto, F., Monti, D.M., Cardi, M. & Fulgione, D. (2010). The blue lizard spandrel and the island syndrome. *BMC Evol. Biol.* **10**, 289.

Roulin, A. & Dubey, S. (2012). The occurrence of reptiles in barn owl diet in Europe. *Bird Study* **59**, 504–508.

Stevens, M. & Merilaita, S. (2011). Animal camouflage: an introduction. In *Animal camouflage: mechanisms and function*: 1–351. Stevens, M. & Merilaita, S. (Eds). Cambridge: Cambridge University Press.

Stuart-Fox, D. & Moussalli, A. (2008). Selection for social signalling drives the evolution of chameleon colour change. *PLoS Biol.* **6**, e25.

Stuart-Fox, D. & Moussalli, A. (2009). Camouflage, communication and thermoregulation: lessons from colour changing organisms. *Philos. Trans. R. Soc. Lond. B. Biol Sci.* **364**, 463–470.

Stuart-Fox, D., Whiting, M.J. & Moussalli, A. (2006). Camouflage and colour change: antipredator responses to bird and snake predators across multiple populations in a dwarf chameleon. *Biol. J. Linn. Soc.* **88**, 437–446.

Stuart-Fox, D., Moussalli, A. & Whiting, M.J. (2008). Predator-specific camouflage in chameleons. *Biol. Lett.* **4**, 326–329.

Thurman, C.L. (1988). Rhythmic physiological color change in crustacea: a review. *Comp. Biochem. Physiol. C: Comp. Pharmacol.* **91**, 171–185.

Untergrasser, A., Cutcutache, I., Koressaar, T., Ye, J., Faircloth, B.C., Remm, M. & Rozen, S.G. (2012). Primer3 - new capabilities and interfaces. *Nucleic Acids Res.* **40**, e115.

Van Der Lek, B., de Heer, J., Burgers, A.C.J. & van Oordt, G.J. (1958). The direct reaction of the tailfin melanophores of *Xenopus* tadpoles to light. *Acta Physiol. Pharmacol. Neerl.* **7**, 409–419.

Vroonen, J., Vervust, B., Fulgione, D., Maselli, V. & Van Damme, R. (2012). Physiological colour change in the moorish gecko, *Tarentola mauritanica* (Squamata: Gekkonidae): effects of background, light, and temperature. *Biol. J. Linn. Soc.* **107**, 182–191.

Wallace, A.R. (1985). *Natural selection and tropical nature: Essays on descriptive and theoretical biology*. London: Macmillan.

Cell. Mol. Life Sci.
DOI 10.1007/s00018-015-2015-y

Cellular and Molecular Life Sciences

ORIGINAL ARTICLE

Femtosecond UV-laser pulses to unveil protein–protein interactions in living cells

Francesco Itri[1] · Daria M. Monti[1,2] · Bartolomeo Della Ventura[3] · Roberto Vinciguerra[1] · Marco Chino[1] · Felice Gesuele[3] · Angelina Lombardi[1] · Raffaele Velotta[3,4] · Carlo Altucci[3,4] · Leila Birolo[1] · Renata Piccoli[1,2] · Angela Arciello[1,2]

Received: 6 May 2015 / Revised: 30 July 2015 / Accepted: 6 August 2015

Abstract A hallmark to decipher bioprocesses is to characterize protein–protein interactions in living cells. To do this, the development of innovative methodologies, which do not alter proteins and their natural environment, is particularly needed. Here, we report a method (LUCK, Laser UV Cross-linKing) to in vivo cross-link proteins by UV-laser irradiation of living cells. Upon irradiation of HeLa cells under controlled conditions, cross-linked products of glyceraldehyde-3-phosphate dehydrogenase (GAPDH) were detected, whose yield was found to be a linear function of the total irradiation energy. We demonstrated that stable dimers of GAPDH were formed through intersubunit cross-linking, as also observed when the pure protein was irradiated by UV-laser in vitro. We proposed a defined patch of aromatic residues located at the enzyme subunit interface as the cross-linking sites involved in dimer formation. Hence, by this technique, UV-laser is able to photofix protein surfaces that come in direct contact. Due to the ultra-short time scale of UV-laser-induced cross-linking, this technique could be extended to weld even transient protein interactions in their native context.

Keywords Protein–protein interactions · Ultra-short UV-laser pulses · UV cross-linking · Living cells irradiation

F. Itri, D.M. Monti were contributed equally to the paper.

Electronic supplementary material The online version of this article (doi:10.1007/s00018-015-2015-y) contains supplementary material, which is available to authorized users.

✉ Angela Arciello
anarciel@unina.it

Carlo Altucci
caltucci@unina.it

Leila Birolo
birolo@unina.it

[1] Department of Chemical Sciences, University of Naples Federico II, 80126 Naples, Italy

[2] Istituto Nazionale di Biostrutture e Biosistemi (INBB), Rome, Italy

[3] Department of Physics, University of Naples Federico II, 80126 Naples, Italy

[4] Consorzio Nazionale Interuniversitario per le Scienze Fisiche della Materia (CNISM), UdR, Naples, Italy

Introduction

Communications between proteins underlie all biological processes, from the formation of multimeric proteins and protein complexes to the regulation of all the mechanisms involved in biological processes. The primary challenges associated with the study of biological systems are targeted to identify protein interactions occurring in a natural context, i.e. in vivo.

Besides the interaction of each single protein with its functional partners, the relationship between the dynamic oligomeric properties of multimeric proteins and their functional diversity plays a key role in cellular processes [1]. On the basis of known protein structures, it emerges that 50–70 % of proteins exists as homomeric complexes in vivo [1, 2].

Chemical stabilization of protein–protein interactions and protein assemblies by cross-linking is a strategy aimed at studying protein association and has been used both in vitro and in vivo, in the complex cellular milieu [3–8]. The strength of this methodology resides in the transformation of

Published online: 12 August 2015

non-covalent interactions into stable covalent bonds. Methods based on in vivo cross-linking are increasingly widespread used in combination with mass spectrometry (XL-MS) to identify interacting proteins as well as topological features [3, 4, 6–11]. Some of these techniques are based on the use of ingenious and attractive chemical reagents, such as PIR reagents [7, 12, 13]. This facilitates fractionation of cross-linked peptides by introducing affinity tags within the cross-linking reagents [14]. Other techniques adopt small reagents, such as formaldehyde and glutaraldehyde [4, 9, 15], which are very reactive and membrane permeable, but rarely allow to obtain structural details. Site-specific incorporation of genetically encoded photo-reactive amino acids is particularly attractive, allowing time- and location-specific cross-linking, although engineering of living cells is required [10, 16, 17].

All these techniques are based on the use of chemical reagents, chemical treatments or engineering of living cells, which may alter the investigated proteins and their natural environment. Therefore, expanding the panel of strategies to explore protein–protein interactions within living cells is still a great challenge.

Following a multidisciplinary approach, we have recently developed a new procedure to cross-link peptides in vitro by UV-laser irradiation [18]. Upon irradiation, aromatic side chains produce radicals able to react and generate covalent bonds with nearby residues. Here, we transfer this know-how from peptides to complex biological systems, by developing a new procedure, named LUCK (Laser UV Cross-linKing), to cross-link interacting proteins in their natural context, i.e. in living cells. This cross-linking is a fast process that essentially occurs when protein surfaces are in direct contact, thus enabling LUCK to "weld" interacting protein chains potentially at zero length. In this methodology, the reactive groups are within the protein itself, without any need of reagents introduction or cell engineering. This represents the novelty and the advantage of our procedure over most of the presently available techniques. Moreover, as the targets of most common chemical cross-linkers are primary amine and thiol nucleophilic groups [19], exposed hydrophobic protein regions, which often play an important role in protein–protein interactions [20], usually escape detection. The procedure herein proposed mainly targets aromatic residues, which are present in almost all proteins. Even though their occurrence on protein surfaces is clearly lower than that of polar residues, all three aromatic residues (Phe, Trp, Tyr) are strong contact formers, as first reported by Jones and Thornton [21] and, more recently, by Mezei [22]. Moreover, it has been recently shown that hot spots of protein–protein interactions frequently contain Trp, Arg and Tyr [23]. Authors also report that mutual interactions between aromatic residues are more frequent than mutual interactions between any other couple of residues [22]. Taken together, all these data further emphasize the need of new cross-linking methodologies that specifically target aromatic residues. To the best of our knowledge, the only strategy developed so far to chemically stabilize hydrophobic interactions is the introduction of photo-leucine, photo-isoleucine and photo-methionine [10, 16].

In this work, we applied our approach in vivo to glyceraldehyde-3-phosphate dehydrogenase (GAPDH), a homo-tetramer made up of four 37 kDa subunits, structurally and functionally well characterized [24]. Although once thought to solely play a role in glycolysis, GAPDH is now considered to be a classic example of a moonlighting protein [25]. Mammalian GAPDH has been implicated in many cellular activities, including apoptosis, nuclear RNA transport, DNA replication and repair, and it is thought to play roles in many diseases, including Parkinson's, Alzheimer's and Huntington's diseases [26]. This array of activities has to be correlated to a number of factors, including the stabilization of dynamic oligomers, since GAPDH largely exists as a tetramer with minor populations of dimers and monomers. Several GAPDH interactors are already known and play a key role in driving the multiple activities of the enzyme. High-resolution crystal structure of human GAPDH has been recently solved [27], giving the opportunity to have a structural understanding of the ongoing processes. This makes GAPDH an ideal candidate to test the idea of welding, by covalent bonds, interacting protein surfaces in their natural environment.

By immunological and mass spectrometry techniques, we demonstrated that, upon irradiation of HeLa living cells with UV-laser ultra-short pulses under controlled conditions, subunit–subunit cross-linking occurs in GAPDH generating dimeric species, as expected by the presence of hydrophobic residues at the symmetric interface between the two dimers which associate to give rise to the homo-tetrameric structure of the enzyme in vivo.

Results

Irradiation of HeLa living cells

Glyceraldehyde-3-phosphate dehydrogenase (GAPDH) was selected as a model protein to analyse the power of UV-laser irradiation in welding protein–protein interactions in living cells. Taking advantage of our previous in vitro studies on laser-induced cross-linking of peptides [18], human living cells (HeLa cell line from human epithelial adenocarcinoma) were irradiated with the fourth harmonic (257 nm) of a PHAROS near-IR fundamental pulse by setting the following irradiation parameters: 50 μJ as energy of each single pulse (E_{pulse}), 2 kHz as pulse

repetition rate (f_{rate}), 10 s as total time of cell irradiation (T_{irr}), with a total irradiation energy of $D = E_{pulse} \times T_{irr} \times f_{rate} = 1.0$ J. To this purpose, the cell suspension (4×10^5 cells/mL) was placed in a cuvette under magnetic stirring to ensure uniform conditions during irradiation with the UV-femtosecond laser source (Fig. 1a). Total proteins were then extracted from irradiated and control cells and analysed in parallel experiments by Western blotting with anti-GAPDH antibodies (Fig. 1b) or Coomassie Blue staining (Fig. 1c). Western blot analyses revealed that, besides the presence of the monomeric form of GAPDH (37 kDa), additional immunopositive protein bands were present in the irradiated sample (Fig. 1b, lane 2), with a protein species of about 90 kDa molecular mass as the most evident, which was found to be absent in control, i.e. non-irradiated cells (Fig. 1b, lane 1). This suggested that UV-laser irradiation induced cross-linking between GAPDH and its protein partners and/or between GAPDH subunits. In either case, this represents a very promising starting point for further studies aimed at investigating the potential of this methodology in different environments. Further, Coomassie Blue staining revealed no significant differences in protein pattern between control (Fig. 1c, lane 1) and irradiated sample (Fig. 1c, lane 2), indicating that irradiation does not significantly alter cell protein profile.

Optimization of irradiation experimental conditions

To maximize the efficiency of UV-laser-induced protein–protein cross-linking, we analysed the influence of three physical parameters, i.e. f_{rate}, E_{pulse} and T_{irr}, on the cross-linking yield. By assuming a linear response of cross-linking yield to laser irradiation, it turns out that the yield of the process depends upon E_{pulse}, T_{irr}, f_{rate} only through D. It is worth noticing that, in place of the pulse energy (E_{pulse}), we should better consider the laser intensity, I [28], proportional to E_{pulse} and defined as $I \approx \frac{E_{pulse}}{S \cdot \tau_{pulse}}$, S being the laser beam section onto the target and τ_{pulse} the laser pulse duration. Typically, I is expressed in W/cm^2 and corresponds to the peak intensity of a single ultra-short laser pulse. In our case, S and τ_{pulse} were fixed to $\sim$0.3 cm^2 and $\sim$250 femtosec, respectively, [29] in all the tested experimental conditions. Thus, in the following, we shall refer to E_{pulse}, rather than I, E_{pulse} being varied between 30 and 70 μJ, that implies 4.0×10^8 W/cm^2 $\leq I \leq 9.3 \times 10^8$ W/cm^2.

Therefore, optimization measurements were carried out at constant D, set at the value of 4.0 J, as a similar value was used to cross-link DNA and proteins by UV-laser irradiation [30]. Through the experiments, each of the three parameters was kept constant, while the other two were varied. In a first subset of experiments, at a fixed repetition rate of 2 kHz, T_{irr} and E_{pulse} were changed; in a second

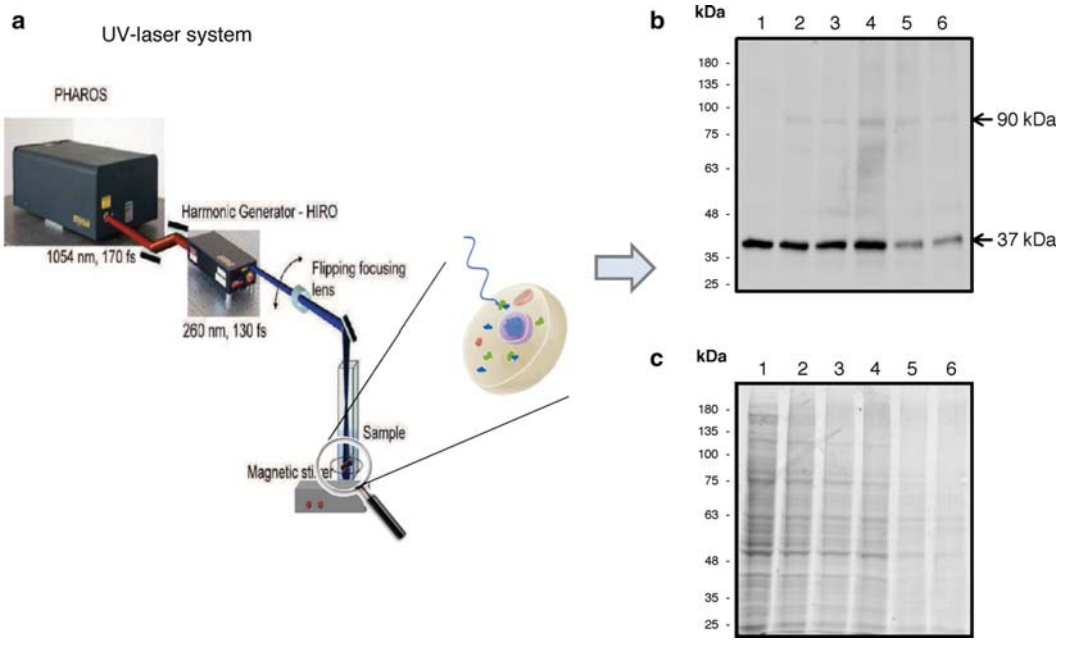

Fig. 1 UV-laser apparatus and analysis of irradiated cells. PHAROS laser apparatus (**a**). SDS-PAGE followed by Western blot with anti-GAPDH antibodies (**b**) or *Coomassie Blue* staining (**c**) of total proteins (40 μg) extracted from untreated cells (*lane 1*) or cells irradiated (*lanes 2–6*) using an energy pulse of 50 μJ and a pulse repetition rate of 2 kHz. The total irradiation energy was: 1.0 J (*lane 2*), 2.0 J (*lane 3*), 4.0 J (*lane 4*), 8.0 J (*lane 5*) and 10.0 J (*lane 6*), with a total irradiation time of 10, 20, 40, 80 and 100 s, respectively

subset, T_{irr} was set at 40 s and E_{pulse} and f_{rate} varied; and in a third subset, E_{pulse} was kept constant at 50 μJ, whereas f_{rate} and T_{irr} were changed. Using this scheme, E_{pulse} was scanned between 30 and 70 μJ, T_{irr} was varied between 30 and 70 s, and f_{rate} was tested between 1 and 6 kHz. The panel of irradiation conditions is reported in the contour plot frame of Fig. 2a, where pulse energy and irradiation time are reported on x- and y-axes, respectively, whereas the colour code refers to laser repetition rate reported in the third dimension. The experimental conditions, represented by rectangles in Fig. 2a, are detailed in ESM_Table 1.

For each set of experiments, the cross-linking yield was determined as follows. Upon UV-laser irradiation of HeLa living cells, total proteins were extracted and analysed by Western blotting using anti-GAPDH specific antibodies (see ESM_Fig. 1). The relative intensities of the two main protein bands recognized by the antibody, corresponding to monomeric GAPDH (37 kDa) and to cross-linked species (∼90 kDa band), were determined by densitometric analyses, normalized to the total protein amount of each sample and expressed as percentage of total GAPDH (monomers + complexes = 100 %). The results clearly showed that in all the conditions tested, at $D = 4.0$ J, the relative amount of GAPDH monomer and cross-linked products remains substantially unvaried, being the percentage of GAPDH cross-linked species (∼90 kDa) nearly stable at ∼10 % (inset in Fig. 2a), independently on E_{pulse}, T_{irr}, f_{rate}, thus confirming our initial assumption that cross-linking yield only depends on D. It is worth noting that, under some irradiation conditions, immunopositive complexes with a molecular mass higher than 90 kDa were also present (ESM_Fig. 1). They may correspond to higher molecular order protein complexes, which in principle may undergo different excitation schemes at a molecular level.

We then analysed the effects of energy dose with the ultimate goal to maximize cross-linking efficiency. We set f_{rate} and E_{pulse} at 2 kHz and 50 μJ, respectively, while the T_{irr} was varied from 24 to 44 s to reach a dose comprised in the 2.4–4.4 J range. The percentage of monomeric GAPDH and of cross-linked species is reported in Fig. 2b and c, respectively, as a function of D. A linear decrease of the 37 kDa monomeric species (from 98 to 92 %, Fig. 2b) and a corresponding linear increase of higher molecular mass species (from 3 to 8 %, Fig. 2c) were observed by increasing the dose. The Pearson's R coefficients of the linear best-fit in Fig. 2b and c were found to be 0.97 and 0.96, respectively, thus confirming the goodness of linearity in the investigated range of laser dose. It is noteworthy that by delivering a total irradiation energy lower than 2.4 J significantly less efficient cross-linking occurs (Fig. 1b, c, lane 2), while at higher energy doses (>4.4 J) total protein amount appeared to be much lower (Fig. 1b, c, lanes 5 and 6), although no significant changes in protein pattern were observed. This is possibly due to extensive and uncontrolled cross-linking generating insoluble protein aggregates, removed by centrifugation prior to electrophoresis. Indeed, the overcrowded conditions of the intracellular environment could promote, at high energy

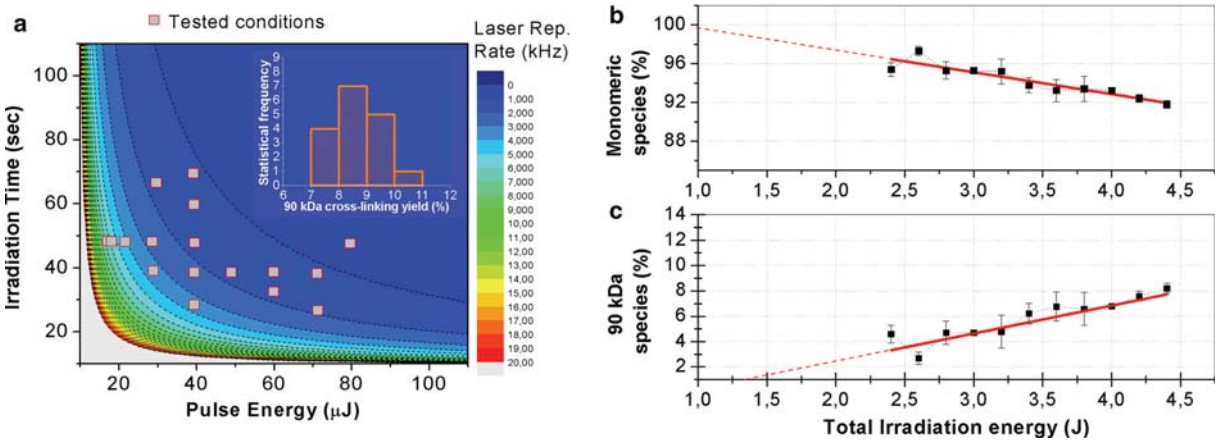

Fig. 2 Optimization of HeLa living cells irradiation conditions. 3D representation of the laser parameter space as a contour plot (**a**), being the pulse energy and the irradiation time the x- and y-axis, respectively, and the *colour* code representing in the third dimension the laser repetition rate. In the plot, the experimental conditions tested (*rectangles*) refer to the selected constant energy dose of 4.0 J. The ∼90 kDa cross-linked species yield (%) at a constant energy dose of 4.0 J is reported in the inset in panel **a**. The percentage of monomeric GAPDH (**b**) and of the ∼90 kDa species (**c**), with GAPDH monomers + GAPDH complexes equal to 100 %, is reported as a function of total irradiation energy. This was varied by increasing the irradiation time between 24 and 44 s, and keeping constant the pulse energy at 50 μJ and the repetition rate at 2 kHz. The Pearson's R coefficients of the linear best-fit in **b** and **c** are 0.97 and 0.96, respectively. In panel **b**, the slope of the *line* is $-(2.2 \pm 0.2) \times 10^{-3}$ J^{-1} and the intercept value is nearly consistent with 100, as expected, within the error bar. In panel **c**, the slope of the *line* is $(2.2 \pm 0.2) \times 10^{-3}$ J^{-1} and the intercept value is nearly consistent with 0

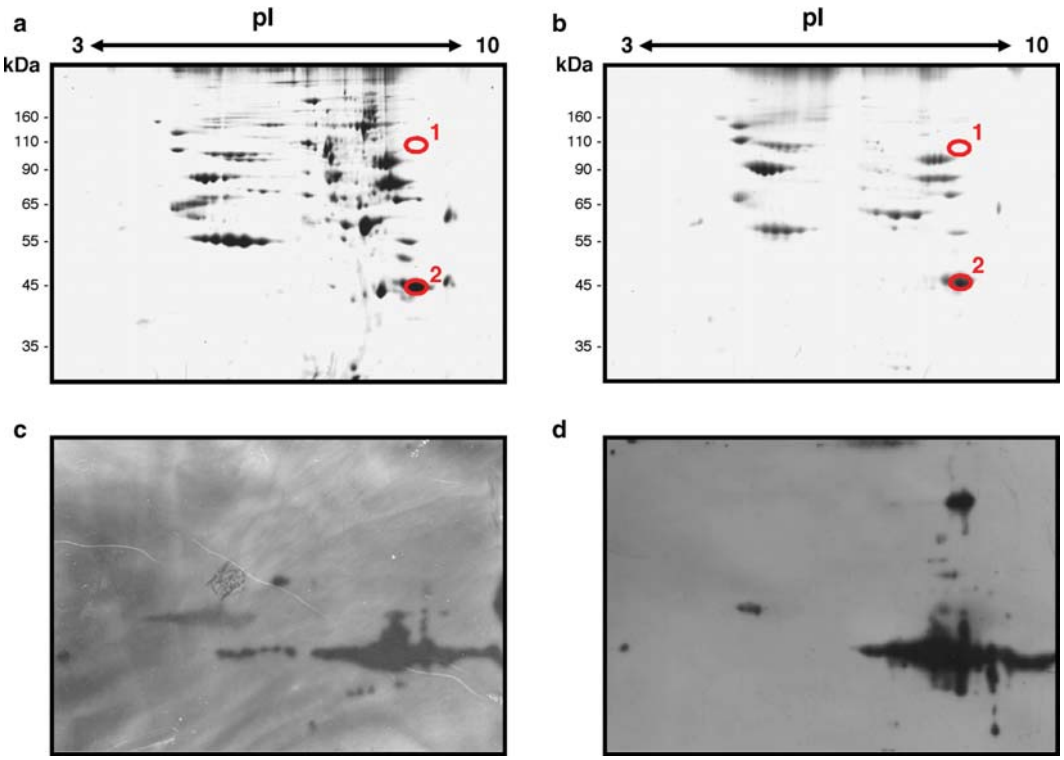

Fig. 3 Two-dimensional electrophoresis of proteins extracted from HeLa cells, untreated (**a**, **c**) or exposed to UV-laser irradiation (**b**, **d**). Duplicate samples of each total protein extract were fractionated in parallel by two-dimensional gel electrophoresis, and analysed by colloidal *Coomassie Blue* staining (**a**, **b**), or transferred onto a PVDF membrane (**c**, **d**) and immunoblotted with anti-GAPDH antibodies. *Circles* on *Coomassie Blue* stained gels correspond to spots that were excised for subsequent analyses

doses, a rapid intermolecular cross-linking, as proteins are in constant contact. This indicates that protein–protein cross-linking efficiency may be modulated, since the phenomenon depends upon the total energy released to the target.

All the data set allowed us to define the optimal irradiation conditions, thereafter used as standard parameters; 40 s irradiation time, 50 μJ pulse energy, 2 kHz repetition rate and 4.0 J total irradiation energy represent the conditions that maximize cross-linked GAPDH signals (Fig. 1b, lane 4) without altering total protein pattern (Fig. 1c, lane 4). Under these conditions, we observed high reproducibility of the cross-linked species yield (10 % ± 1, $n = 30$ independent experiments).

The linear correlation between the yield of cross-linked products and the total irradiation energy suggests that the process is triggered by the absorption of a single UV-laser photon by side chains of aromatic amino acids. In this hypothesis, it is possible to define the value of the energy required to induce protein–protein cross-linking as approximately the energy associated to a single 257 nm photon (4.81 eV).

Identification of GAPDH cross-linked species

To identify the protein species covalently bound to GAPDH upon living cells irradiation, mass spectrometry analyses of total proteins extracted from control and irradiated HeLa cells were performed. By superimposing the Western blot (Fig. 1b) to the corresponding Coomassie Blue stained gel (Fig. 1c), the gel area corresponding to the immunopositive signal of ∼90 kDa molecular mass was localized (Fig. 1b, c, lane 4), excised from gel and treated as described in the "Materials and methods". As control, the equivalent gel section was also excised from the non-irradiated sample lane (Fig. 1c, lane 1). Proteins were identified by standard proteomic procedures by LC–MS/MS and database search in the human subset of NCBI with a licensed version of MASCOT software. In agreement with the immunopositive signal revealed by Western blot analysis (Fig. 1b, lane 4), LC–MS/MS analysis indicated the presence of GAPDH in the ∼90 kDa protein band, based on the identification of 8 peptides covering 35 % of GAPDH sequence. This represents a clear evidence of the formation of cross-linked GAPDH species upon living cells

irradiation. No photo-oxidized peptides were detected in the analysed samples.

In order to identify the GAPDH cross-linked species, total proteins extracted from control and irradiated cells were fractionated by two-dimensional gel electrophoresis (2D gel). Gels were either stained with colloidal Coomassie Blue (Fig. 3a, b, for control and irradiated cells, respectively) or analysed by Western blotting with anti-GAPDH specific antibodies (Fig. 3c, d, for control and irradiated cells, respectively). As shown in Fig. 3, a high molecular mass protein spot (spot 1) was recognized by anti-GAPDH antibodies in the irradiated sample, migrating as a ~90 kDa species, and with the same pI as monomeric GAPDH (spot 2). By superimposition of 2D blot and 2D gel of the irradiated sample, protein spots of interest were localized, excised from gel and in situ digested with trypsin. As control, the corresponding spots were excised from the gel of the non-irradiated sample. The resulting peptide mixtures were analysed by nanoLC-MS/MS experiments, as described above, and, in agreement with immunostaining, the high molecular mass protein spot of irradiated sample was found to contain GAPDH (ESM_Table 2). Most interestingly, no other proteins were identified in the same spot, thus suggesting that GAPDH intersubunit cross-linking occurred.

To further investigate this point, total proteins were extracted from control and irradiated cells and immunoprecipitated with anti-GAPDH specific antibodies. The immuno-selected proteins were then analysed by SDS-PAGE, followed by Coomassie Blue staining (ESM_-Fig. 2). From gels of irradiated and control samples, 12 slices were excised, as indicated in ESM_Fig. 2, and analysed by nanoLC-MS/MS as described above. The comparative analysis of the identified proteins (ESM_ Table 3) indicated that at ~90 kDa molecular mass (slice 5), and even at higher molecular masses (slices 2–4), GAPDH was present in the irradiated sample but not in control cells. Since no other proteins were found, this clearly confirmed that intermolecular cross-linking between GAPDH subunits was induced by UV-laser irradiation of living cells.

It is worth noting that no known photo-oxidation products of Trp and Tyr [31] were detected in the analysed irradiated samples, while classical methionine oxidation was observed both in irradiated and control samples (ESM_Table 2, ESM_Table 3).

In silico and in vitro GAPDH spectroscopic analyses

To shed light on GAPDH intersubunit cross-linking, we irradiated in vitro pure GAPDH from rabbit muscle (95 % identity with human GAPDH) and compared the electrophoretic mobility of cross-linked products to that of immunopositive GAPDH species obtained upon irradiation of living cells. As shown by Western blot analysis (Fig. 4a), a species with an apparent molecular mass of ~90 kDa, comparable to that of the GAPDH species cross-linked in living cells, was found to be present in the in vitro irradiated sample.

Moreover, we analysed the high-resolution GAPDH crystal structure to investigate on the exclusive formation of dimers. The protein is a D_2-symmetric homo-tetramer in its functional form, with three independent interfaces [27]. Cross-distance matrix between aromatic residues

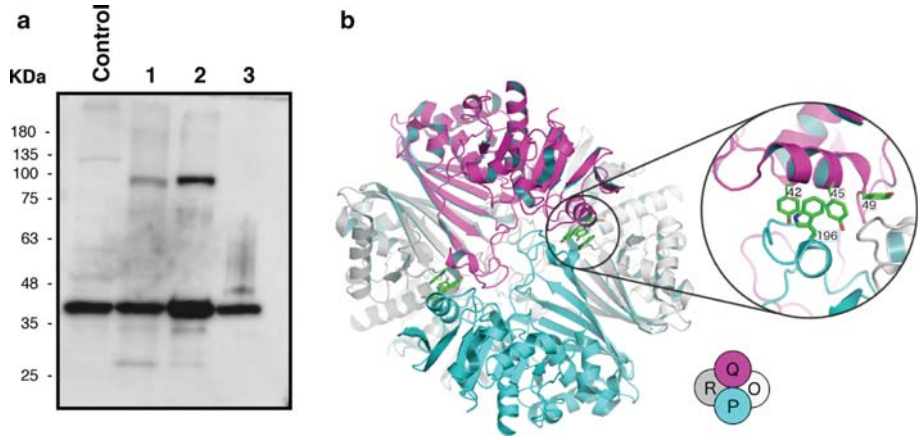

Fig. 4 Irradiation of GAPDH in vitro and human GAPDH crystal structure. Comparative Western blot analysis of in vitro irradiated GAPDH from rabbit muscle and endogenous GAPDH from irradiated cells (**a**). Total proteins were extracted from untreated cells (control) and irradiated cells (*lane 1*) and analysed with anti-GAPDH antibodies. Pure GAPDH was analysed before (*lane 3*) and after (*lane 2*) in vitro irradiation. Human GAPDH crystal structure (PDB ID 1U8F[27]) (**b**). The four symmetry-related subunits are specified as in the bottom balloons. W196 from P subunit, and Y42, Y45, Y49 from Q subunit are showed as green sticks. This figure was generated using the PyMOL molecular graphics system, by Delano Scientific (www.pymol.org)

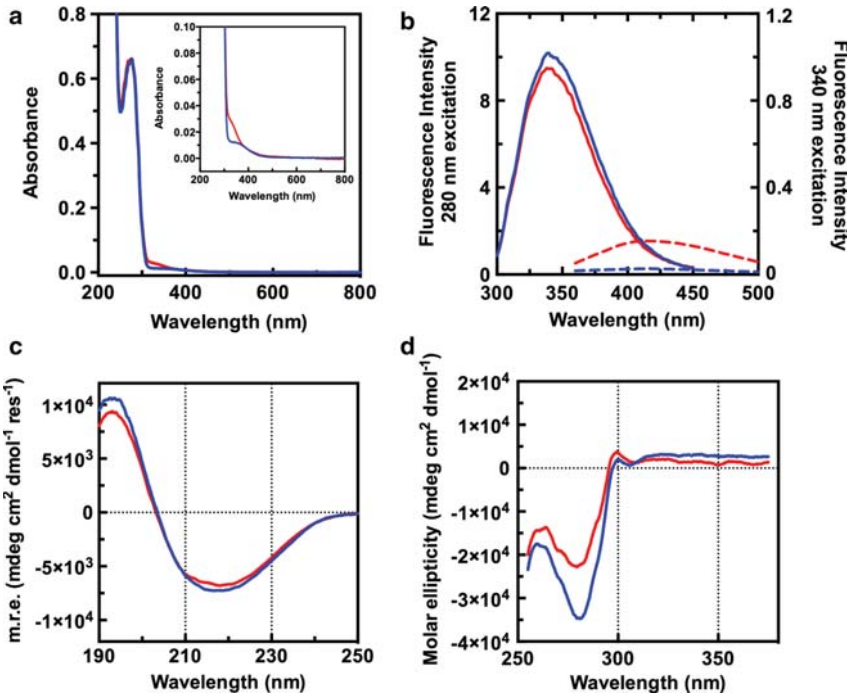

Fig. 5 Spectroscopic characterization of irradiated GAPDH from rabbit muscle. *Blue lines* are relative to control GAPDH, *red lines* are relative to irradiated samples (65 μM in 50 mM phosphate buffer pH 7.5). UV–Vis absorption spectra (**a**) including a magnification in the *inset*; intrinsic fluorescence spectra (**b**); far-UV and aromatic region circular dichroism spectra (**c**, **d**). In **b**, intrinsic fluorescence emission was registered upon excitation at 280 nm (*continuous lines*) or at 340 nm (*dashed lines*)

(ESM_Fig. 3) clearly shows that only one interface (the so-called *R* interface) presents aromatic residues prone to cross-link. In particular, W196 is in close proximity with three tyrosine residues (Y42, Y45, Y49) from the nearby subunit (Fig. 4b). Therefore, only dimers can be generated by UV-laser cross-linking, whereas higher oligomers cannot be predicted based on GAPDH intrinsic symmetry and on the assumption that aromatic residues are essential for laser-induced cross-linking.

To deeply analyse the involvement of aromatic residues in the intersubunit cross-linking, we performed a spectroscopic characterization of the irradiated GAPDH from rabbit muscle in vitro. UV–Vis spectrum of irradiated sample clearly showed a new band centred around 330 nm (Fig. 5a), which can be interpreted as a conjugated aromatic chromophore [32], whereas the absorption intensity of the 280 nm band remains substantially unchanged, with a slight increase in the 250–270 nm region. Tryptophan intrinsic fluorescence analyses of the irradiated GAPDH showed only a decrease in intensity (Fig. 5b), without any difference in the emission maximum wavelength, suggesting a quenching of the fluorescence probably due to a higher solvent exposure, or a decrease in the number of fluorophores that are excited at 280 nm. The latter hypothesis was further supported by a concomitant increase of emission at 420 nm, upon 340 nm excitation, thus indicating that a fraction of aromatic residues was involved in the red-shifted fluorescence.

Circular dichroism (CD) analysis was performed both in the amide and in the aromatic regions. CD spectra in the far-UV (Fig. 5c) were typical of an α/β protein, in good agreement with previously published GAPDH CD analyses [33, 34]. Irradiated sample showed only slight spectral differences in this region with respect to control GAPDH, indicating that the secondary structure content is almost unaltered. Spectral differences between irradiated and control samples in the near-UV region (Fig. 5d) were more evident, in agreement with fluorescence and absorption data. Global profiles of the spectra remained unaltered, with bands centred at the same wavelengths. However, we found a significant decrease of the molar ellipticity of the minimum at 280 nm in the case of the irradiated sample.

Discussion

We conceived and set up a simple, reliable method to "weld" protein surfaces that come in direct contact, by establishing cross-links at zero length. By in vitro studies on peptides, we demonstrated that a radical mechanism is at the basis of the phenomenon as, upon absorption of UV light, aromatic side chains produce radicals able to react and generate covalent bonds with nearby residues [18]. Hence, reactive groups belong to the interacting proteins themselves, without the need of introducing reagents, which may alter the protein natural environment. This

represents a great advantage of the methodology. Furthermore, cross-linking occurs in a very rapid time scale and is triggered by the absorption of a single UV-laser photon by an aromatic side chain.

Using HeLa cells as the natural context and endogenous GAPDH (37 kDa) as a model protein, we demonstrated, for the first time, that UV-laser irradiation of living cells freezes GAPDH complexes of high molecular mass, among which we focused on species of about 90 kDa for protein identification. We defined a wide energy range in which the yield of these cross-linked products is a linear function of total irradiation energy with no apparent perturbation of cell proteome. Within this range, we set up optimal conditions to induce cross-linking by UV-laser irradiation of living cells.

By immunological, 2D-electrophoretic and mass spectrometric analyses, we demonstrated that UV-laser irradiation of HeLa living cells induces cross-linking between two GAPDH chains, generating cross-linked dimers. Analysis of the high-resolution GAPDH crystal structure [27] supports our findings. A detailed analysis of the distances between aromatic residues shows that W196 and Y42, Y45, Y49 form the most important set of aromatic interactions between the two subunits (Fig. 4b). Given the one-photon excitation mechanism of the here proposed technique, it is likely to hypothesize that the covalent GAPDH homo-dimer formation upon photochemical cross-coupling involves W196 and one of the three tyrosine residues in its proximity, both tryptophan and tyrosine being indeed amino acid residues amongst the most involved in excitation mechanisms induced by UVC light (200–280 nm) [35]. Most notably, these aromatic residues lie at the C_2 symmetric *R* interface, thus a covalent bond would produce only dimers, as experimentally found both in living cells and in vitro.

Spectroscopic analyses, performed on pure GAPDH irradiated in vitro, clearly support the involvement of aromatic residues in the covalent cross-linking between two subunits. Taken together, all the spectroscopic data suggest that a new chromophore, absorbing around 330 nm, is produced upon laser irradiation. Concomitant changes were detected in both UV–Vis and fluorescence spectra. In particular, fluorescence emission generated upon 340 nm excitation can be attributed to the presence of highly conjugated aromatic moieties, in agreement with literature data [32]. Aryl substituted tryptophans in position 2 have been previously synthesized via Pd-catalysed Suzuki–Miyaura cross-coupling [32]. Taking these unnatural amino acids as models for a tyrosyl-tryptophan cross-coupling product, we found that their UV–Vis and fluorescence spectral features fairly correlate with our results, thus suggesting that a cross-coupled aromatic moiety is produced upon laser irradiation.

Analysis of CD spectra gives further insights into the molecular mechanism occurring after cross-coupling. The lower intensities of the positive and negative bands in the far-UV region, upon laser irradiation, can be related to a decrease in the secondary structure content, or to a change in the oligomerization state, as already reported for GAPDH [33, 34]. A more evident decrease in spectrum amplitude is observed in the near-UV region, further confirming that aromatic residues are involved in the cross-coupling event. The observed CD variations are generally interpreted as a partial transition to a molten globule state [36], which in the case of the GAPDH has been correlated to a lower oligomerization state [33, 34]. It can be argued that the observed changes in the CD signals are related to degenerative oxidative processes, triggered by the laser in vitro, differently from what observed in living cells. The decrease of the near-UV signal amplitude has been indeed reported for GAPDH, upon exposure to chemical oxidative stress [37, 38] and it has been related to non-native amyloid-like aggregates. In that case, differently from our results, such a decrease in the near-UV region was accompanied by an increased signal amplitude in far-UV region. Our results well fit with a mechanism of tetramer destabilization upon covalent dimer formation. In conclusion, the results herein reported strongly confirm the formation of specific cross-linked species through aromatic residues triggered by laser irradiation.

The procedure herein proposed is a fast, reproducible and controlled process. It is fast, as the time needed for cross-linking induction is much shorter (seconds) than that required for conventional methodologies applied to living cells. It is a controlled process, as the energy dose can be modulated accurately to optimize cross-linking in a given experimental system.

The linear response of protein–protein cross-linking in living cells to the laser intensity led us to highlight that the cross-linking event is triggered by the absorption of a single UV-laser photon by aromatic side chains. This makes the process basically different from that occurring in the case of protein-DNA photoinduced cross-linking, from a microscopic point of view. For DNA–protein cross-linking, in fact, the reaction proceeds in two steps: (1) bi-photonic UV light absorption [39–41] and excitation of the DNA bases, in the nanosec-, picosec- or even femtosec-time scale; (2) cross-linking with proteins interacting with the DNA excited site and therefore lying nearby (zero-length cross-linking), which is completed in less than 1 millisec [39–41].

It is also important underlying the reproducibility and high cross-linking efficiency of this novel technique as compared to many of the presently available alternatives, based on the use of chemicals. The yield of the cross-linked products was found to be about 10 %, suggesting that 10 %

of total GAPDH chains are cross-linked as dimers upon UV-laser irradiation. Hence, our method turns out to be approximately 5 times more efficient than conventional formaldehyde cross-linking [41], and its efficiency is comparable to that of recently developed single-molecular-interaction sequencing (SMI-seq) technology for in vitro analyses [42]. Therefore, LUCK technology has the potentiality to become a universal technique to photo-fix protein interactions, as in principle it may be applicable to any biological context, such as the intracellular milieu of living cells, to unveil protein–protein interactions in a native context.

Moreover, due to the ultra-short time scale of UV-laser-induced cross-linking, this technique might allow to unveil transient interactions between proteins in a native context, differently from most of the methods based on the chemical induction of bonds between partners.

Materials and methods

Materials

All reagents were purchased from Sigma-Aldrich, unless differently specified. Protein G Sepharose was from GE Healthcare. The chemiluminescence detection system (SuperSignal® West Pico) was purchased from Pierce. Protease inhibitors cocktail was from Roche. HeLa cells (ATCC) were cultured in Dulbecco's modified Eagle medium (DMEM) supplemented with 10 % foetal bovine serum (FBS), 4 mM L-glutamine and penicillin–streptomycin (50 U/mL), in a 5 % CO_2 humidified atmosphere at 37 °C. Anti-GAPDH antibodies were from Ambion (monoclonal) and from Proteintech (polyclonal). Anti-mouse and anti-rabbit secondary antibodies conjugated to horseradish peroxide enzyme (HRP) were from Thermo Scientific.

UV-laser irradiation of living HeLa cells

To irradiate HeLa living cells, a powerful source of UV radiation, a custom-made version of the PHAROS laser system (Light Conversion Ltd., Vilnius, Lithuania, see the company website at http://www.lightcon.com/) was used. This is a very compact femtosecond amplified laser source—a single-unit integrated system, combining up to millijoule pulse energies and high average output power. This system, based on the new Yb:KGW lasing medium and on a very compact Chirped Pulse Amplification scheme, emits 1.3 mJ, 170 femtosec pulses, centred at 1030 nm, at a repetition rate of 2 kHz, corresponding to an average power of 2.5–2.6 W. The repetition rate can be increased up to 200 kHz, where the average output power reaches nearly 7 W. The IR pulse is then frequency up-converted into a harmonic generator stage (HIRO) where II (515 nm), III (343 nm), and VI (257 nm) harmonic pulses, lasting about 250 femtosec, are obtained. The system is equipped with a sophisticated pulse picker which allows one to separately select any possible repetition rate, from single-shot to 200 kHz.

For UV-laser irradiation, HeLa cells were detached by trypsin–EDTA and suspended in phosphate buffer (PBS 1X) at a density of 4×10^5 cells/mL. Cells were then placed in a cuvette containing a magnetic stirrer to ensure continuous agitation of the cell suspension during irradiation and uniform irradiation conditions.

UV-laser irradiation of GAPDH in vitro

In vitro cross-linked GAPDH was prepared by irradiating the protein isolated from rabbit muscle (65 μM, 500 μL total volume). To this purpose, lyophilized GAPDH was dissolved in 50 mM phosphate buffer pH 7.5 and placed in a cuvette containing a magnetic stirrer. Irradiation was then performed under the following conditions: 5 s irradiation time, 100 μJ pulse energy, 2 kHz repetition rate and 1.0 J total irradiation energy.

Cell extracts and immunoprecipitation

Following irradiation, cells were centrifuged at 2300*g* for 5 min. For total protein extraction, the cell pellet was resuspended at a density of 1×10^4 cells/μL in PBS 1X containing 1 % NP-40 and protease inhibitors cocktail (Roche, Germany). After 30 min on ice, lysates were centrifuged at 14,000 g for 30 min at 4 °C. Soluble protein concentration was determined by the Bradford assay. UV-laser-induced cross-linking was analysed by Western blotting of total proteins extracted from control and irradiated cells by the use of monoclonal anti-GAPDH antibodies.

For immunoprecipitation (IP) experiments, protein extracts (300 μg) were diluted in 0.01 % Tween-20 in PBS (1 μg/μL final concentration) and incubated with polyclonal anti-GAPDH-specific antibodies (3 μg) overnight at 4 °C on a shaker. After incubation with protein G Sepharose (60 μL) for 1.5 h at room temperature, the sample was centrifuged, washed, and bound proteins eluted in 2 % SDS and 10 % glycerol in 0.125 M Tris–HCl, pH 6.8. Selected proteins were analysed by Western blotting with anti-GAPDH monoclonal antibodies.

Two-dimensional gel electrophoresis

Protein extracts were obtained as described above. For each sample, 200 μg of proteins were precipitated using the 2D

Clean-Up Kit (GE Healthcare). After precipitation, the pellet was mixed with 125 μL of rehydration buffer (6 M urea, 2 M tiourea, 0.4 % CHAPS, 1 % bromophenol blue), 3 μL of 1 M DTT and 2.5 μL of pH 3–10 nl IPG buffer (GE Healthcare). Samples were loaded in duplicates onto 7 cm Immobiline^{TM}DryStrip gels strips (GE Healthcare) with a non-linear pH range of 3–10 using an isoelectric focusing system (EttanIPGphoreIII). Strips were rehydrated (20 °C, 16 h) and isoelectric focused (500 V for 1 h, 1000 V for 1 h, 5000 V for 3 h, held at 5000 V, 6000 V for 3 h, and held at 6000 V for 5 h to reach 15,000 V total energy). The maximum current was maintained at 50 μA per strip. Strips were subsequently reduced and alkylated twice (15 min each) in equilibration buffer [50 mM Tris–HCl pH 8.8, 6 M urea, 30 % (v/v) glycerol, 2 % (w/v) SDS, and 0.03 % bromophenol blue] with 65 mM DTT and 135 mM iodoacetamide. Strips were subjected to the second-dimensional separation (Ettan DALTsix) using a SDS–polyacrylamide gel (12.5 %). SDS-PAGE was carried out by standard methods with a constant voltage (180 V) at room temperature. A set of samples was then stained with colloidal Coomassie Brilliant Blue, while a second set of samples was electroblotted for Western blot analysis.

Protein identification

Protein identification by mass spectrometry was performed on Coomassie Blue stained spots from 2D gels and on bands excised from monodimensional gels. Excised spots/bands were destained by repetitive washes with 0.1 M NH_4HCO_3, pH 7.5 and acetonitrile. Enzymatic digestion was carried out with 100 ng of proteomic grade trypsin (Sigma) in 10 mM NH_4HCO_3 buffer, pH 7.5. Samples were incubated for 2 h at 4 °C, then trypsin solution was removed and a fresh trypsin solution was added and samples were incubated for 18 h at 37 °C. Peptides were then extracted by washing the gel spots/bands with acetonitrile and 0.1 % formic acid at room temperature and then were filtered using 0.22 μm PDVF filters (Millipore) following the recommended procedure.

The resulting peptide mixtures were analysed by nanoLC–MS/MS, on a CHIP MS 6520 QTOF equipped with a capillary 1200 HPLC system and a chip cube (Agilent Technologies, Palo Alto, Ca). After sample loading, the peptide mixture was first concentrated and washed at 4 μL/min in 40 nL enrichment column (Agilent Technologies chip), with 0.1 % formic acid in 2 % acetonitrile. The sample was then fractionated on a C18 reverse-phase capillary column (75 μm × 43 mM in the Agilent Technologies chip) at a flow rate of 400 nL/min, with a linear gradient of eluent B (0.1 % formic acid in 95 % acetonitrile) in A (0.1 % formic acid in 2 % acetonitrile) from 7 to 60 % in 50 min. Peptide analysis was performed using data-dependent acquisition of one MS scan (mass range from 300 to 2000 *m/z*) followed by MS/MS scans of the five most abundant ions in each MS scan. MS/MS spectra were measured automatically when the MS signal surpassed the threshold of 50,000 counts. Double and triple charged ions were preferably isolated and fragmented. Each LC-MS/MS analysis was preceded and followed by blank runs to avoid carryover contamination.

Data handling

The acquired MS/MS spectra were transformed in Mascot Generic format (.mgf) and used to query the SwissProt database 2015_01 (547,357 sequences; 194,874,700), with taxonomy restriction to Human (142,140 sequences), for protein identification with a licensed version of MASCOT software (www.matrixscience.com) version 2.4.0. Mascot search parameters were: trypsin as enzyme; 3, as allowed number of missed cleavages; carbamidomethylation of cysteines as fixed modification; 10 ppm MS tolerance and 0.6 Da MS/MS tolerance; peptide charge from +2 to +3. Possible oxidation of methionine and the formation of pyroglutamic acid from glutamine residues at the N-terminal position of peptides were considered as variable modifications. We also searched for known photo-oxidation products, as described by Plowman [31]. Peptide score threshold provided from MASCOT software to evaluate quality of matches for MS/MS data was 10. Individual ion score threshold provided by MASCOT software to evaluate the quality of matches in MS/MS data was 22. Only proteins presenting two or more peptides were considered as positively identified.

UV, fluorescence and CD spectroscopies

The spectroscopic characterization was carried out with commercially available GAPDH from rabbit muscle in 50 mM phosphate buffer pH 7.5, at a final concentration of 65 μM ($\varepsilon_{280} = 29{,}910\ M^{-1}\ cm^{-1}$). All acquired spectra were conveniently subtracted from blank contribution. The UV–Vis absorption spectra were recorded in 0.33 cm path length quartz cuvette. Wavelength scans were performed in the 200–800 nm range, with a 300 nm/min scan rate, 1.0 nm data interval and an average time of 0.0125 s, with the temperature set at 25 °C.

Fluorescence experiments were performed on a Horiba Jobin–Yvon Fluoromax-4 fluorimeter. The spectra were recorded with a reduced volume quartz cuvette with a 1.0 cm path length. Temperature of 25 °C was kept constant by the peltier unit with 2 nm slits. Spectra were recorded in the 300–450 nm region and in the 360–500 nm region with excitation wavelengths of 280 and 340 nm,

respectively. Fluorescence spectra were smoothed adopting a Savitzky–Golay filter with a 15 points window.

CD experiments were performed on a Jasco J-815 circular dichroism spectropolarimeter, calibrated for intensity with ammonium [D_{10}] camphorsulfonate [($\theta_{290.5\text{-}}$) = 7910 °C cm^2 dmol^{-1}). Depending on the observed region, the cell path length was 0.01 or 0.33 cm. CD spectra were recorded in the 190–250 nm (far-UV) and 255–375 nm (Soret) regions, at 0.2 nm intervals, with a 20 nm/min scan rate, 1.0 nm bandwidth and a 16 s response. In order to improve the signal to noise ratio, 3 accumulations were collected for the near-UV region. Spectra in the far-UV region are reported in terms of mean residue ellipticity, calculated by dividing the total molar ellipticity by the number of amino acids in the molecule, whereas spectra in the near-UV region are reported in terms of molar ellipticity.

Acknowledgments This research was partially supported by "Programma STAR" of University of Naples Federico II, "Compagnia di San Paolo" and "Istituto Banco di Napoli—Fondazione". We acknowledge the STRAIN PROJECT (POR Campania FSE 2007/2013 CUP B25B0900000000), which provided a postdoctoral fellowship to M.C. The authors are deeply indebted to Professor Gennaro Marino for his interest in this work and very useful comments and suggestions.

Compliance with ethical standards

Conflict of interest The authors declare no competing financial interests.

References

1. Goodsell DS, Olson AJ (2000) Structural symmetry and protein function. Annu Rev Biophys Biomol Struct 29:105–153
2. Levy ED, Pereira-Leal JB, Chothia C, Teichmann SA (2006) 3D complex: a structural classification of protein complexes. PLoS Comput Biol 2:e155
3. Tang X, Bruce JE (2009) Chemical cross-linking for protein-protein interaction studies. Methods Mol Biol 492:283–293
4. Subbotin RI, Chait BT (2014) A pipeline for determining protein-protein interactions and proximities in the cellular milieu. Mol Cell Proteomics 13:2824–2835
5. Sinz A (2006) Chemical cross-linking and mass spectrometry to map three-dimensional protein structures and protein-protein interactions. Mass Spectrom Rev 25:663–682
6. Bruce JE (2012) In vivo protein complex topologies: sights through a cross-linking lens. Proteomics 12:1565–1575
7. Zhang H, Tang X, Munske GR, Tolic N, Anderson GA, Bruce JE (2009) Identification of protein-protein interactions and topologies in living cells with chemical cross-linking and mass spectrometry. Mol Cell Proteomics 8:409–420
8. Walzthoeni T, Leitner A, Stengel F, Aebersold R (2013) Mass spectrometry supported determination of protein complex structure. Curr Opin Struct Biol 23:252–260
9. Guerrero C, Tagwerker C, Kaiser P, Huang L (2006) An integrated mass spectrometry-based proteomic approach: quantitative analysis of tandem affinity-purified in vivo cross-linked protein complexes (QTAX) to decipher the 26 S proteasome-interacting network. Mol Cell Proteomics MCP 5:366–378
10. Sinz A (2014) The advancement of chemical cross-linking and mass spectrometry for structural proteomics: from single proteins to protein interaction networks. Expert Rev Proteomics 11:733–743
11. Gingras A, Gstaiger M, Raught B, Aebersold R, Raught RAB (2007) Analysis of protein complexes using mass spectrometry. Nat Rev Mol Cell Biol 8:645–654
12. Chavez JD, Weisbrod CR, Zheng C, Eng JK, Bruce JE (2013) Protein interactions, post-translational modifications and topologies in human cells. Mol Cell Proteomics 12:1451–1467
13. Zheng C, Yang L, Hoopmann MR, Eng JK, Tang X, Weisbrod CR et al (2011) Cross-linking measurements of in vivo protein complex topologies. Mol Cell Proteomics 10(M110):006841
14. Kaake RM, Wang X, Burke A, Yu C, Kandur W, Yang Y et al (2014) A new in vivo cross-linking mass spectrometry platform to define protein-protein interactions in living cells. Mol Cell Proteomics 13:3533–3543
15. Lougheed KE, Bennett MH, Williams HD (2014) An in vivo crosslinking system for identifying mycobacterial protein-protein interactions. J Microbiol Methods 105:67–71
16. Suchanek M, Radzikowska A, Thiele C (2005) Photo-leucine and photo-methionine allow identification of protein-protein interactions in living cells. Nat Methods 2:261–267
17. Lin S, He D, Long T, Zhang S, Meng R, Chen PR (2014) Genetically encoded cleavable protein photo-cross-linker. J Am Chem Soc 136:11860–11863
18. Leo G, Altucci C, Bourgoin-Voillard S, Gravagnuolo AM, Esposito R, Marino G et al (2013) Ultraviolet laser-induced cross-linking in peptides. Rapid Commun Mass Spectrom 27:1660–1668
19. Petrotchenko EV, Borchers CH (2010) Crosslinking combined with mass spectrometry for structural proteomics. Mass Spectrom Rev 29:862–876
20. Keskin O, Gursoy A, Ma B, Nussinov R (2008) Principles of protein-protein interactions: what are the preferred ways for proteins to interact? Chem Rev 108:1225–1244
21. Jones S, Thornton JM (1996) Principles of protein-protein interactions. Proc Natl Acad Sci 93:13–20
22. Mezei M (2015) Statistical properties of protein-protein interfaces. Algorithms 8:92–99
23. Falchi F, Caporuscio F, Recanatini M (2014) Structure-based design of small-molecule protein–protein interaction modulators: the story so far. Future Med Chem 6:343–357
24. Sirover MA (2014) Structural analysis of glyceraldehyde-3-phosphate dehydrogenase functional diversity. Int J Biochem Cell Biol 57:20–26
25. Henderson B, Martin AC (2014) Protein moonlighting: a new factor in biology and medicine. Biochem Soc Trans 42:1671–1678
26. Chuang DM, Ishitani R (1996) A role for GAPDH in apoptosis and neurodegeneration. Nat Med 2:609–610b
27. Jenkins JL, Tanner JJ (2006) High-resolution structure of human D-glyceraldehyde-3-phosphate dehydrogenase. Acta Crystallogr D Biol Crystallogr 62:290–301
28. Boyd RW (2008) Nonlinear optics. Elsevier Academic Press, ISBN:0123694701
29. Valadan M, D'Ambrosio D, Gesuele F, Velotta R, Altucci C (2015) Temporal and spectral characterization of femtosecond deep-UV chirped pulses. Laser Phys Lett 12: 025302. IOP Select http://iopscience.iop.org/1612-202X/12/2/025302/article
30. Altucci C, Nebbioso A, Benedetti R, Esposito R, Carafa V, Conte M et al (2012) Nonlinear protein—nucleic acid crosslinking induced by femtosecond UV laser pulses in living cells. Laser Phys Lett 9:234–239

31. Plowman JE, Deb-Choudhury S, Grosvenor AJ, Dyer JM (2013) Protein oxidation: identification and utilisation of molecular markers to differentiate singlet oxygen and hydroxyl radical-mediated oxidative pathways. Photochem Photobiol Sci 12:1960–1967
32. Williams TJ, Reay AJ, Whitwood AC, Fairlamb IJ (2014) A mild and selectivePd-mediated methodology for the synthesis of highly fluorescent 2-arylated tryptophans and tryptophan-containing peptides: a catalytic role for Pd(0) nanoparticles? Chem Commun (Camb) 50:3052–3054
33. Pappenberger G, Schurig H, Jaenicke R (1997) Disruption of an ionic network leads to accelerated thermal denaturation of D-glyceraldehyde-3-phosphate dehydrogenase from the hyperthermophilic bacterium Thermotoga maritima. J Mol Biol 274:676–683
34. He RQ, Li YG, Wu XQ, Li L (1995) Inactivation and conformation changes of the glycated and non-glycated D-glyceraldehyde-3-phosphate dehydrogenase during guanidine-HCl denaturation. Biochim Biophys Acta 1253:47–56
35. Pattison DI, Rahmanto AS, Davies MJ (2011) Photo-oxidation of proteins. Photochem Photobiol Sci 11:38–53
36. Fasman GD (1996) Circular dichroism and the conformational analysis of biomolecules. Springer Science & Business Media, New York
37. Nakajima H, Amano W, Fukuhara A, Kubo T, Misaki S, Azuma YT et al (2009) An aggregate-prone mutant of human glyceraldehyde-3-phosphate dehydrogenase augments oxidative stress-induced cell death in SH-SY5Y cells. Biochem Biophys Res Commun 390:1066–1071
38. Nakajima H, Amano W, Kubo T, Fukuhara A, Ihara H, Azuma YT et al (2009) Glyceraldehyde-3-phosphate dehydrogenase aggregate formation participates in oxidative stress-induced cell death. J Biol Chem 284:34331–34341
39. Kryukov P, Letokhov V, Nikogosyan D, Borodavkin A, Budowsky E, Simukova N (1979) Multiquantum photoreactions of nucleic acid components in aqueous solution by powerful ultraviolet picosecond radiation. Chem Phys Lett 61:375–379
40. Nikogosyan DN (1990) Two-quantum UV photochemistry of nucleic acids: comparison with conventional low-intensity UV photochemistry and radiation chemistry. Int J Radiat Biol 57:233–299
41. Klockenbusch C, Kast J (2010) Optimization of formaldehyde cross-linking for protein interaction analysis of non-tagged integrin B1. J Biomed Biotechnol 2010:927585
42. Gu L, Li C, Aach J, Hill DE, Vidal M, Church GM (2014) Multiplex single-molecule interaction profiling of DNA-barcoded proteins. Nature 515:554–557

Biochimica et Biophysica Acta 1860 (2016) 434–444

Contents lists available at ScienceDirect

Biochimica et Biophysica Acta

journal homepage: www.elsevier.com/locate/bbagen

Protein conformational perturbations in hereditary amyloidosis: Differential impact of single point mutations in ApoAI amyloidogenic variants

Rita Del Giudice [a], Angela Arciello [a,e], Francesco Itri [a], Antonello Merlino [a,b], Maria Monti [a,e], Martina Buonanno [b,c], Amanda Penco [d], Diana Canetti [a,e], Ganna Petruk [a], Simona Maria Monti [b], Annalisa Relini [d,e], Piero Pucci [a,e], Renata Piccoli [a,e], Daria Maria Monti [a,e,*]

[a] Department of Chemical Sciences, University of Naples Federico II, 80126 Naples, Italy
[b] Institute of Biostructures and Bioimaging-CNR, Via Mezzocannone 16, 80134 Naples, Italy
[c] Dipartimento di Scienze e Tecnologie Ambientali, Biologiche e Farmaceutiche, Seconda Università di Napoli, Caserta, Italy
[d] Department of Physics, University of Genoa, Genoa, Italy
[e] Istituto Nazionale di Biostrutture e Biosistemi (INBB), Rome, Italy

ARTICLE INFO

Article history:
Received 17 July 2015
Received in revised form 15 October 2015
Accepted 23 October 2015
Available online 26 October 2015

Keywords:
Apolipoprotein A I
Protein stability
Amyloidosis
Conformational diseases

ABSTRACT

Amyloidoses are devastating diseases characterized by accumulation of misfolded proteins which aggregate in fibrils. Specific gene mutations in Apolipoprotein A I (ApoAI) are associated with systemic amyloidoses. Little is known on the effect of mutations on ApoAI structure and amyloid properties. Here we performed a physico-chemical characterization of L75P- and L174S-amyloidogenic ApoAI (AApoAI) variants to shed light on the effects of two single point mutations on protein stability, proteolytic susceptibility and aggregation propensity. Both variants are destabilized in their N-terminal region and generate fibrils with different morphological features. L75P-AApoAI is significantly altered in its conformation and compactness, whereas a more flexible and pronounced aggregation-competent state is associated to L174S-AApoAI. These observations point out how single point mutations in ApoAI gene evocate differences in the physico-chemical and conformational behavior of the corresponding protein variants, with the common feature of diverting ApoAI from its natural role towards a pathogenic pathway.

1. Background

Amyloidoses are characterized by protein aggregation in insoluble fibrils and their deposition in tissues and organs, with consequent alteration of their functionality. To date, almost 30 amyloidogenic proteins have been identified [1]; although these proteins do not show any sequence or structure homology, they have the ability to give rise to amyloid fibrils characterized by a highly ordered and rigid structure [2–5].

Apolipoprotein A I (ApoAI) is the main component of high density lipoproteins (HDL) and is mostly involved in the removal of cholesterol from peripheral tissues and its transfer, via the plasma, to the liver, where it is either recycled back to plasma as a component of newly formed lipoproteins, or excreted from the body via bile [6]. Due to ApoAI conformational plasticity, in its lipid-free or lipid-poor form, this protein is able to bind to phospholipids and to unesterified cholesterol to give rise to nascent HDL [7].

Some of the mutations in ApoAI gene are associated with hereditary systemic amyloidoses, characterized by extracellular fibrillar deposits in specific tissues, mainly heart, liver, kidneys and testes [8–10]. It has been reported that in the HDLs of heterozygous patients, in which both the wild-type protein and an amyloidogenic variant (L75P-AApoAI, L174S-AApoAI or L64P-AApoAI) are present, the wild-type protein is more abundant than the variant [11–13]. This finding is in line with our recent observation that in stably transfected human hepatic cells over-expressing L75P-AApoAI the secretion of the amyloidogenic variant is down-regulated [14], which in turn is in line with the observation of Marchesi and coworkers, who reported a decreased secretion efficiency of L75P- and L174S-AApoAI variants in transiently transfected COS cells [15]. Moreover, it has been hypothesized that AApoAI variants have a lower affinity for HDLs when compared to the wild-type protein; this would shift the ApoAI distribution from HDL-bound to lipid-poor/free state, which is relatively unstable and susceptible to proteolysis. The

Abbreviations: ANS, 8-anilino-1-naphthalensulfonic acid; ApoAI, apolipoprotein A I; AApoAI, amyloidogenic apolipoprotein A I; CD, circular dichroism; DLS, dynamic light scattering; GdnHCl, guanidine hydrochloride; HDL, high-density lipoproteins; MD, molecular dynamics; ThT, thioflavin T; TM-AFM, tapping mode atomic force microscopy; LC-MS, liquid chromatography-mass spectrometry.

* Corresponding author at: Department of Chemical Sciences, University of Naples Federico II, 80126 Naples, Italy.
E-mail address: mdmonti@unina.it (D.M. Monti).

http://dx.doi.org/10.1016/j.bbagen.2015.10.019
0304-4165/

resolution at 2.2 Å of the crystal structure of lipid-free Δ(185–243)-ApoAI revealed that ApoAI associates in domain swapped dimers held together by two four-helix bundles each constituted by the N-terminus of one subunit and the C-terminus of its partner. Interestingly, all the 19 amyloidogenic mutations so far identified cluster in two regions: the amino-terminus (residues 1–100) and within residues 173–178 [16], which, in the dimeric structure, define a 3D hot-spot mutation site [17]. To date, only few full-length AApoAI variants, out of 19 identified so far, have been investigated, which show significant peculiarities on the conformational transitions [18–21]. Recently, a model has been proposed, prompting that AApoAI mutations perturb one of the 4 predicted hot spots of the protein (14–22, 53–58, 69–72 and 227–232), with consequent full-length protein aggregation via the N-terminal region. This event would be followed by proteolytic cleavage at the exposed loop (83–100) and release of the N-terminal fibrillogenic polypeptide [21], which has been found to be the main protein constituent of ex-vivo fibrils [8]. It has been hypothesized that perturbation in the hot spots is one of the prerequisite for AApoAI misfolding, even though other factors may influence this process [21]. Here we analyzed the effects of two point mutations, L75P and L174S, on AApoAI conformational stability, being the former an "inside" mutation, i.e. located within the N-terminal fibrillogenic polypeptide, and the latter an "outside" mutation. Leu 75 is located in the middle of the short helix 70–76 that contributes to define the relative helical orientation in the four-segment bundle, whereas Leu 174 is located in the "bottom" of the hydrophobic cluster [22]. The variant with leucine to proline substitution at position 75 (L75P-AApoAI) is associated with a hereditary systemic amyloidosis characterized by preferential accumulation of fibrils in the kidneys and liver [11]. Instead, in the case of leucine to serine substitution at position 174 (L174S-AApoAI), a predominant accumulation of fibrils in the heart, skin, testes and larynx was observed [12]. The molecular basis of this differential localization of amyloid fibrils is still unknown.

We report structural stability, proteolytic susceptibility and aggregation propensity of full-length recombinant, lipid-free, human AApoAI harboring L75P or L174S mutation, to reveal the effects of a single point mutation on AApoAI structure and amyloidogenic potential.

This study is aimed to add knowledge to the largely unknown field of systemic amyloidoses. Starting from the general hypothesis suggesting that single point mutations, occurring in the 3D hot spot mutation site, direct the protein towards an amyloidogenic pathway, our study is aimed at revealing common and different impacts of mutations on protein stability.

2. Methods

2.1. Production of recombinant proteins

A bacterial expression system consisting of ApoAI expressing pET20 plasmid in *Escherichia coli* strain BL21(DE3) pLysS (Invitrogen) was used to prepare AApoAI proteins, as previously described [18]. Primer-directed PCR mutagenesis was used to introduce the L75P and L174S mutations. The mutation was verified by dideoxy automated fluorescent sequencing. Human ApoAI proteins were purified from bacterial cell lysate by immobilized metal affinity chromatography (HiTrap columns, GE Healthcare, Waukesha, WI) under denaturing conditions (4 M urea). Following binding, an extensive wash with 500 mM NaCl and 4 M urea in sodium phosphate buffer, 20 mM, pH 7.4 (wash buffer) was performed and bound proteins were then eluted with 500 mM imidazole in wash buffer. Proteins were dialyzed versus refolding buffer (50 mM Tris–HCl, pH 7.4), concentrated with 30 kDa molecular weight cut-off Amicon Ultra centrifugal filter devices (Millipore), and stored at −20 °C.

Purity and identity of the wild-type and variants were confirmed by LC–MS analyses, as reported below. Chromatographic traces recorded for each protein preparation, showed a single sharp peak, corresponding to the recombinant protein and the measured molecular masses were in agreement with the theoretical ones, according to the amino acid sequences of his-tagged expressed constructs (wild-type ApoAI: measured molecular mass: 29,799.6 ± 1.1 Da, theoretical molecular mass: 29,798.5 Da; L75P-AApoAI: measured molecular mass: 29,783.0 ± 1.8 Da, theoretical molecular mass: 29,782.5 Da; L174S-AApoAI: measured molecular mass: 29,772.8 ± 1.5 Da, theoretical molecular mass: 29,772.4 Da). For all the experiments His-tag containing proteins were used, as in preliminary conformational analyses (data not shown) we did not observe any significant difference comparing the His-tag containing wild-type protein to the protein after His-tag removal, or to commercial ApoAI (Sigma-Aldrich).

2.2. CD spectroscopy

Circular dichroism (CD) measurements were performed on a Jasco J815 spectropolarimeter (Jasco, Essex, UK), equipped with a temperature control system, using a 1-mm quartz cell in the far-UV range 194–260 nm (50 nm/min scan speed). Each spectrum was the average of three scans with the background of the buffer solution subtracted. Measurements were performed at 25 °C at a protein concentration of 0.15 mg/mL in 50 mM Tris HCl pH 7.4. Raw spectra were corrected for buffer contribution and converted to mean residue ellipticity, θ (mdeg cm^2 $dmol^{-1}$). Estimation of the secondary structure was carried out according to the Variable Selection Method (CDSSTR) using DICHROWEB [23].

2.3. Intrinsic fluorescence analysis

Emission fluorescence spectra were recorded in the range 300–450 nm, following excitation at 280 (tyrosine/tryptophan) or 295 nm (tryptophan). Measurements were carried out at 25 °C in a 10 mm cell by using a Perkin-Elmer LS50 spectrofluorimeter. Emission spectra were acquired at a scanning speed of 300 nm/min, with 10 and 5 slit widths for excitation and emission, respectively. Proteins (3 μM) were analyzed in 50 mM Tris HCl at pH 7.4.

2.4. Dye-binding assays

2.4.1. ThT binding assay

Proteins (0.3 mg/mL) were incubated at 25 °C in 50 mM Tris HCl at pH 7.4 in the presence of 10 μM thioflavin T (ThT). ThT fluouorescence emission spectra were acquired in the range 470–490 nm at 1 h intervals with scan speed of 300 nm/min, upon excitation at 450 nm. Excitation and emission slits were set at 5 and 10 nm, respectively. Fluorescence intensity values at 482 nm were plotted as a function of time. The determination of apparent $t_{1/2}$ values was obtained by non-linear regression fit of the data according to a double Boltzmann equation. The reported values represent the means from three independent experiments.

2.4.2. 1-Anilinonaphthalene-8-sulfonic acid (ANS) binding assay

Emission fluorescence spectra of recombinant proteins (3 μM) were acquired in the presence of the dye ANS (350 μM). Analyses were performed in 50 mM Tris HCl at pH 7.4, at 25 °C. Emission fluorescence spectra were recorded in the range 400–600 nm, following excitation at 380 nm. Excitation and emission slits were set at 5 and 10 nm, respectively.

2.5. Protein stability to denaturing agents

2.5.1. Chemical denaturation

Equilibrium denaturation was carried out on samples using guanidine (GdnHCl) and urea. Proteins were incubated for 24 h at 4 °C at 0.05 mg/mL prior to addition of denaturant. Incubated proteins were combined with denaturant, diluted from 8 M stock solutions. Samples were stored at 4 °C for 24 h prior to data collection. Changes in tryptophan fluorescence were recorded. The unfolding transition was

monitored by recording the wavelength at maximum fluorescence intensity (λ_{max}). The λ_{max} of triplicate dilutions of each sample was averaged and plotted against the denaturant concentration. Experimental points, describing sigmoidal curves, were fitted using the Boltzmann equation and $D_{1/2}$ (the concentration of denaturant at which the protein is half folded) was calculated. Assuming a two-state model (folded and unfolded), the free energy of denaturation was calculated as described by Petrlova et al. [18] by using the equation: $\Delta G_D^\circ = -RTlnK_D$. ΔG_D° and m values were obtained by plotting ΔG_D versus denaturant concentration to give the linear equation [24] $\Delta G_D = \Delta G_D^\circ - m[denaturant]$, where ΔG_D° is the free energy of protein folding in water (0 M denaturant), and m the cooperativity of denaturation.

2.5.2. Thermal denaturation

Temperature-induced denaturation of proteins (0.05 mg/mL) was performed as a function of increasing temperature (20–100 °C). Protein samples were incubated at the desired temperature for 15 min before taking the measurements. Denaturation of proteins was performed by recording changes in tryptophan fluorescence.

2.6. Homology modeling and molecular dynamics simulations

The starting structure of wild-type ApoAI for molecular dynamics simulation was taken from the protein data bank (PDB) file 3R2P [17]. The structure, which has been solved at 2.2 Å resolution, includes residues 3–182 of two chains. Based on the evidence of dynamic light scattering experiments, this dimeric structure was considered as representative of the protein conformation in solution. Models of the mutants were built on the structure of wild-type ApoAI by manual residue replacement.

Molecular dynamics (MD) and trajectory analysis were performed with the software package GROMACS 4.6.6 [25–27] using the Gromos43a1 force field. Appropriate number of counterions (Na^+) was added to neutralize the systems. The structures were immersed in a rectangular box filled with SPC water molecules at a density of 1000 kg/m^3 [28] with periodic boundary conditions. Long-range electrostatic interactions were treated with the particle-mesh Ewald method with a grid spacing of 12 Å and cutoff of 8 Å. [29]. The molecules were submitted to initial energy minimisation with the steepest descent for 5000 steps followed by 500 ns NVT and 500 ps NPT equilibration with position restraints. Production runs were performed for 10 ns with a 2 fs step. To the best of our knowledge, these simulations are the first ever performed on mutants of ApoAI.

Temperature and pressure coupling were obtained with the v-rescale [30] and the Parrinello-Rahman [31] algorithms, respectively. Bond lengths were constrained using LINCS [32]. The overall flexibility of the systems was evaluated comparing the traces obtained by diagonalizing the covariance matrix of the coordinate fluctuations, as previously described [33]. Only Cα atoms were included in the definition of the covariance matrices. Figures were prepared with Pymol (www.pymol.org).

2.7. Complementary proteolysis experiments and mass spectrometry analysis

Complementary proteolysis experiments were carried out by treating 0.4 mg/mL solutions of proteins with trypsin, chymotrypsin, and endoproteinase Glu-C in 50 mM Tris HCl, pH 7.4. Different E:S ratios were optimized for each proteolytic probe as reported: 1:8000 for chymotrypsin and trypsin, 1:10,000 for endoprotease Glu-C. The extent of digestion was monitored on a time-course basis by sampling the reaction mixture at 15 and 30 min and blocking the reactions with 2% trifluoroacetic acid (TFA). Peptide mixtures were analyzed by liquid chromatography-mass spectrometry (LC–MS) onto a QuattroMicro LC-MS system (Micromass, Waters) interfaced with a 1100 HPLC (Agilent Technologies, Palo Alto, CA). Peptide mixtures from the different proteolysis experiments were fractionated by reverse-phase HPLC on a Phenomenex Jupiter C18 column (250 mm × 2.1 mm, 300 Å pore size) and eluted by using a step gradient from 5% to 60% of solvent B (5% formic acid and 0.05% TFA in acetonitrile) over 60 min and from 60% to 95% in 5 min (solvent A 5% formic acid and 0.05% TFA in water). The flow rate was kept at 200 μL/min and directly introduced in the mass spectrometers ESI source. Horse heart myoglobin was used to calibrate the instrument (average molecular mass 16,951.5 Da) at 5 scans/s.

2.8. Determination of critical concentration

Proteins were incubated at different concentrations (from 0.15 to 2 mg/mL) in 50 mM Tris HCl pH 7.4 for 14 days at 37 °C. Then, samples were centrifuged at 14,000 *g* for 30 min at r.t., supernatants were filtered with a 20 nm cut off filter and the absorbance at 280 nm measured.

2.9. Dynamic light scattering

Dynamic light scattering (DLS) measurements were carried out using a Malvern nano zetasizer (Malvern, UK) [34]. Proteins (0.55 mg/mL) were diluted in 50 mM Tris HCl at pH 7.4, filtered with a 0.22 μm cut off filter and incubated at 37 °C over time. Samples were placed in a disposable cuvette and held at 25 °C during analysis. The aggregation rate was monitored at time 0 and after 24 h, 48 h and 7 days of incubation. For each sample, spectra were recorded six times with 11 sub-runs using the multimodal mode. The Z average diameter was calculated from the correlation function using the Malvern technology software.

2.10. Atomic force microscopy

For AFM inspection, ApoAI samples were incubated at 0.3 mg/mL at 37 °C. Incubation times in the range from 4 to 7 weeks were considered. At the end of incubation, proteins were centrifuged at 1700 *g* for 10 min, the pellet was suspended in an equal volume of water, and a 10 μL aliquot was deposited on freshly cleaved mica and dried under mild vacuum. Tapping mode AFM images were acquired in air using a Multimode SPM, equipped with "E" scanning head (maximum scan size 10 μm) and driven by a Nanoscope V controller, and a Dimension 3100 SPM, equipped with a 'G' scanning head (maximum scan size 100 μm) and driven by a Nanoscope IIIa controller (Digital Instruments, Bruker AXS GmbH, Karlsruhe, Germany). Single beam uncoated silicon cantilevers (type OMCL-AC160TS, Olympus, Tokyo, Japan) were used. The drive frequency was between 290 and 340 kHz, the scan rate was between 0.3 and 0.8 Hz. Aggregate sizes were estimated from the heights in cross section of the topographic AFM images.

3. Results

3.1. Effects of amyloidogenic mutations on ApoAI secondary structure

The secondary structure content of AApoAI variants was estimated by far-UV CD spectroscopy at pH 7.4, at 0.15 mg/mL protein concentration to approximate physiological conditions. As shown in Fig. 1, wild-type ApoAI and the two amyloidogenic variant proteins were predominantly in an α-helical state, with a slightly lower α-helix content of the variants with respect to the wild-type protein (Table 1). When the proteins were incubated at 37 °C over time, no significant changes in the spectra of the wild-type protein were observed, consistently with literature data [18 and references therein]; on the contrary, the α-helicity of both variants decreased over time accompanied by an increase in β-strand, indicating an alteration of the protein native conformation towards an aggregation competent state.

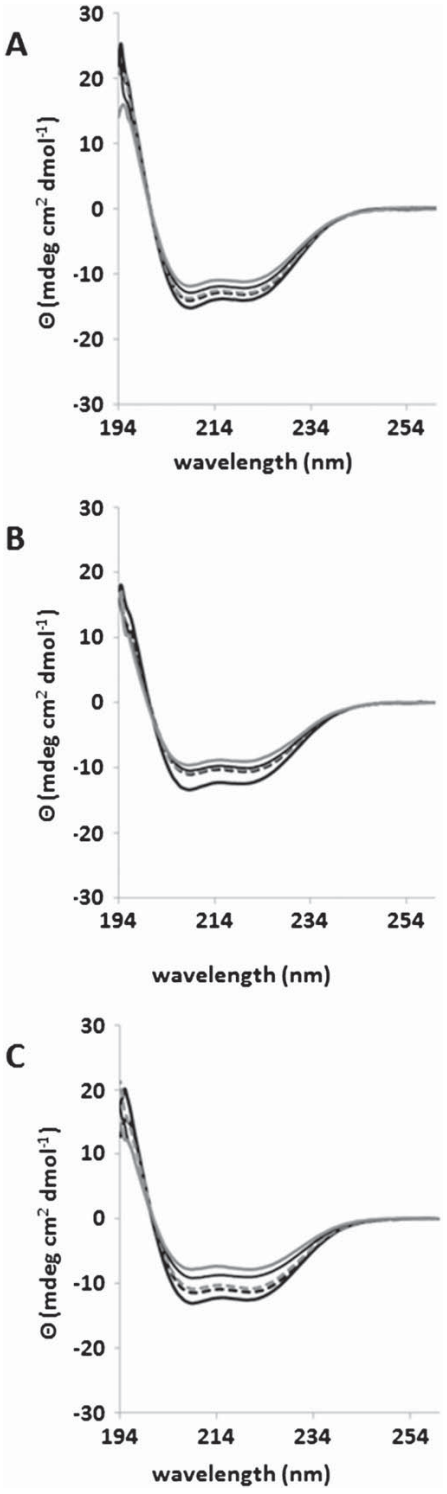

Fig. 1. Far-UV CD spectra of wild-type ApoAI and its amyloidogenic variants upon incubation at 37 °C. A, wild-type ApoAI; B, L75P-AApoAI; C, L174S-AApoAI. Spectra were acquired at 25 °C with 0.15 mg/mL protein concentration in 50 mM TrisHCl buffer, pH 7.4. Spectra were recorded at time 0 (bold black line), after 24 h (black dashed line), 48 h (gray dashed line), 72 h (black fine line) and after 7 days (bold gray line) incubation.

Table 1
α-Helix and β-strand contents (%) for wild-type ApoAI and its amyloidogenic variants, upon incubation at 37 °C. Data shown are the means from three independent experiments. The accuracy of the secondary structure content estimation is approximately 2% for wild-type ApoAI and 4% for its amyloidogenic variants.

Incubation time (h)	Wild-type ApoAI		L75P-AApoAI		L174S-AApoAI	
	α-Helix (%)	β-Strand (%)	α-Helix (%)	β-Strand (%)	α-Helix (%)	β-Strand (%)
0	49	29	40	36	45	28
24	49	28	34	36	40	21
48	47	29	32	39	35	37
72	40	34	31	39	29	41
168	38	33	29	40	20	53

3.2. Effects of amyloidogenic mutations on ApoAI conformation

During amyloid formation protein aggregation leads to an increase in the exposure of hydrophobic regions to the aqueous environment. ANS binding studies revealed a 3-fold increase of ANS fluorescence intensity in the presence of wild-type ApoAI (Fig. 2A, black line), due to the exposure of ANS accessible hydrophobic surfaces, as previously reported [35–38]. A larger increase of ANS fluorescence was measured for both variants compared to wild-type ApoAI, particularly evident for L174S-AApoAI variant, indicating that both mutations trigger the exposure of hydrophobic regions (Fig. 2A, gray line and dashed line for L75P-AApoAI and L174S-AApoAI, respectively).

To compare the tertiary structure of AApoAI variants with that of the wild-type protein, the intrinsic fluorescence emission intensity was registered and the shift of maximum emission wavelength (λ_{max}), due to changes in solvent exposure of tyrosine and tryptophan residues, was evaluated. As the four Trp residues of the wild-type protein (at positions 8, 50, 72 and 108), as well as the five Tyr residues (at positions 18, 29, 100, 115, 166), are located within the four-helix bundle domain and are all conserved in the amyloidogenic variants under study, this analysis is a measure of the stability of AApoAI N-terminal region. Fluorescence spectra were collected either upon excitation at 295 nm, where the contribution of tyrosine residues is negligible (Fig. 2B), or upon excitation at 280 nm, where both Tyr and Trp residues significantly contribute to the absorption (Fig. 2C). As shown in Fig. 2B, in the case of L75P-AApoAI (gray line) the maximum fluorescence intensity emission wavelength ($\lambda_{max} = 344.7 \pm 0.3$ nm) is higher than that of wild-type ApoAI ($\lambda_{max} = 335.7 \pm 0.6$ nm). These data suggest that the substitution L75P is able to induce changes in the conformation of the N-terminal domain with consequent exposure of hydrophobic protein surfaces, since proline is known to interrupt protein α-helical structure. On the contrary, L174S-AApoAI (Fig. 2B, dashed line) showed a $\lambda_{max} = 336.3 \pm 1.2$ nm, a value similar to that recorded for wild-type ApoAI. Similar results were observed when the contribution of both Tyr and Trp was analyzed (Fig. 2C and Table S1).

3.3. Effects of mutations on ApoAI stability

To get insights into the structural features that favor AApoAI amyloidogenicity, we compared the folding of the L75P-AApoAI and L174S-AApoAI to that of wild-type ApoAI by investigating protein stability in the presence of chemical denaturing agents, such as guanidine hydrochloride (GdnHCl) and urea. Upon excitation at 295 nm, the unfolding transition was monitored by evaluating the change in λ_{max} as a function of chemical agent concentration. As the equilibrium unfolding of wild-type ApoAI by GdnHCl has been well characterized, it can be used as a reference for the stability of the variants. As shown in Fig. 3(A–B), sigmoidal curves (filled squares) were obtained in the case of wild-type protein, confirming a cooperative unfolding pattern that well fits the two-state model [18,39]. As shown in Table 2, the mid-point of the denaturation process ($D_{1/2}$ values), ΔG_D° and

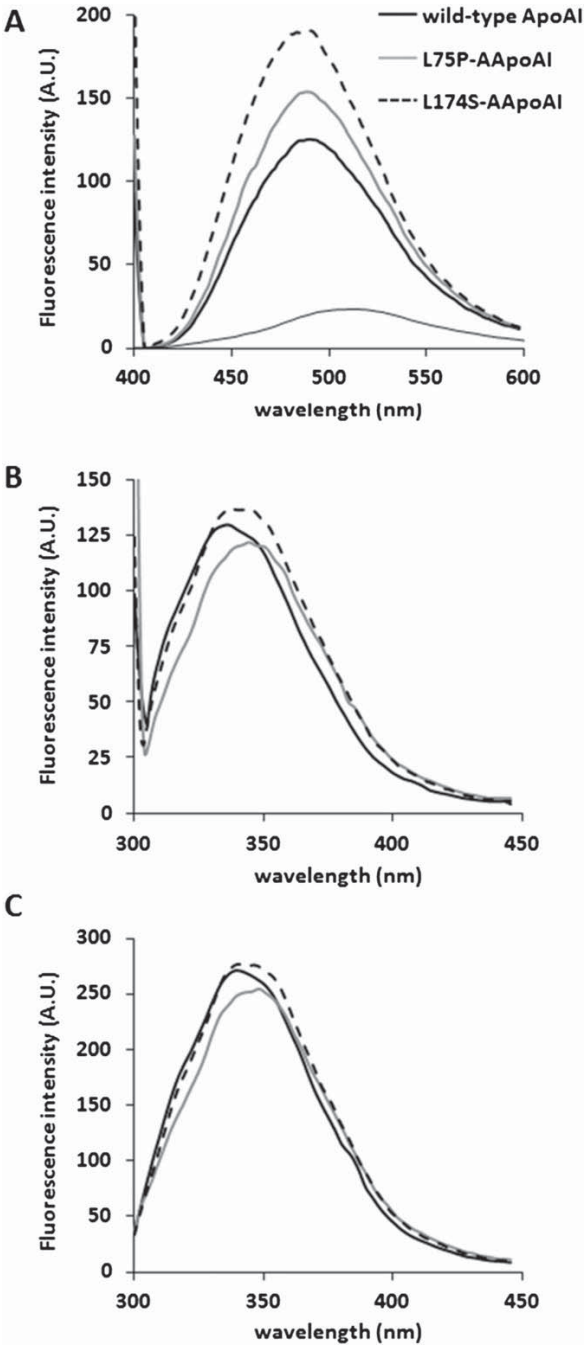

Fig. 2. Fluorescence analyses of AApoAI variants. A, binding of ANS to wild-type ApoAI (black line) and to its amyloidogenic variants L75P (gray line) and L174S (dashed line). ANS spectrum is reported as a fine black line. ANS emission fluorescence spectra were recorded in the range from 400 to 600 nm at the excitation wavelength of 395 nm. ANS emission was monitored at pH 7.4. B and C, tryptophan and tyrosine emission spectra at pH 7.4 of wild-type ApoAI (bold black line), L75P-AApoAI (gray line) and L174S-AApoAI (dashed line). Fluorescence was excited at 295 nm (B) and at 280 nm (C).

cooperativity (m) values were similar to those previously reported [18 and references therein].

A completely different behavior was observed in the case of L75P-AApoAI and L174S-AApoAI, as the denaturation curves are shifted to lower denaturant concentrations compared to wild-type ApoAI, indicating a decreased structural stability. In particular, for L75P-AApoAI variant (empty circles in Fig. 3 (A–B), protein unfolding was found not to be a cooperative process and a higher λ_{max} was recorded even in the absence of the denaturing agent. On the other hand, for

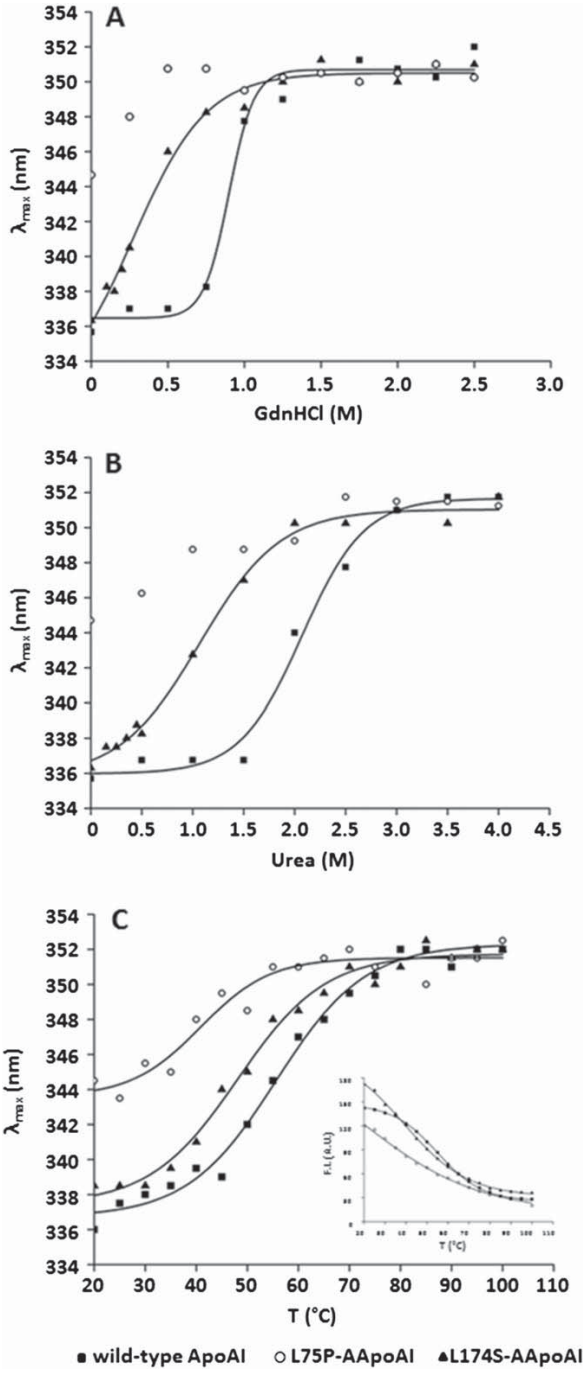

Fig. 3. Unfolding of wild-type ApoAI (filled squares) and of its amyloidogenic variants L75P (empty circles) and L174S (filled triangles) induced by the addition of increasing amounts of GdnHCl (A), urea (B), or by temperature changes (C). Following excitation at 295 nm, emission spectra were recorded and curves were obtained by reporting the maximum emission fluorescence as a function of the denaturing agent concentration value. Tryptophan fluorescence intensity as a function of temperature is reported as an inset in C.

Table 2
Denaturation parameters for the unfolding of AApoAI variants. Data shown are the means from three independent experiments.

Protein	$D_{1/2}$ (M)	ΔG_D° (kcal/mol)	m	$D_{1/2}$ (M)	ΔG_D° (kcal/mol)	m	Tm (°C)	ΔH (kcal/mol)
	GdnHCl			Urea			Temperature	
Wild-type ApoAI	0.90 ± 0.01	2.9 ± 0.5	2.76 ± 0.32	2.1 ± 0.3	4.4 ± 0.4	2.0 ± 0.1	55.3 ± 0.5	26.9 ± 0.1
L75P-AApoAI	n.a.	n.a.	n.a.	n.a.	n.a.	n.a.	40.8 ± 2.2	15.0 ± 0.4
L174S-AApoAI	0.39 ± 0.01	0.20 ± 0.04	0.9 ± 0.2	1.1 ± 0.4	1.3 ± 0.2	1.0 ± 0.2	43.5 ± 4.6	22.4 ± 0.4

L174S-AApoAI variant, a hyperbolic curve (filled triangles in Fig. 3A) was obtained in the presence of GdnHCl, indicative of a fast and non-cooperative unfolding process. Following the addition of increasing amounts of urea, a sigmoidal curve was obtained for L174S variant (Fig. 3B, filled triangles) even though less pronounced when compared to the wild-type protein, indicating a loss in unfolding cooperativity. Denaturation parameters for the unfolding process of AApoAI variants are reported in Table 2. The lower GdnHCl $D_{1/2}$ values obtained for wild-type ApoAI and L174S variant, compared to urea $D_{1/2}$, may suggest the importance of electrostatic interactions, efficiently weakened by GdnHCl, in the stabilization of the two proteins [40]. Loss in cooperativity during denaturation is a common feature of amyloidogenic variants, as variants G26R and L178H [18], and the recently published R173P [20] share this behavior.

Finally, by thermal denaturation (Fig. 3C) we observed that the proteins are all structurally stable up to 50 °C, although enthalpy and midpoint values, reported in Table 2, were found to be lower for the variants than for wild-type ApoAI, confirming their lower stability with respect to the native protein.

3.4. Structural features of wild-type ApoAI, L75P-AApoAI and L174S-AApoAI: a molecular dynamics study

To address differences in the structural features of the two variants when compared to the wild-type protein, models of the variants were obtained and used as inputs for a molecular dynamics (MD) study. In wild-type ApoAI, L75 is located in the middle of the short helix 70–76 that contributes to define the relative helical orientation in the four-segment bundle and interacts with L14 in the "bottom" hydrophobic cluster formed by V11, L14, F71 and L82. L174, instead, is located in the packed "bottom" hydrophobic cluster so that its substitution with Ser was expected to disrupt this cluster [17,22]. On the other hand, from the MD simulations it emerged that the replacement of L174 with a Ser has only a moderate effect on the overall structure of the protein. In fact, in the L174S variant, the serine side chain can be well accommodated within the helix 141–180, since it can form a hydrogen bond with the carbonylic oxygen of Y170 (Fig. 4A). On the contrary, the L75P substitution has a stronger destabilizing effect, since the presence of Pro breaks helix 70–76 and disturbs the stabilizing hydrophobic interactions that play a major role in orienting the helices of the four-segment bundle (Fig. 4B).

During the MD simulations, no significant changes in the overall structure from the corresponding crystal structure occurred in wild-type ApoAI, while the two variants show subtle, but significant variations. In particular, the average structures extracted from the trajectories for the three proteins suggest that L174S-AApoAI, which has an overall structure similar to that of wild-type protein, presents a slight reduced radius of gyration (5.91 ± 0.02 nm vs 5.98 ± 0.03 nm of wild-type ApoAI), while L75P-AApoAI adopts a less compact structure (+2% in the total solvent accessible surface area), with a significant loss of α-helical content (about −2%). These differences well reflect in the average distances between donor and acceptor atoms involved in the formation of 3_{10}-, α- and π-helices (Table S2). These data are in overall agreement with those obtained by CD spectra (Fig. 1).

To verify if the conformational changes induced by the mutations also affects the overall dynamics of the proteins, the trace of the covariance matrix of CA atoms for the three structures, which is a measure of the overall flexibility [33], has been evaluated. The values for wild-type ApoAI, L75P-AApoAI and L174S-AApoAI were 75 nm^2, 105 nm^2 and 98 nm^2, respectively. These data clearly indicate that the mutations enhance the overall flexibility of the protein.

To obtain a more detailed picture of the observed differences, the percentage of α-helical content of each residue (helicity) during the simulation was plotted as a function of the residue number (Fig. S1). Interestingly, although the plots have an overall similar profile for the three proteins, some differences can be evidenced: wild-type ApoAI is generally more structured; however in the regions encompassing residues 18–30, 80–81 and 126–131 it is slightly less structured than the two variants. L75P-AApoAI shows a lower helical content in correspondence of residues 66–73, 135–137, 157–160 and 172–177, but it is more structured than both wild-type ApoAI and L174S in the regions 125–129 and 140–142. L174S-AApoAI has a lower α-helical content in correspondence of residues 107–110, 140–141, but it is more structured in the regions 77–80 and 158–160. These differences are associated with slight variations also in the solvent accessible surface area per residue. Notably, although in the L75P variant the region encompassing residues 135–137 presents a lower helical content when compared to the other proteins (Fig. S1), it becomes more buried than in L174S-AApoAI and the wild-type protein, as the average solvent accessible surface area of residue 136 is: 76, 62 and 76 $Å^2$, in wild-type, L75P-AApoAI and L174S-AApoAI, respectively.

3.5. Complementary proteolysis experiments

In order to define ApoAI regions structurally altered by the presence of mutations, the surface topology of wild-type protein, L75P-AApoAI and L174S-AApoAI variants was investigated by a complementary proteolysis approach coupled with mass spectrometry identification of cleavage sites (LC–MS) [41]. Complementary proteolysis refers to limited proteolysis experiments carried out in conditions able to generate a single proteolytic event on the protein which originates two "complementary" peptides. Further cleavages occurring on the two complementary peptides are not considered. Conformational changes induced by mutations and affecting protein topology were monitored by the appearance of preferential cleavage sites located in exposed and flexible regions of the proteins, which become more susceptible to proteolysis [42,43]. Complementary proteolysis experiments were performed using trypsin, chymotrypsin and endoprotease Glu-C as conformational probes. All reactions were carried out in parallel on the three proteins by using the same E:S ratio and were monitored on a time-course basis by sampling the incubation mixture after 15 and 30 min of hydrolysis. Following this time course approach, primary and secondary cleavage sites, always produced by a single proteolytic event, were only defined on kinetic basis. The LC–MS profiles showed that both variants were more susceptible to proteases than the wild-type protein, as demonstrated by the higher number of peptides released at the same hydrolysis time (data not shown). This observation suggests that both AApoAI variants are more flexible and/or less structured than the wild-type protein, in agreement with both spectroscopic and molecular dynamics data.

The distribution of the proteolytic sites is outlined in Fig. 4C. A similar pattern of proteolytic accessibility could be observed in all the

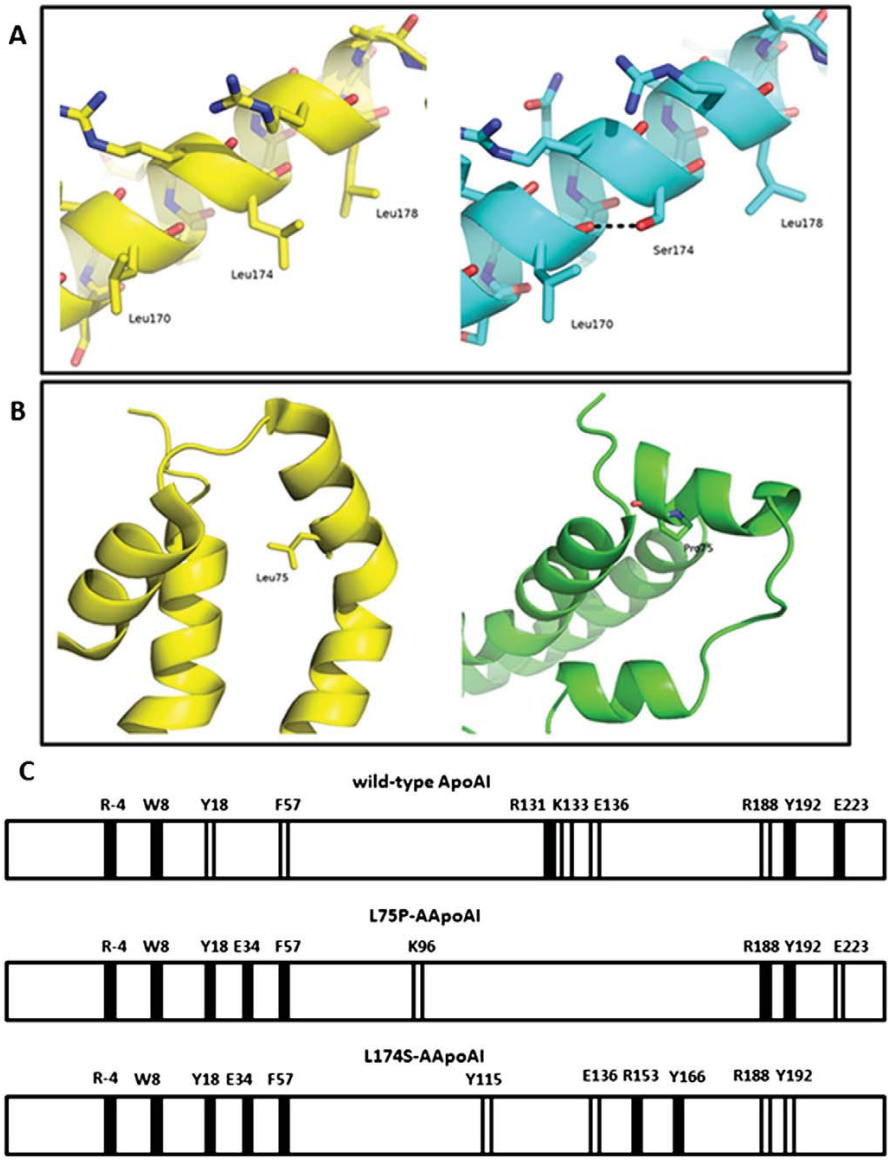

Fig. 4. Structural features of AApoAI variants. A, insight of the structure of helix encompassing residues 141–180 in wild-type ApoAI (yellow) and in L174S variant (cyan). B, ribbon representation of the helix bundle in proximity of L75 in the structure of wild-type ApoAI (yellow) and of L75P variant (green). For sake of clarity, one helix from the second chain of the dimer was removed. C, pattern of preferential proteolytic sites in native and AApoAI variants. Schematic representation of the results obtained from limited proteolysis experiments on wild-type ApoAI (upper), L75P-AApoAI (middle) and L174S-AApoAI (lower). Proteolytic sites are designed as primary (filled) or secondary sites (empty) merely on kinetic basis. The R-4 cleavage site was not taken in consideration, as it is located in the his-tag peptide sequence occurring in the recombinant proteins.

proteins, with preferential cleavage sites gathering at both the N- and C-terminal regions. However, hydrolysis at Y18 and F57 occurred much faster in the mutants than in wild-type ApoAI and E34 was not recognized in the native protein, suggesting a higher flexibility in the N-terminal region of the variants. Moreover, cleavage at K96 and Y115, in L75P- and L174S-AApoAI, respectively, suggests a slight conformational change in the region including the putative proteolytic site in AApoAI variants, responsible for the release of the fibrillogenic polypeptide. On the contrary, in wild-type ApoAI this region, as reported in the crystal structure [17], is in a predominantly α-helical structure, which protects the protein from proteolytic cleavage.

Also at the C-terminus, wild-type ApoAI and L75P variant are characterized by a quite similar proteolytic profile, showing accessibility at residues R188, Y192 and E223. This region seems to be protected in the L174S variant, as showed by the disappearance of the E223 cleavage site and by a slower kinetic of hydrolysis at level of R188 and Y192 residues, thus suggesting that a slight conformational change occurred in this region. Further differences in the proteolytic patterns of the three proteins were located in the region encompassing the 131–136 sequence that was exposed in the wild-type ApoAI, as demonstrated by cleavages at R131, K133 and E136. On the contrary, this region became completely inaccessible in the L75P variant, in perfect agreement with the molecular dynamics simulation. The accessibility of this sequence changed also in the L174S variant, where E136 was still recognized, but with slow kinetics and the appearance of new cleavage sites at R153 and Y166 was detected. It is noteworthy that these cleavages occurred quite close to the mutation site 174, indicating a higher accessibility of this region, as suggested by molecular dynamics calculations.

From MD and complementary proteolysis experiments we can conclude that both L75P- and L174S-AApoAI variants have an increased exposure of the N-terminal region.

3.6. Effects of mutations on ApoAI aggregation

As structural and conformational alterations have been associated with the presence of a single point mutation, the impact of pathogenic substitutions on the aggregation propensity of full-length AApoAI was investigated by using different approaches. First, to get information about the critical concentration [44] of AApoAI variants, proteins were incubated at different concentrations for 14 days at 37 °C. Their final concentration (c_f) was measured spectrophotometrically following the removal of aggregated species, as described in the Methods section. In the graph (Fig. S2), we reported $1 - c_f / c_i$ versus c_i, where c_i is the initial protein concentration and $1 - c_f / c_i$ is a measure of protein aggregated species. We calculated a critical concentration of 0.18 ± 0.05 mg/mL for L75P variant and 0.15 ± 0.04 mg/mL for L174S variant. No aggregation occurred for the wild-type protein.

Next, we measured the kinetics of aggregation of AApoAI variants by ThT binding assays. Proteins were incubated (0.3 mg/mL) at pH 7.4 in the presence of ThT, and the increase of ThT emission fluorescence at 482 nm was measured over time (Fig. 5A). A much higher increase in ThT fluorescence intensity was observed in the case of L174S-AApoAI variant with respect to L75P-AApoAI, whereas no aggregation of the wild-type protein was observed, in line with previous results [18]. For both AApoAI variants, a double-sigmoidal curve of ThT emission was observed, less evident in the case of L75P-AApoAI variant (inset of Fig. 5A). For both variants, the first transition occurred with a smaller amplitude increase in ThT fluorescence intensity with respect to the second one. The apparent $t_{1/2}$ values were: 29 ± 9 h and 96 ± 10 h for L75P-AApoAI and 35 ± 6 h and 83 ± 7 h for L174S-AApoAI. In agreement with data reported by Grudzielanek and coworkers on insulin aggregation [45], we hypothesize that the first transition is associated to with the formation of partially folded species able to bind ThT, whereas the second transition can be due to the formation of amyloid nuclei (Fig. 5A). Similar results were obtained in the presence of physiological amount of NaCl (0.15 M). Hence, in our experimental conditions, low salt concentration has no significant effect on the aggregation propensity of AApoAI variants.

Then, we analyzed the stability of protein tertiary structure upon incubation at 37 °C, as destabilization represents a crucial step during fibrillogenesis [46]. Proteins were incubated at 37 °C up to 1 week and at time intervals ANS binding experiments and intrinsic fluorescence analyses were performed (Fig. S3). In the presence of either amyloidogenic variants an increase in ANS fluorescence, more evident for L174S-AApoAI (Fig. S3C, gray line), was detected after 72 h, suggesting conformational changes leading to the exposure of hydrophobic surfaces. A decrease in ANS binding was observed after a prolonged incubation (1 week, Fig. S3C, dashed lines), suggesting shielding of hydrophobic patches due to their direct involvement in fibril formation. No changes in ANS binding was observed instead in the case of wild-type ApoAI (Fig. S3A). These results were confirmed by intrinsic fluorescence experiments (Fig. S3D–I and Table S1), showing a decrease of the emission maximum after 72 h incubation to be related to protein aggregation. As a consequence, Trp residues are hindered and remain buried instead of being exposed to the solvent.

Furthermore, we evaluated the apparent hydrodynamic diameter of the three proteins by means of dynamic light scattering (DLS). For wild-type ApoAI we obtained an apparent hydrodynamic diameter of 11.0 ± 1.1 nm, consistent with the size of a protein dimer, as previously reported by X-ray crystallography [22]. The hydrodynamic diameter of the

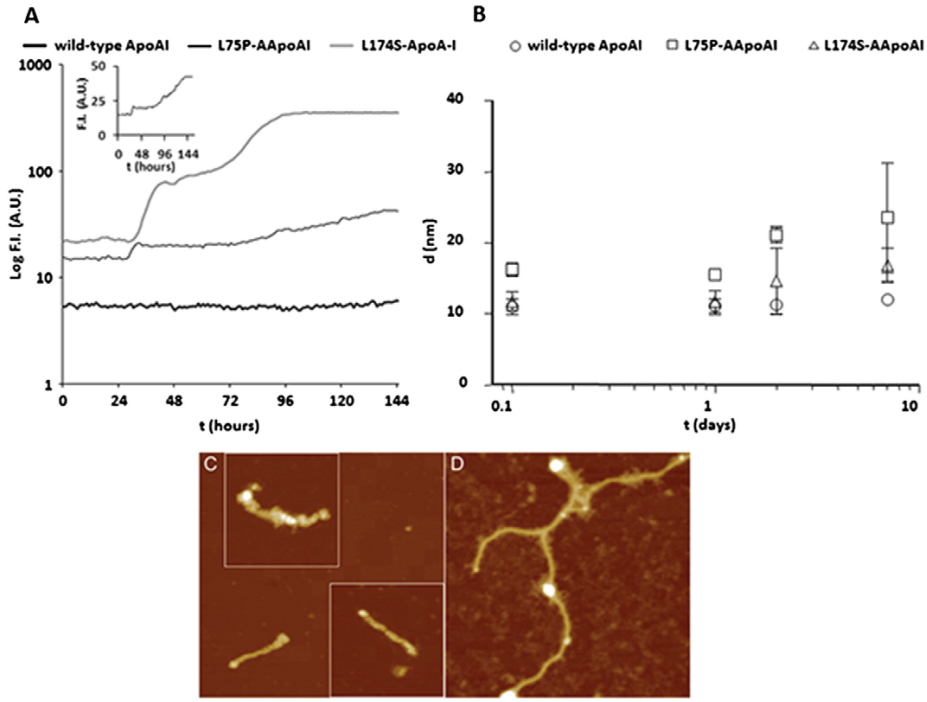

Fig. 5. AApoAI aggregation. A, ThT binding assay. Proteins under test were incubated for 144 h at 25 °C in 50 mM Tris HCl, pH 7.4. During the incubation, emission fluorescence values at 482 nm were recorded every 60 min. A typical curve for wild-type ApoAI (black bold line), L75P-AApoAI (black fine line) and L174S-AApoAI (gray bold line) are shown. The inset shows an enlargement of L75P-AApoAI curve. B, apparent hydrodynamic diameter of AApoAI variants over time. Wild-type ApoAI (empty circles), L75P-AApoAI (empty squares) and L174S-AApoAI variant (empty triangles) were incubated at 37 °C for different length of time. The hydrodynamic diameter, d (nm), is reported as a function of time, t (days), expressed as logarithm of time. C, D, tapping mode AFM images (height data) of L75P-AApoAI (C) and L174S-AApoAI (D) aggregates obtained after seven weeks incubation. Scan size 750 nm, Z range 29 nm (C and insets), 12 nm (D). The insets in C are at the same scale of the background image (inset scan size, 500 nm).

L174S-AApoAI variant was 11.8 ± 1.4 nm, similar to the value obtained for the wild-type protein, whereas the L75P-AApoAI variant showed a diameter of 16.3 ± 0.9 nm, consistent with a less-compact structure than the native protein, according to intrinsic fluorescence experiments and MD simulations (Fig. 2B-C). When proteins were analyzed after 24 h incubation, no formation of higher molecular aggregated species were detected in the three samples, as indicated in Fig. 5B, where the diameter values are plotted as a function of the incubation time. Indeed, wild-type ApoAI showed a constant apparent diameter up to 7 days (Fig. 5B) in agreement with ANS binding experiments, intrinsic fluorescence analyses and ThT binding (Figs. 2 and 5A), thus confirming no aggregation for the wild-type protein. On the contrary, the variants showed a different behavior with respect to ApoAI, with peculiar characteristics differentiating one from the other. The apparent diameter of L174S-AApoAI gradually increased up to 16.9 ± 2.4 nm after 7 days incubation, whereas L75P-AApoAI reached an apparent diameter value of 23.6 ± 7.8 nm, suggesting a pronounced decrease of protein compactness over time.

Finally, AFM experiments were performed to inspect the aggregate morphology after incubation times ranging from 4 to 7 weeks. We found that L75P-AApoAI formed scanty, short fibrils with length of 200–350 nm and height of 4–6 nm (Fig. 5C). These fibrils exhibit a beaded morphology, resulting from the assembly of different subunits of variable size, with not very regular packing. The L174S-AApoAI variant displayed a higher density of fibrillar aggregates as compared to L75P-AApoAI. These aggregates were generally smoother, longer and thinner than those formed by L75P-AApoAI, exhibiting typical lengths between 200 nm and 4 μm and heights between 1 and 3 nm; Fig. 5D shows L174S-AApoAI fibrils detected after 7 weeks incubation. In addition, a minority of thick, beaded fibrils (length 400–500 nm, height 5–6 nm) was also observed (not shown). No fibrils were detected for wild-type ApoAI in the same conditions. All the data collected indicate that the AApoAI variants are prone to aggregate and generate fibrils qualitatively similar to the fibrillar structures reported in the literature for other AApoAI variants [18,19].

4. Discussion

Using an array of independent methodologies, the effects of the "inside mutation" L75P and the "outside mutation" L174S on ApoAI propensity to undergo an amyloidogenic pathway have been analyzed with the aim of elucidating common and different features of amyloidogenic mutations in the development of the disease. We found that both variants display: (i) a slightly lower α-helical content with respect to the native protein and a time dependent increase of β-strand structure; (ii) more exposed hydrophobic regions, particularly evident for L174S variant; (iii) reduced stability and loss of unfolding cooperativity; (iv) increased flexibility; and (v) enhanced susceptibility to protease cleavage in the N-terminal region.

Nevertheless, the two variants show significant differences, which contribute to add knowledge to the emerging picture of the cause and effect relationship in ApoAI associated amyloidosis. As supposed, the substitution of L75 with proline has a destabilizing effect, as it breaks helix 70–76. This helix overlaps with one of the three predicted N-terminal amyloid "hot spots", whose perturbation has been recently suggested to be a prerequisite for misfolding [21]. This leads to the exposure of hydrophobic residues mainly located in the N-terminal region, as demonstrated by the increased intrinsic fluorescence intensity and ANS binding, as well as by the exposure of a proteolytic site at Y18, belonging to the major hot spot 14–22, as also found for G26R and L178H variants [18]. Furthermore, the accessibility of further proteolytic sites at E34 and F57 (the latter belonging to the minor hot spot 53–58), both hindered in the native protein, is the consequence of the propagation of the local perturbation (helix 70–76) to the other two predicted hot spots and the cause of the decreased protein compactness. In fact, DLS measurements of the hydrodynamic diameter demonstrated that the L75P variant is a much less compact protein with respect to both the wild-type protein and the L174S variant, with an increased diameter of 50%. Therefore, as a response to the occurrence of the "internal" mutation L75P, the protein acquires a "looser" structure at the N-terminal domain, with significant alteration of protein conformation and compactness, while the "external" mutation L174S is responsible for a less destabilized but more flexible structure to which a more pronounced aggregation-competent state is associated.

In the 3D structure, residue 174 is in close proximity to hot spot 14–22 which appears to be destabilized, as indicated by the appearance of a cleavage site at Y18. This perturbation could affect the hot spot 53–58, in line with cleavage at F57. Moreover, in the L174S variant cleavages at R153 and Y166 occur. The structural differences between L75P- and L174S-AApoAI variants are mainly due to differences in the exposed regions of the proteins. We believe that in L75P variant the N-terminal region is more unstructured, as indicated by Trp intrinsic fluorescence (Fig. 2B) and suggested by DLS measurements (Fig. 5B) and MD simulations (Fig. 4B), whereas in L174S the region encompassing residues 153–166 seems to be more unstructured, as demonstrated by limited proteolysis experiments (Fig. 4C).

We propose that these structural features represent the molecular basis of the different aggregation propensity of the two variants. Following incubation at 37 °C, L174S shows a higher propensity to aggregate than the L75P variant, as demonstrated by CD and fluorescence analyses, ThT binding and AFM imaging. The time-dependent increase of β-sheet structure, shown by L75P and L174S variants, is similar to that of G26R-AApoAI [18], whereas for L178H-AApoAI an increase in the α-helical content has been described over time, accompanied by the formation of very short fibrillar structures [18]. Upon 7 days incubation at 37 °C, DLS measurements revealed an over time increase of protein diameter by about 50% and 44% for the L75P and L174S variants, respectively, compared to the wild-type protein. Noteworthy, L75P-AApoAI lower compactness well correlates with the beaded morphology of its fibrils, whereas even though L174S-AApoAI is relatively compact and less unstructured than the other variant, it presents higher aggregation propensity than L75P-AApoAI. It is likely that in this case a balance between protein compactness, partial unfolding, group exposure and flexibility regulates protein amyloidogenicity.

Our data indicate that both amyloidogenic mutations induce protein destabilization in a region close to the mutated residue. The propagation of the destabilization to the N-terminal hot spots region, allowed by their proximity in the 3D structure, is a sine qua non condition for aggregation, as recently suggested by Das and coworkers [21]. The polymorphic behavior observed in our experimental system is not surprising, as polymorphism is a common feature of amyloid aggregation; in this case it could be also favored by the direct involvement of the N-terminal region alone in triggering aggregation, thus resulting in possible multiple arrangements of the rest of the protein.

Differently from the accepted pathway in which AApoA-I is cleaved prior to aggregation, Das and coworkers [21] suggested that AApoAI cleavage can occur only after aggregation of the full-length protein. Therefore, aggregation of the N-terminal region of the full-length protein would represent the first step in the fibrillogenic process. Following the specific cleavage of the full-length variant, the formation of mature fibrils could be observed. Our observation that L75P- and L174S-AApoA-I are able to aggregate as full-length proteins is consistent with this model, and the scantiness of mature fibrils can be explained by the lack of the proteolytic cleavage. Our findings highlight a potential key element in the evolution of the disease, i.e. the partial exposure of K96 and Y115 cleavage sites in L75P- and L174S-AApoAI, respectively. In fact, in this region, which is fully hindered in the native protein, the cleavage sites that allow the release of the fibrillogenic N-terminal polypeptide(s) are expected to be present. It is tempting to speculate that this region becomes fully exposed upon aggregation of the full-length variants.

In conclusion, our study adds knowledge, at a molecular level, to the general mechanism by which amyloidogenic mutations determine

ApoAI systemic amyloidosis, providing a new *tessera* in the puzzle of such a severe disease.

Supplementary data to this article can be found online at http://dx.doi.org/10.1016/j.bbagen.2015.10.019.

Author contribution

R.D.G and D.M.M. conceived the experiments; F.I. and R.D.G. constructed mutants; G.P. express and purified recombinant proteins; R.D.G. performed the biochemical experiments; M.M. and D.C. carried out proteolysis experiments; M.B. performed DLS experiments; A.M. performed the MD analyses; A.P. performed the AFM experiments; R.D.G., D.M.M., A.A., A.R., S.M.M., R.P. and P.P. analyzed the results; R.D.G., and D.M.M. wrote the paper with the contribution of all authors.

Funding

The authors thank the Italian MIUR (Ministero dell'Università e della Ricerca Scientifica, Progetti di Rilevante Interesse Nazionale) Project (PRIN 2009STNWX3) and the University of Genoa (Projects PRA2013 and PRA2014) for the financial support to the activities reported in the present study.

Transparency document

The Transparency document associated with this article can be found, in the online version.

References

[1] M. Eriksson, S. Schonland, S. Yumlu, U. Hegenbart, H. von Hutten, Z. Gioeva, P. Lohse, J. Büttner, H. Schmidt, C. Röcken, Hereditary apolipoprotein AI-associated amyloidosis in surgical pathology specimens: identification of three novel mutations in the APOA1 gene, J. Mol. Diagn. 11 (2009) 257–262.
[2] A. Relini, S. Torrassa, R. Rolandi, A. Gliozzi, C. Rosano, C. Canale, M. Bolognesi, G. Plakoutsi, M. Bucciantini, F. Chiti, M. Stefani, Monitoring the process of HypF fibrillization and liposome permeabilization by protofibrils, J. Mol. Biol. 338 (2004) 943–957.
[3] P. Westermark, M.D. Benson, J.N. Buxbaum, A.S. Cohen, B. Frangione, S. Ikeda, C.L. Masters, G. Merlini, M.J. Saraiva, J.D. Sipe, A primer of amyloid nomenclature, Amyloid 14 (2007) 179–183.
[4] S.T. Ferreira, F.G. De Felice, A. Chapeaurouge, Metastable, partially folded states in the productive folding and in the misfolding and amyloid aggregation of proteins, Cell Biochem. Biophys. 44 (2006) 539–548.
[5] S.T. Ferreira, M.N. Vieira, F.G. De Felice, Soluble protein oligomers as emerging toxins in Alzheimer's and other amyloid diseases, IUBMB Life 59 (2007) 332–345.
[6] K.A. Rye, P.J. Barter, Formation and metabolism of prebeta-migrating, lipid-poor apolipoprotein A-I, Arterioscler. Thromb. Vasc. Biol. 24 (2004) 421–428.
[7] G. Cavigiolio, E.G. Geier, B. Shao, J.W. Heinecke, M.N. Oda, Exchange of apolipoprotein A-I between lipid-associated and lipid-free states: a potential target for oxidative generation of dysfunctional high density lipoproteins, J. Biol. Chem. 285 (2010) 18847–18857.
[8] L. Obici, G. Franceschini, L. Calabresi, S. Giorgetti, M. Stoppini, G. Merlini, V. Bellotti, Structure, function and amyloidogenic propensity of apolipoprotein A-I, Amyloid 13 (2006) 1–15.
[9] D. Rowczenio, A. Dogan, J.D. Theis, J.A. Vrana, H.J. Lachmann, A.D. Wechalekar, J.A. Gilbertson, T. Hunt, S.D. Gibbs, P.T. Sattianayagam, et al., Amyloidogenicity and clinical phenotype associated with five novel mutations in apolipoprotein A-I, Am. J. Pathol. 179 (2011) 1978–1987.
[10] M. Gomaraschi, L. Obici, S. Simonelli, G. Gregorini, A. Negrinelli, G. Merlini, G. Franceschini, L. Calabresi, Effect of the amyloidogenic L75P apolipoprotein A-I variant on HDL subpopulations, Clin. Chim. Acta 412 (2011) 1262–1265.
[11] L. Obici, G. Palladini, S. Giorgetti, V. Bellotti, G. Gregorini, E. Arbustini, L. Verga, S. Marciano, S. Donadei, V. Perfetti, et al., Liver biopsy discloses a new apolipoprotein A-I hereditary amyloidosis in several unrelated Italian families, Gastroenterology 126 (2004) 1416–1422.
[12] P. Mangione, M. Sunde, S. Giorgetti, M. Stoppini, G. Esposito, L. Gianelli, L. Obici, L. Asti, A. Andreola, P. Viglino, et al., Amyloid fibrils derived from the apolipoprotein A1 Leu174Ser variant contain elements of ordered helical structure, Protein Sci. 10 (2001) 187–199.
[13] C.L. Murphy, S. Wang, K. Weaver, M.A. Gertz, D.T. Weiss, A. Solomon, Renal apolipoprotein A-I amyloidosis associated with a novel mutant Leu64Pro, Am. J. Kidney Dis. 44 (2004) 1103–1109.
[14] R. Del Giudice, D.M. Monti, C. Sarcinelli, A. Arciello, R. Piccoli, G.F. Hu, Amyloidogenic variant of apolipoprotein A-I elicits cellular stress by attenuating the protective activity of angiogenin, Cell Death Dis. 5 (2014), e1097.
[15] M. Marchesi, C. Parolini, C. Valetti, P. Mangione, L. Obici, S. Giorgetti, S. Raimondi, S. Donadei, G. Gregorini, G. Merlini, et al., The intracellular quality control system down-regulates the secretion of amyloidogenic apolipoprotein A-I variants: a possible impact on the natural history of the disease, Biochim. Biophys. Acta 1812 (2011) 87–93.
[16] A. Andreola, V. Bellotti, S. Giorgetti, P. Mangione, L. Obici, M. Stoppini, J. Torres, E. Monzani, G. Merlini, M. Sunde, Conformational switching and fibrillogenesis in the amyloidogenic fragment of apolipoprotein A-I, J. Biol. Chem. 278 (2003) 2444–2451.
[17] X. Mei, D. Atkinson, Crystal structure of C-terminal truncated apolipoprotein A-I reveals the assembly of HDL by dimerization, J. Biol. Chem. 286 (2011) 38570–38582.
[18] J. Petrlova, T. Duong, M.C. Cochran, A. Axelsson, M. Mörgelin, L.M. Roberts, J.O. Lagerstedt, The fibrillogenic L178H variant of apolipoprotein A-I forms helical fibrils, J. Lipid Res. 53 (2012) 390–398.
[19] J.O. Lagerstedt, G. Cavigiolio, L.M. Roberts, H.S. Hong, L.W. Jin, P.G. Fitzgerald, M.N. Oda, J.C. Voss, Mapping the structural transition in an amyloidogenic apolipoprotein A-I, Biochemistry 46 (2007) 9693–9699.
[20] S.A. Rosú, O.J. Rimoldi, E.D. Prieto, L.M. Curto, J.M. Delfino, N.A. Ramella, M.A. Tricerri, Amyloidogenic propensity of a natural variant of human apolipoprotein a-I: stability and interaction with ligands, PLoS ONE 10 (2015), e0124946.
[21] M. Das, X. Mei, S. Jayaraman, D. Atkinson, O. Gursky, Amyloidogenic mutations in human apolipoprotein A-I are not necessarily destabilizing- a common mechanism of apolipoprotein A-I misfolding in familial amyloidosis and atherosclerosis, FEBS J. 281 (2014) 2525–2542.
[22] O. Gursky, X. Mei, D. Atkinson, The crystal structure of the C-terminal truncated apolipoprotein A-I sheds new light on amyloid formation by the N-terminal fragment, Biochemistry 51 (2012) 10–18.
[23] L. Whitmore, B.A. Wallace, DICHROWEB: an online server for protein secondary structure analyses from circular dichroism spectroscopic data, Nucleic Acids Res. 32 (2004) 668–673.
[24] M. Koyama, M. Tanaka, P. Dhanasekaran, S. Lund-Katz, M.C. Phillips, H. Saito, Interaction between the N- and C-terminal domains modulates the stability and lipid binding of apolipoprotein A-I, Biochemistry 48 (2009) 2529–2537.
[25] B. Hess, C. Kutzner, D. van der Spoel, E. Lindahl, GROMACS 4: algorithms for highly efficient, load-balanced, and scalable molecular simulation, J. Chem. Theory Comput. 4 (2008) 435–447.
[26] S. Pronk, S. Pall, R. Schulz, P. Larsson, P. Bjelkmar, R. Apostolov, M.R. Shirts, J.C. Smith, P.M. Kasson, D. van der Spoel, et al., GROMACS 4.5: a high-throughput and highly parallel open source molecular simulation toolkit, Bioinformatics 29 (2013) 845–854.
[27] D. van der Spoel, R. van Druner, H.J.C. Berendsen, GROningenMAchine for chemical simulations, BIOSON Research Institute, Groningen, The Netherlands, 1994.
[28] H.J.C. Berendsen, J.P.M. Postma, W.F. van Gusteren, A. Di Nola, J.R. Haak, Molecular dynamics with coupling to an external heat bath, J. Chem. Phys. 81 (1984) 3684–3690.
[29] T. Darden, D. York, L. Pedersen, Particle mesh Ewald — an N·log(N) method for Ewald sums in large systems, J. Chem. Phys. 98 (1993) 10089–10092.
[30] G. Bussi, D. Donadio, M. Parrinello, Canonical sampling through velocity rescaling, J. Chem. Phys. 126 (2007) 014101.
[31] M. Parrinello, A. Rahman, Polymorphic transitions in single crystals: a new molecular dynamics method, J. Appl. Phys. 52 (1981) 7182–7190.
[32] B. Hess, H. Bekker, H.J.C. Berendsen, J.G.E.M. Frajie, LINCS: a linear constraint solver for molecular simulations, J. Comput. Chem. 18 (1997) 1463–1472.
[33] A. Merlino, L. Mazzarella, A. Carannante, A. Di Fiore, A. Di Donato, E. Notomista, F. Sica, The importance of dynamic effects on the enzyme activity: X-ray structure and molecular dynamics of onconase mutants, J. Biol. Chem. 280 (2005) 17953–17960.
[34] I. Di Lelio, S. Caccia, M. Coppola, M. Buonanno, G. Di Prisco, P. Varricchio, E. Franzetti, G. Corrado, S.M. Monti, R. Rao, et al., A virulence factor encoded by a polydnavirus confers tolerance to transgenic tobacco plants against lepidopteran larvae, by impairing nutrient absorption, PLoS ONE 9 (2014), e113988.
[35] H. Saito, P. Dhanasekaran, D. Nguyen, P. Holvoet, S. Lund-Katz, M.C. Phillips, Domain structure and lipid interaction in human apolipoproteins A-I and E, a general model, J. Biol. Chem. 278 (2003) 23227–23232.
[36] M. Tanaka, P. Dhanasekaran, D. Nguyen, S. Ohta, S. Lund-Katz, M.C. Phillips, H. Saito, Contributions of the N- and C-terminal helical segments to the lipid-free structure and lipid interaction of apolipoprotein A-I, Biochemistry 45 (2006) 10351–10358.
[37] J.A. Beckstead, B.L. Block, J.K. Bielicki, C.M. Kay, M.N. Oda, R.O. Ryan, Combined N- and C-terminal truncation of human apolipoprotein A-I yields a folded, functional central domain, Biochemistry 44 (2005) 4591–4599.
[38] D.P. Rogers, C.G. Brouillette, J.A. Engler, S.W. Tendian, L. Roberts, V.K. Mishra, G.M. Anantharamaiah, S. Lund-Katz, M.C. Phillips, M.J. Ray, Truncation of the amino terminus of human apolipoprotein A-I substantially alters only the lipid-free conformation, Biochemistry 36 (1997) 288–300.
[39] M. Tanaka, P. Dhanasekaran, D. Nguyen, M. Nickel, Y. Takechi, S. Lund-Katz, M.C. Phillips, H. Saito, Influence of N-terminal helix bundle stability on the lipid-binding properties of human apolipoprotein A-I, Biochim. Biophys. Acta 1811 (2011) 25–30.
[40] V. Granata, G. Graziano, A. Ruggiero, G. Raimo, M. Masullo, P. Arcari, L. Vitagliano, A. Zagari, Chemical denaturation of the elongation factor 1 alpha isolated from the hyperthermophilic archaeon *Sulfolobus solfataricus*, Biochemistry 45 (2006) 719–726.
[41] F. Dal Piaz, A. Casapullo, A. Randazzo, R. Riccio, P. Pucci, G. Marino, L. Gomez-Paloma, Molecular basis of phospholipase A2 inhibition by petrosaspongiolide M, Chembiochem 3 (2002) 664–671.
[42] G. Esposito, R. Michelutti, G. Verdone, P. Viglino, H. Hernàndez, C.V. Robinson, A. Amoresano, F. Dal Piaz, M. Monti, P. Pucci, et al., Removal of the N-terminal hexapeptide from human β2-microglobulin facilitates protein aggregation and fibril formation, Protein Sci. 9 (2000) 831–845.

[43] M. Monti, S. Principe, S. Giorgetti, P. Mangione, G. Merlini, A. Clark, V. Bellotti, A. Amoresano, P. Pucci, Topological investigation of amyloid fibrils obtained from β2-microglobulin, Protein Sci. 11 (2002) 2362–2369.
[44] H. Yagi, K. Hasegawa, Y. Yoshimura, Y. Goto, Acceleration of the depolymerization of amyloid β fibrils by ultrasonication, Biochim. Biophys. Acta 1834 (2013) 2480–2485.
[45] S. Grudzielanek, V. Smirnovas, R. Winter, Solvation-assisted pressure tuning of insulin fibrillation: from novel aggregation pathways to biotechnological applications, J. Mol. Biol. 356 (2006) 497–509.
[46] M. Lindgren, P. Hammarström, Amyloid oligomers: spectroscopic characterization of amyloidogenic protein states, FEBS J. 277 (2010) 1380–1388.